THE UNIVERSITY OF CALGARY

WEIGHTED FOUR POINT IMPLICIT METHOD OF SOLUTION OF THE ST. VENANT EQUATIONS

BY

ABDALLA ALI EL-MAAWY

A THESIS

SUBMITTED TO THE FACULTY OF GRADUATE STUDIES

IN PARTIAL FULFILMENT OF THE REQUIREMENTS FOR THE

DEGREE OF MASTER OF SCIENCE

DEPARTMENT OF CIVIL ENGINEERING

CALGARY, ALBERTA

OCTOBER, 1991

ISBN 0-315-75163-0

THE UNIVERSITY OF CALGARY

FACULTY OF GRADUATE STUDIES

The undersigned certify that they have read, and recommend to the Faculty of Graduate Studies for acceptance, a thesis entitled, "Weighted Four Point Implicit Method of Solution of the St. Venant Equations", submitted by Abdalla Ali El-Maawy in partial fulfilment of the requirements for the degree of Master of Science.

Chairman, Dr. D.H. Manz
Department of Civil Engineering

Dr. R.L. Day
Department of Civil Engineering

Richard D. Rowe

Dr. R.D. Rowe
Department of Mechanical Engineering

Date Oct. 31/91

ABSTRACT

The most commonly used equations for hydraulic routing of unsteady open channel flow are the St. Venant equations for which no analytical solution exists. Of the many existing numerical techniques to solve the St. Venant is the weighted four point implicit scheme, which is considered one of the best. This scheme is favoured because it is not restricted to using very small time steps imposed by the stringent stability conditions such as the Courant stability criteria and/or limits on friction. It can readily be used with unequal distance intervals and its stability-convergence properties can be controlled.

An investigation was performed on the numerical and simulation properties of the weighted four point implicit scheme for hydraulic routing of unsteady open channel flow. This included an evaluation of the stability, convergence, verification, and factors affecting the calibration properties of the method.

Several series of numerical experiments were performed. Analysis of the experimental results permitted the following conclusions to be made:

1. The stability and convergence properties of the weighted four point implicit finite difference scheme are:

   (a) When values of time step (Δt_c) and distance interval (Δx_c) are selected such that the term $\Delta t_c/\Delta x_c \cdot C \approx 1$ (C is the wave celerity of undisturbed water), simulations can be expected to be stable and convergent and provide a more accurate representation of the flow profile. However, if values of distance interval are selected much greater than Δx_c, serious instabilities may result.

   (b) The time interval chosen to obtain experimental observations must be sufficiently small to ensure adequate detail of the flow is provided to the numerical model.

(c) The maximum value of time interval which would ensure solution stability decreases as the relative change in the abrupt increase or decrease in flow increases. The value of time interval is the same if relative changes in flow, increase or decrease, are of similar magnitude, convergence considerations withstanding.

(d) The magnitude of the time interval had a much greater impact on solution convergence than either distance interval or weighting factor.

(e) A value of weighting coefficient approaching 0.6 permits stable, convergent and accurate representation of the wave profile of surge flow. Weighting coefficients approaching 0.55 may be used successfully for gradual changes in flow.

2. Using a high quality experimental channel data set, an appropriately configured simulation model which employed the weighted four point implicit method successfully predicted the measured flow conditions and may be considered verified.

3. Techniques were developed to determine optimum estimate of resistance coefficient, channel bottom slope and channel geometry.

4. Knowledge of the effects of variations of the resistance coefficient, channel bottom slope and cross section geometry of the channel predicted depth and discharge hydrographs can be used to develop strategies for performing calibration studies.

ACKNOWLEDGEMENTS

In the name of ALLAH most gracious most merciful.

I wish to extend my appreciation to my supervisor, Dr. D.H. Manz for his continued guidance and assistance during my study. I am deeply indebted for his invaluable patience and assistance in proofreading of this manuscript. Also I am thankful for his teachings, programming and use of the Irrigation Conveyance System Simulation Model.

Grateful acknowledgement is given to the staff of the Inter-Library Loan department for providing the assistance in getting the necessary reference materials for this study. Special thanks are extended to Dr. and Mrs. R. Day for the editing and typing of this manuscript.

Last, but not least, I thank my parents, brother, sister and friends for their moral support and prayers during my studies.

TABLE OF CONTENTS

LIST OF TABLES

LIST OF FIGURES

LIST OF SYMBOLS

A	cross-sectional area of channel
B	width of the water surface of the channel
C	celerity of wave in undisturbed water (or water at rest), computed depth or discharge values
C_m	celerity of kinematic wave
C_p	maximum (peak) value of depth or discharge computed values
D	exact solution of finite difference equation
d/s	downstream boundary of channel reach length
d	subscript for variable evaluated at downstream boundary of the channel
E	mass conservation error
F, G, f	functions
i	grid point index along x
j	grid point index along t
k	label for kth interation cycle
L	length of channel
M	measured depth or discharge values, point on the (x,t) plane (see Fig. 2.1)
M_p	maximum (peak) value of measured depth or discharge
N	number of subreaches in a system, numerical solution of partial difference equations

n	Manning's resistance coefficient, total number of hydrograph values being computed
P	wetted perimeter, system performance variable
P_e	peak error
Q	discharge
Q_0	discharge at uniform flow
Q_1	discharge at entrance section of channel reach
Q_2	discharge at exit section of channel reach
q	lateral inflow
RS	relative root mean square error
r	residual error, subscript for variable evaluated at downstream or upstream boundary of the channel
S	exact solution of partial differential equations, not mean square error
S_o	channel bottom slope, storage at t=0
S_t	storage at t=t
S_f	channel friction slope
S_w	slope of wind energy line
t	time
V	average velocity of flow
x	distance
y	water depth

y_0	water depth at uniform flow
z	water depth above reference plane
Δt	time step (interval)
Δt_c	selected time interval
Δx	distance interval
Δx_c	selected distance interval
∂	partial derivative
β	momentum correction coefficient, numerical error
δ	truncation error
α	a grid function
ε	convergence criteria parameter in Newton Iteration Method
θ	finite difference weighting parameter

CHAPTER 1: INTRODUCTION

1.1 INTRODUCTION

The analysis of the dynamics of the flow of water through man-made or natural open channels (including rivers, estuaries, irrigation channels, drainage channels, and hydroelectric power canals) is complex. The flow is typically unsteady, that is, the depth, velocity and discharge varies with time locally and throughout channel length. Depth, velocity and discharge along open channels may vary rapidly (abrupt change over comparatively short distance) or gradually. The propagation phenomenon is a function of several factors: variation in cross-section, variation of channel flow resistance, variation in channel bottom slope, local inflows and outflows, branches, wind effects, and lateral inflows (e.g. rainfall) or outflows (e.g. seepage, evaporation) along the channel reach. The need to predict the behaviour of the unsteady flow in open channels provides the impetus to develop flow routing models. For example, to control water distribution in irrigation channels, for flood forecasting in rivers, to determine (approximately) the channel roughness for vegetative infested open channels, etc. The theory describing the unsteady flow has been known and confirmed since the 19th century, by De Saint Venant in 1871.

The most commonly used equations for hydraulic routing unsteady flows in open channels are the one-dimensional partial differential equations of gradually varied unsteady flow consisting of equations of continuity and of momentum, collectively known as the St. Venant equations. The St. Venant equations describe the hydraulics of long water waves (water waves in open channels means the depth, velocity and discharge as they vary with time). The St. Venant equations are nonlinear hyperbolic equations and defy analytical solution except in their simplest form. Before the advent of high speed computers it was necessary to simplify the St. Venant equations and develop approximate solution

technique (for details see, for example, Gunaratnam and Perkins, 1970). The high speed computer made feasible techniques to solve the complete form of the St. Venant equations which are usually superior to the approximate methods in describing the complex unsteady open channel flow phenomena.

The development of numerical methods to solve the complete form of the St. Venant equations was pioneered by Stoker (1953) and can be categorized into the explicit finite difference schemes, implicit finite difference, and method of characteristics. Of these techniques the weighted four point implicit scheme developed by Amein (1968), belonging to the category of implicit finite difference scheme, was selected for study. The weighted four point implicit scheme is favoured because it is not restricted to using small time steps imposed by stringent stability conditions. It can be readily used with variable distance interval; and the stability-convergence properties can be controlled.

Since hydraulic modelling using the complete form of St. Venant equation is still in its infant stage of development, previous studies conducted on the weighted four point implicit scheme did not completely describe the numerical properties and application characteristics of the technique.

1.2 OBJECTIVE OF RESEARCH PROGRAM

The objective of the research program was to investigate the numerical modelling and simulation properties of the weighted four-point implicit finite difference scheme for hydraulic routing of unsteady open channel flows.

Past research on numerical modelling and simulation properties, numerical computational properties, and numerical simulation properties, of the weighted four-point implicit scheme are investigated in order to permit the development of guidelines for the application of the technique.

CHAPTER 2 - RESEARCH METHOD

2.1 WEIGHTED FOUR POINT IMPLICIT METHOD FOR UNSTEADY FLOW SIMULATION

2.1.1 GOVERNING EQUATIONS

The basic hydrodynamic equations for one dimensional flow simulation in open channels are the St. Venant equations of continuity and of momentum. Derivations of these equations may be found in various handbooks or literature on open channel hydraulics (e.g. Lai, 1986; Manz, 1985). The actual forms of the equations vary with choice of the independent variables and the number and kind of terms added to account for flow complexity and conditions. The particular form of the St. Venant equations chosen for solution in terms of dependent variables, cross-sectional mean flow velocity, V, and depth of flow, y, are given below.

Continuity equation

$$\frac{A}{B}\cdot\frac{\partial V}{\partial x} + V\cdot\frac{\partial y}{\partial x} + \frac{\partial y}{\partial t} - \frac{q}{B} = 0 \qquad \text{...(2.1a)}$$

Momentum equation.

$$\frac{\partial V}{\partial t} + V\cdot\frac{\partial V}{\partial x} + g\cdot\frac{\partial y}{\partial x} + g\cdot(S_f - S_0) + q\cdot\frac{V}{A} = 0, \text{ in which} \qquad \text{...(2.1b)}$$

$$S_f = n^2\cdot V\cdot|V|\cdot\left[\frac{P^{4/3}}{A^{4/3}}\right]$$

and A, B, and P are the cross-sectional area, surface width, and wetted perimeter of flow, respectively; g is the gravitational acceleration; q is the lateral inflow per unit length per unit time; S_0 and S_f are the channel bottom and frictional slope, respectively; and n is Manning's resistance coefficient. The distance, x, in the longitudinal direction of the channel, and time, t, are the two independent variables.

These equations are only applicable to prismatic channels (ie. a channel with unvarying cross-section and constant bottom slope). It is assumed that the lateral inflow possesses no momentum in the direction of flow when entering the channel. Wind effects are neglected, and the channel bottom is rigid or relatively stable and fixed with respect to time.

2.1.2 FINITE DIFFERENCE APPROXIMATIONS SCHEME

The continuous x-t regions in which solutions of depth, y and velocity, V are sought is represented by a rectangular net of discrete points as shown in Figure 2.1. The computational algorithm for the chosen scheme is as follows (Manz, 1985):

Define any variable, α at point m by the relation:

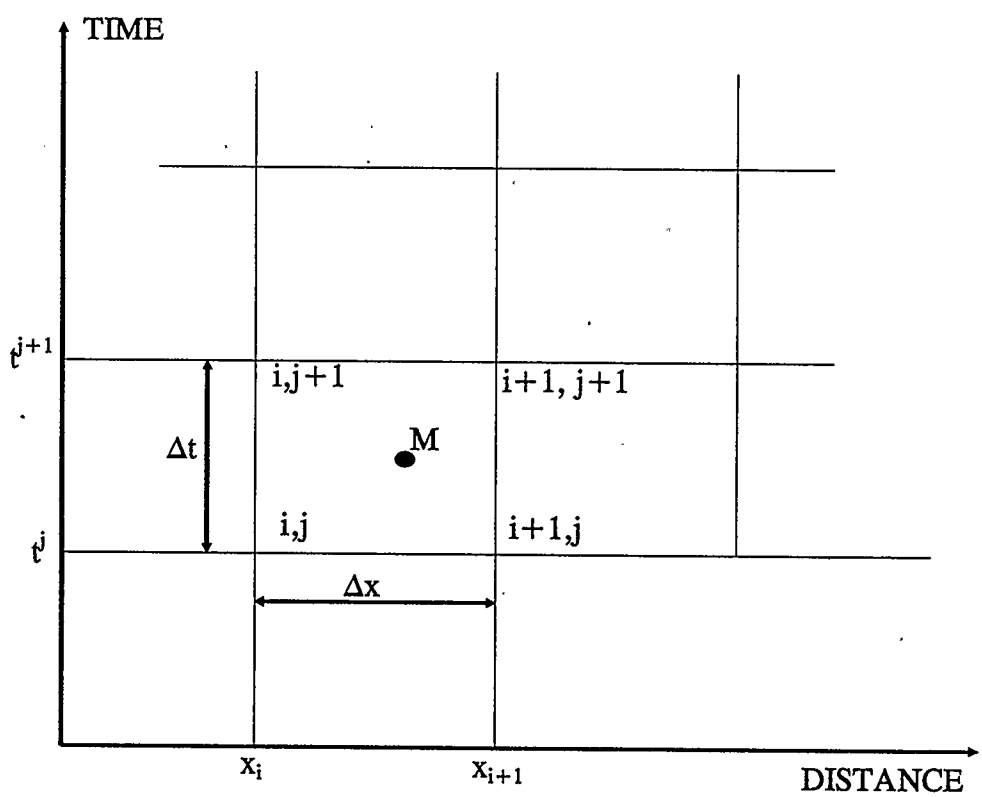

FIGURE 2.1
Distance-Time Grid for Finite Difference Solution

$$\alpha(m) = \frac{\theta}{2}\cdot\left[\alpha_{i+1}^{j+1}+\alpha_i^{j+1}\right] + \frac{(1-\theta)}{2}\cdot\left[\alpha_{i+1}^{j}+\alpha_i^{j}\right] \qquad \ldots(2.2)$$

Derivative of the variable, α with respect to time, t, at point M is given by the relation:

$$\frac{\partial\alpha(m)}{\partial t} = \frac{1}{2}\cdot\left[\frac{\alpha_{i+1}^{j+1}-\alpha_{i+1}^{j}}{\Delta t}\right] + \frac{1}{2}\cdot\left[\frac{\alpha_i^{j+1}-\alpha_i^{j}}{\Delta t}\right] \qquad \ldots(2.3)$$

Derivative of variable, α with respect to distance, x, at point M:

$$\frac{\partial\alpha(m)}{\partial x} = \theta\cdot\left[\frac{\alpha_{i+1}^{j+1}-\alpha_i^{j+1}}{\Delta x}\right] + (1-\theta)\cdot\left[\frac{\alpha_{i+1}^{j}-\alpha_i^{j}}{\Delta x}\right] \qquad \ldots(2.4)$$

where θ is the weighting function which varies as $0.5 \leq \theta \leq 1.0$.

By substituting the finite difference operators (Equations 2.2, 2.3, and 2.4) into Equations 2.1(a) and (b), the finite difference forms of the continuity and momentum equations may be derived. These may be written in the following form:

$$F_i\cdot\left(V_i^{j+1}, V_{i+1}^{j+1}, y_i^{j+1}, y_{i+1}^{j+1}\right) = 0 \qquad \ldots(2.5a)$$

$$G_i\cdot\left(V_i^{j+1}, V_{i+1}^{j+1}, y_i^{j+1}, y_{i+1}^{j+1}\right) = 0 \qquad \ldots(2.5b)$$

where F_i and G_i denote the finite difference form of the equations of continuity and momentum, respectively (see Appendix A for details). At any time, t^j, the channel is represented by N discrete points. There are (N - 1) points like M in the space-time grid between the time t^j and t^j+1. Therefore, equations 2.5(a) and (b) provide 2 (N-1) equations with i taking values 1, 2,....(N-1) containing N unknown depths y_i and N unknown velocities, V_i. Two additional equations are obtained by considering the boundary conditions at end of the channel:

$$G_0\cdot\left(y_1^{j+1}, V_i^{j+1}\right) = 0 \qquad \ldots(2.6a)$$

$$F_N\cdot\left(y_N^{j+1}, V_N^{j+1}\right) = 0 \qquad \ldots(2.6b)$$

where G_0 and F_N denote the functional relationship of the equations of momentum and continuity at upstream and downstream boundary, respectively (see Appendix A for details).

2.1.3 METHOD OF SOLUTION OF THE FINITE DIFFERENCE EQUATIONS

The non-linear partial differential equations (Equations 2.1(a) and (b)) have been replaced, using a weighted finite difference scheme, by a set of 2N non-linear simultaneous equations, Equations 2.5(a) and (b) and 2.6(a) and (b). The form of these equation is particularly suitable for the generalised iteration method of Newton. In this method the non-linear equations are reduced to a set of linear equations. Trial values are assigned to unknowns and substituted into the system of equations: the right hand side in general will not be zero but acquire values known as the residuals. Solutions are obtained by adjusting the values until each residual vanishes (zero) or is reduced to a tolerable limit, known as convergence criterion, ε. The set of simultaneous equations solved are assembled as follows:

$$G_0 \cdot \left[y_1^k , V_1^k \right] = r_1^k$$

$$F_1 \cdot \left[y_1^k , V_1^k , y_2^k , V_2^k \right] = r_2^k$$

$$G_1 \cdot \left[y_1^k , V_1^k , y_1^k , V_2^k \right] = r_3^k$$

$$\ldots \text{ etc. } \ldots$$

$$F_i \cdot \left[y_i^k , V_i^k , Y_{i+1}^k , V_{i+1}^k \right] = r_{2i}^k$$

$$G_i \cdot (y_i^k , V_i^k , y_{i+1}^k , V_{i+1}^k) = r_{2i+1}^k$$

$$\ldots \text{ etc. } \ldots$$

$$F_N \cdot \left[y_N^k , V_N^k \right] = r_{2N}^k$$

where superscript k denoting the values of unknown value computed until the kth iteration cycle; $r_i k$ ($i = 1,2,\ldots,2N$) are the residuals; and the subscript ($j + 1$) is omitted

as the values are determined at j + 1 term. The computation may be organized in a series of iteration steps and values of y_i and V_i for i = 1...N are obtained at j + 1 time when each residual r_i^k and (i=1,2,... 2N) equal to zero, or are equal or below prescribed convergence criterion value, ε. Details of the procedure are given in Appendix A

2.2 RESEARCH BACKGROUND

The various numerical techniques developed for the solution of the St. Venant equations can be categorized into the explicit finite difference scheme, implicit finite difference scheme, and method of characteristics: details may be found in the literature, (e.g. Gunaratnam and Perkins, 1970). The weighted four point implicit scheme belongs to the category of implicit finite difference schemes and is favoured because:

- the weighted four point implicit scheme (in general an implicit finite difference scheme) is not restricted to the small time intervals (Δt) that are imposed on the explicit and characteristic schemes for reasons of stringent stability conditions, i.e. Courant criteria and the friction;
- of the various implicit finite difference schemes, the "four point" implicit schemes appear most advantageous since they can be readily used with unequal distance interval (Δx); and
- of the various "four point" implicit schemes, the weighted four point implicit scheme provides the flexibility in weighting factor (θ) to control the stability-convergence properties (Fread, 1974).

The assessment of the weighted four point implicit scheme for unsteady flow simulation of open channel flow was conducted in two ways:

1. The assessment of the computational scheme to approximate by discrete finite difference steps the continuous differential equations (described in Section 2.1)

based on stability, and convergence or some kind of numerical accuracy of the scheme. Collectively, these assessments are called the numerical analysis of the solution scheme.

2. Once the properties in (1) are verified, a working numerical model is available for simulating the prototype systems. The second type of assessment was calibration of the model and verification of the model. Calibration infers the determination of the channel hydraulic control parameters in the model so that the prototype system for a range of flow condition is accurately replicated. Verification infers the evaluation of the mathematical relations used by the model to describe the relevant hydraulic processes (including methods used to manipulate and/or solve the equations). The calibration and verification assessments were based on accuracy criterion defined as the degree of difference between observed real-life data (such as measured hydrographs) and computed results.

2.2.1 ANALYSES OF WEIGHTED FOUR POINT IMPLICIT SCHEME

Numerous books and papers have been written on the numerical analysis of the weighted four point implicit scheme, and the computation properties were usually made based on computational stability and convergence or some kind of numerical accuracy. The stability and convergence were defined by computational errors, i.e. numerical error defined as round-off error and truncation error. If S (x, t), D (x, t), and N (x, t) represent, respectively, exact solution of the partial differential equation, exact solution of the finite difference equation, and numerical solution of partial difference equations at a fixed point (x, t) then $\delta = S - D$ is called truncation error while $\beta = D - N$ is numerical error.

The errors and/or growth or decay of these errors during the application of finite difference scheme were largely a function of three parameters: time increment, Δt, the

distance interval, Δx and the weighting parameter, θ. The computational aspects were investigated by various researchers and results are as follow:

2.2.1.1 Stability Analysis

A finite difference scheme is considered computationally stable if small truncation and round-off or numerical errors, introduced in the computation procedure, are not amplified into unlimited error. That is, $|\beta|$ remains small and bounded for all i ($i \cdot \Delta x = x$) as t increases ($t = j \cdot \Delta t$, Δt remaining fixed). Some investigators, for example Strelkoff (1970), Gunaratnam and Perkins (1970), Fread (1974), presented analytical stability analysis of the weighted four point implicit scheme, while others have demonstrated the stability of the weighted four point implicit scheme via numerical experiments, e.g., Gunaratnam and Perkins (1970), Chaudhry and Contractor (1973), Fread (1974). The commonly used analytical technique was by Fourier analysis of the error propagation properties of linearized forms of the partial differential equations, known as the Von Neumann Method (see for example, Fread, 1974). Note that the inability to include in the stability analysis the non-linearities of the partial differential equations, as well as the effects of boundary conditions, causes the Von Neumann techniques to be heuristic and somewhat inconclusive. Comments regarding stability criterion were:

1. The weighted four point implicit scheme formulation of gradually varied form of unsteady flow equations is unconditionally stable for any ratio of $\Delta t/\Delta x$ when the weighting factor is restricted to the range, $0.5 \leq \theta \leq 1.0$ (for example, Fread, 1974). However,

2. It is noted in numerical experiments that the weighted four point implicit scheme with θ values in the range of 0.5 did exhibit instabilities under condition of rapid transient flow (abrupt change in depth) and in cases when the time steps were quite large relative to wave period. The weighted four point implicit

scheme was found to become stable for such severe conditions if θ was increased such that θ approached 1. And,

3. The necessary condition for the weighted four point implicit scheme to become unconditionally stable for the severe condition in (2) with θ increasing from 0.5 to 1 is that the value of time interval, Δt, should be less than a maximum value Δt_0 (irrespective of the ratio $\Delta t/\Delta x$), however, the value of Δt_0 cannot be explicitly determined. For example, Gunaratnam and Perkins (1970) reported an approximate range of Δt for unconditional stability as:

$$\Delta t \ll \frac{V_0}{2 \cdot S_0 \cdot g} \qquad \text{...(2.8)}$$

where V_o is velocity about which the St. Venant equations are linearized. In this case V_o is the mean velocity of uniform flow of the channel, S_o is channel bottom slope, and g is gravitational acceleration.

4. It is noted in the numerical experiments for surge flow in open channels (rapidly varied unsteady flows), that the weighted four point implicit scheme was found to become stable with θ values in range, $0.6 \leq \theta \leq 1.0$ for low channel resistance and $0.5 < \theta < 0.6$ for high channel resistance (Chaudhry and Contractor, 1973).

2.2.1.2 <u>Convergence Analysis</u>

Convergence is the condition in which the solution of the finite difference equations approaches the analytical solution of the partial differential equation. That is, convergence is the condition where $|S-D| \rightarrow 0$ as $\Delta x, \Delta t \rightarrow 0$ and $i,j \rightarrow \infty$, with $i \cdot \Delta x = x$ and $j \cdot \Delta t = t$ remained fixed. Extensive analysis on convergence using an analytical approach and numerical experiments on the weighted four point implicit scheme have been made by Fread (1974). Additional information has been reported by Gunaratnam and Perkins

(1970), and others. The investigation of convergence of the weighted four point implicit scheme was performed as follows:

1. If the analytical solution of the partial differential equation is known, convergence was investigated quantitatively by determining the functional form of truncation error, i.e. determining the parameters of the finite difference equations that produced the best numerical accuracy ($\delta \rightarrow 0$).

2. Convergence criteria using truncation error may distort the computed transients via numerical dispersion and damping, which in combination are called numerical distortion. It is important to develop criteria which produce the least or most numerical distortion.

3. If the analytical solution of the partial differential equation is unknown, convergence is indicated by the extent to which the scheme conserves mass, known as mass conservation error (e.g. Fread, 1974).

The results from the various investigations are summarized:

- The weighted four point implicit scheme, for dominantly gradually varied forms of unsteady flow, is convergent or most numerically accurate at $\Delta x/\Delta t$ approximately equal to the kinematic wave speed (wave celerity in moving water), for $\theta=0.5$, that is,

$$\frac{\Delta x}{\Delta t} \approx \frac{3}{2} \cdot \frac{Q}{A} = C_m \qquad \text{...(2.9)}$$

  where C_m is the kinematic wave speed and Q and A is the rate and cross-sectional area of the flow, respectively, (Price, 1974)

- For rapidly varied forms, Cunge (1975) suggested that the Preismann (Sogreah) implicit scheme (this scheme uses the same finite difference operators (Equations 2.2, 2.3, 2.4) but different finite difference approxi-

mation technique from the one described in Section 2.1.2; for details see Cunge, 1975) is convergent or most numerically accurate at $\Delta x/\Delta t$ approximately equal to wave celerity of undisturbed flow or flow at rest) or

$$\frac{\Delta x}{\Delta t} \approx \sqrt{g \cdot \frac{A}{B}} = C \qquad \text{...(2.10)}$$

where C is the celerity of a wave in undisturbed water, A and B is the cross-section area and surface width of the flow and A/B is the hydraulic depth.

- Numerical distortion increases as θ departs from 0.5 and approaches 1.0. This effect on numerical distortion becomes more pronounced as the time interval increases and less significant with increasing number of distance intervals (i.e. by reducing Δx).
- Mass conservation error is a function of time interval and departure of θ from 0.5 (Fread, 1974).
- The weighted four point implicit scheme, when used to model rapidly varied unsteady flow, was observed to develop significant mass conservation error during initial stages (Gunaratnam and Parkins, 1970).

2.2.1.3 Relationships Between Convergence And Stability.

As can be discerned from investigations described in the previous sections, stable solutions are not necessarily convergent while convergent solutions are always stable. Thus convergence as measured by truncation errors is a more important criterion under conditions when the stability condition is satisfied. Therefore the values of Δt, Δx, and θ in the finite difference approximation are subjected to limitations imposed by convergence considerations and should result in stable numerical solutions. In other words, the weighted four point implicit scheme with $0.5 \leq \theta \leq 1.0$ is unconditionally linearly stable

if the computational time and distance steps are selected to achieve a reasonable degree of convergence.

2.2.2 CALIBRATION AND VERIFICATION

Once the mathematical model has been constructed, the stability and convergence of the calculation scheme must be assessed and the time interval, Δt, distance interval, Δx, and weighting factor θ must be chosen so that the computation is stable and convergent. When this has been completed, a working model is available; however, the depth and velocity or discharge of flow are not necessarily the same as in the prototype and the model must be calibrated and verified. Verification infers evaluation of the mathematical relationships used by the model to describe relevant hydraulic processes (including methods used to manipulate and/or solve the equations) by comparing model results to those obtained from adequately controlled experimental programs. If the mathematical relations used by the model have been verified, calibration of the model is possible. Calibration is the reverse of the verification process. In calibration, control parameters are determined by repeated comparison of model output to observed field conditions, perhaps using some form of the optimization technique. Criteria used to access model verification and calibration may have a similar form; however, that used for model verification is more stringent. At the time of writing, literature describing the experimental verification of the weighted four point implicit technique could be not be found presumably because of the significant expense associated with conducting the experiments. However, verification of the model has been made using data collected as part of field experimental programs, Amein and Chu (1975), Balzter and Lai (1968), Amein and Fang (1970), and others. The numerical models using the weighted four point implicit scheme differ by the modifications made to the basic numerical scheme to simulate the different channel conditions. It was noted that in all cases the time and distance increments used in the computations were limited by the manner in which the data were collected and not by

pre-established convergence criteria. For example, if the measured data was recorded at 6 hour intervals, a time step of 6 hours was used in computation. The distance steps were determined using criteria similar to that associated with routine backwater computational procedures. In most cases the weighting factor, θ, was set equal to 1 to ensure numerical stability.

Results of the calibration of a model to a specific prototype channel cannot be used for other prototype systems without exercising caution. In most cases calibration involves a trial and error technique to permit determination of channel hydraulic control parameters (e.g. resistance coefficient). In some instances an optimization technique is used to reduce the cost and time of the trial and error procedure, (Fread and Smith (1978) report an optimization technique to determine resistance coefficient). The most important channel hydraulic control parameters were found to be channel bottom slope, cross-sectional geometry and resistance coefficient. Variation of these parameters has the following effects:

1. Errors in channel bottom slope result in errors in computed discharge. Positive (negative) errors in channel slope result in the increase (decrease) in the discharge at the downstream end of the channel.

2. Errors in channel geometry have the effect of altering the predicted characteristics of the flow.

3. Errors in estimation of the resistance coefficient (never directly measured) may be very significant. Estimates which are too large result in underestimation of predicted flow rate and overestimation of predicted depth. Estimates which are too low result in overestimation of predicted flow rates and underestimation of predicted depth. Errors in these hydraulic control parameters may occur singularly or in combination with each other. Other parameters which consider

lateral in or out flows or the effect of wind may also need to be considered when their effects are expected to be significant.

2.3 DESCRIPTION OF RESEARCH PROGRAM

The research program consists of a sensitivity analysis of the parameters affecting the unsteady flow computation performed using the weighted four point implicit scheme, demonstration of the numerical model verification process, and an investigation of numerical model calibration procedures. All components of the research program were performed on a prismatic channel of rectangular cross-section. The geometry of the channel and the hydraulic data used as the basis for the verification and point of departure for sensitivity analysis and investigation of calibration procedures were taken from Treske (1980). A brief description of the experimental procedures used by Treske and some of the experimental results used are given in Appendix C.

The sensitivity analysis of the parameters affecting the unsteady flow computation was performed by verifying time interval, distance interval, weighting factor and convergence criteria parameters. The analysis was performed on hypothetical abrupt increases and decreases in inflow to the channel.

The verification was performed by simulating the channel used by Treske to obtain his experimental observations and comparing the simulated results to Treske's measurements. The investigation of numerical model calibration procedure was performed by examining the effect on model output of variations in control channel hydraulic parameters, including flow resistance, channel bottom slope and channel geometry. Calibration optimization procedures were also demonstrated.

CHAPTER 3: SENSITIVITY ANALYSIS

3.1 GENERAL DESCRIPTION

For any open channel the precision of unsteady flow calculations is largely a function of the time interval, Δt, the distance interval, Δx, the weighting factor, θ, and the convergence criterion parameter ε in the Newton Iteration method.

The convergence and stability may be significantly affected by choosing different values of these parameters. Cungè (1975) has suggested that a suitable measure of the finite difference approximation for rapidly varied unsteady flows or surge flows is given by $\Delta x/\Delta t \approx C$, (where C is the celerity of wave in undisturbed water$=\sqrt{g\cdot(A/B)}$) with $\theta > 0.6$ so that the stability of the computations is never endangered. Thus the first series of numerical experiments consisted of varying the ratio of $\Delta x/\Delta t$ and the abrupt change in discharge $Q=Q(t)$ at the upstream boundary. Another series of numerical experiments was performed to examine the influence of θ and ε.

Numerical experiments were conducted using Treske's channel (see Appendix C). The numerical computations were conducted, using the Irrigation Conveyance System Simulation (ICSS) Model described in Appendix D.

3.2 CONVERGENCE ANALYSIS

Convergence analysis attempts to consider the significance of the difference between the exact solution of the partial differential equations and the numerical solution. Frequently, however, the exact solution is unknown. Consequently, indirect means must be taken. Gunaratnam and Perkins (1970) suggested that the ability of the computations to preserve flow volume balance or conservation of mass at any time may be used as a

convergence indicator. The error of flow volume at any time, t, can be determined using the following equation:

$$E = \frac{(S_t - S_0) - \int_0^t (Q_1 - Q_2)\cdot dt}{\int_0^t Q_1 \cdot dt} \times 100\% \qquad \ldots(3.1)$$

in which S_0 and S_t are the storage in the reach of the channel at t=0 and t=t respectively and Q_1 and Q_2 are the inflow and outflow to/from the reach.

3.3 STUDY CHANNEL

A 210 m long section of the Treske channel is used in this study. A summary of the open-channel hydraulic parameters is described in Table 3.1. For the model application, the upstream condition is discharge as a function of time, Q(t), while the downstream condition is controlled by a rating curve (depth-discharge relationship) established from measured data (Appendix C, Table C.2) as:

$$y(n) = 1.344 \cdot Q(n) + 0.08565 \qquad \ldots(3.2)$$

where y(n) and Q(n) are depth and discharge measured in m and m^3/s, respectively. The lateral flow is zero and the initial condition to be simulated by the steady flow simulation capability of the ICSS Model (Manz, 1985) is provided by specifications of the depth Y_0 and discharge (Q_0) at the downstream boundary, see Table 3.1.

Table 3.1
Data Summary of Channel Conditions in Sensitivity Analysis

Reach length, L	210 m
Channel bottom width, b	1.25 m
Channel bed slope, S_o	0.00019
Channel resistance, n	0.0120
Initial uniform flow rate, Q_0	0.103 m^3/s
Initial uniform flow depth, Y_0	0.225 m

3.4 NUMERICAL EXPERIMENTS

To evaluate the relative significance of these parameters on the quality of the numerical solutions, a series of simple numerical experiments were performed as follows:

3.4.1 VARIATION IN THE TIME INTERVAL AND DISTANCE INCREMENT

This series of experiments consisted of varying the ratios of $\Delta x/\Delta t$ and the flows at the inlet of the channel. The other channel conditions remained constant as described in Section 3.3 with the weighting coefficient of the finite difference scheme maintained at a constant value $\theta=0.6$ as suggested by Chaudhry and Contractor (1973) and convergence criterion of the Newton's Iteration set equal to $\varepsilon=0.0001$, a value assumed to be sufficiently small.

Table 3.2
Data Summary Of Selected $\Delta x/\Delta t$ Ratios

Δx_c(m)	10	42	105
Δt_c(s)	7	28	70

3.4.1.1 Abrupt Increase in Flow

The flow at the inlet was instantaneously increased from 0.103 m^3/s to three different flow rates viz., to 0.186 m^3/s ($\approx 2\times 0.103$); to 0.387 m^3/s ($\approx 4\times 0.103$); to 0.618 m^3/s (6×0.103). Note the values of Q=0.198 and 0.387 m^3/s are the maximum discharges measured in Treske's experiment for the most rapid flow form of experiment conducted (see Appendix C and Treske, 1980). Since the celerity computed with the formulas $\sqrt{g\cdot A/B}$ is of the order of 1.485 m/s (i.e. $1{,}485=\sqrt{9.81\times 0.225}$, where $A/B=0.225$) three pairs of values ($\Delta x_c,\Delta t_c$) were selected, such that $\Delta x_c/\Delta t_c \approx 1.485$ for all of them (Table 3.2). The experiments were conducted as follows:

TEST 1

In this series of experiments the distance increment was held constant at 10 m and the time interval, Δt, was varied from 7 seconds to the point where significant instability occurred in multiplier of Δt_c. Figures 3.1, 3.2 and 3.3 show the results of computed discharge hydrographs at the downstream end with the corresponding computed mass conservation error E in Figures 3.4, 3.5 and 3.6 for three different times of instantaneous inlet flows Q=0.186 m^3/s, 0.387 m^3/s and 0.618 m^3/s respectively. It will be noted that as Δt increases, the curves tend to flatten and displace forward in time (Figures 3.1 to

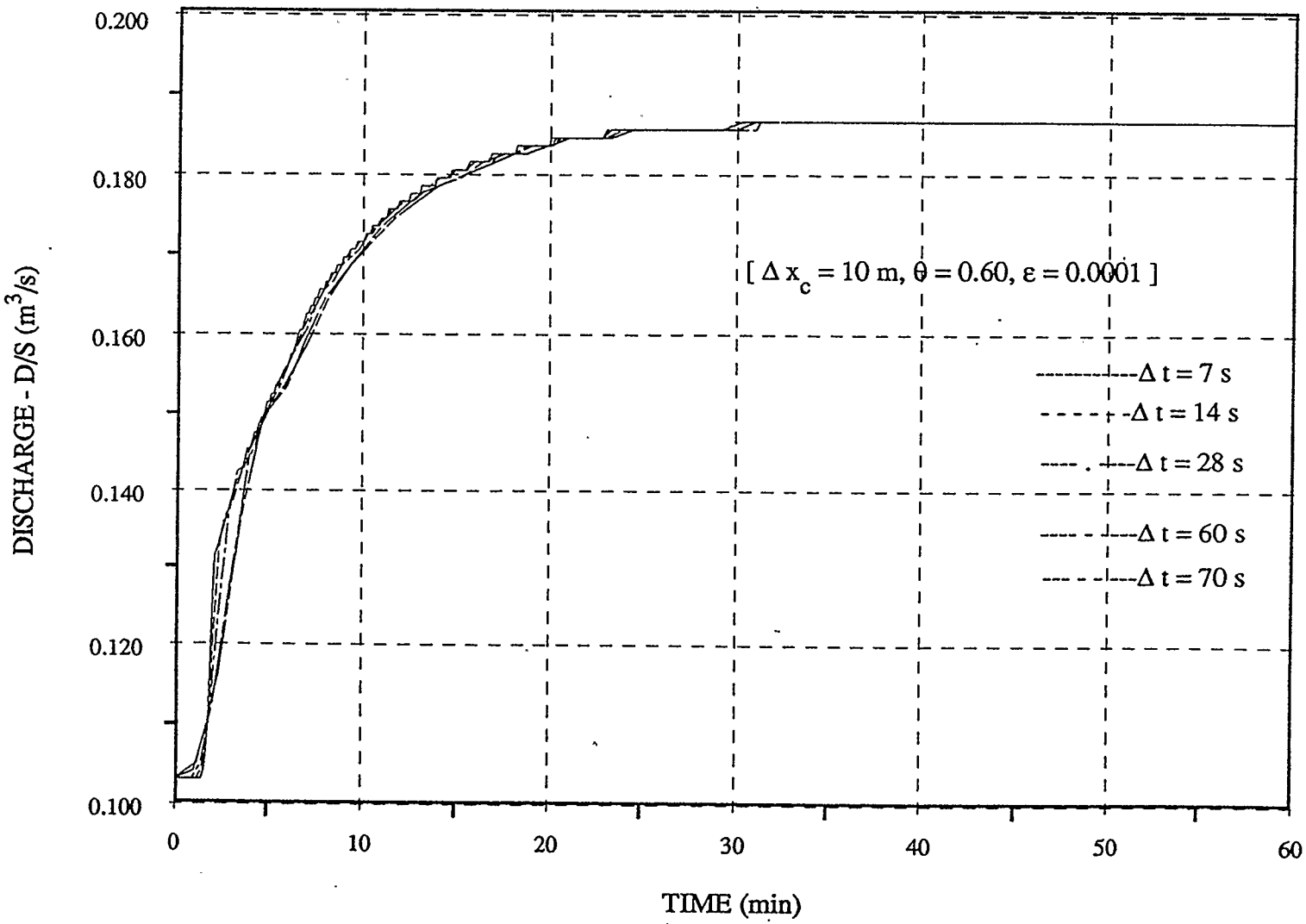

Figure 3.1 (a)

Comparisons of computed discharge hydrographs at the downstream boundary (D/S) for various values of time interval, Δt, for the abrupt increase in inlet flow from 0.103 to 0.186 m^3/s

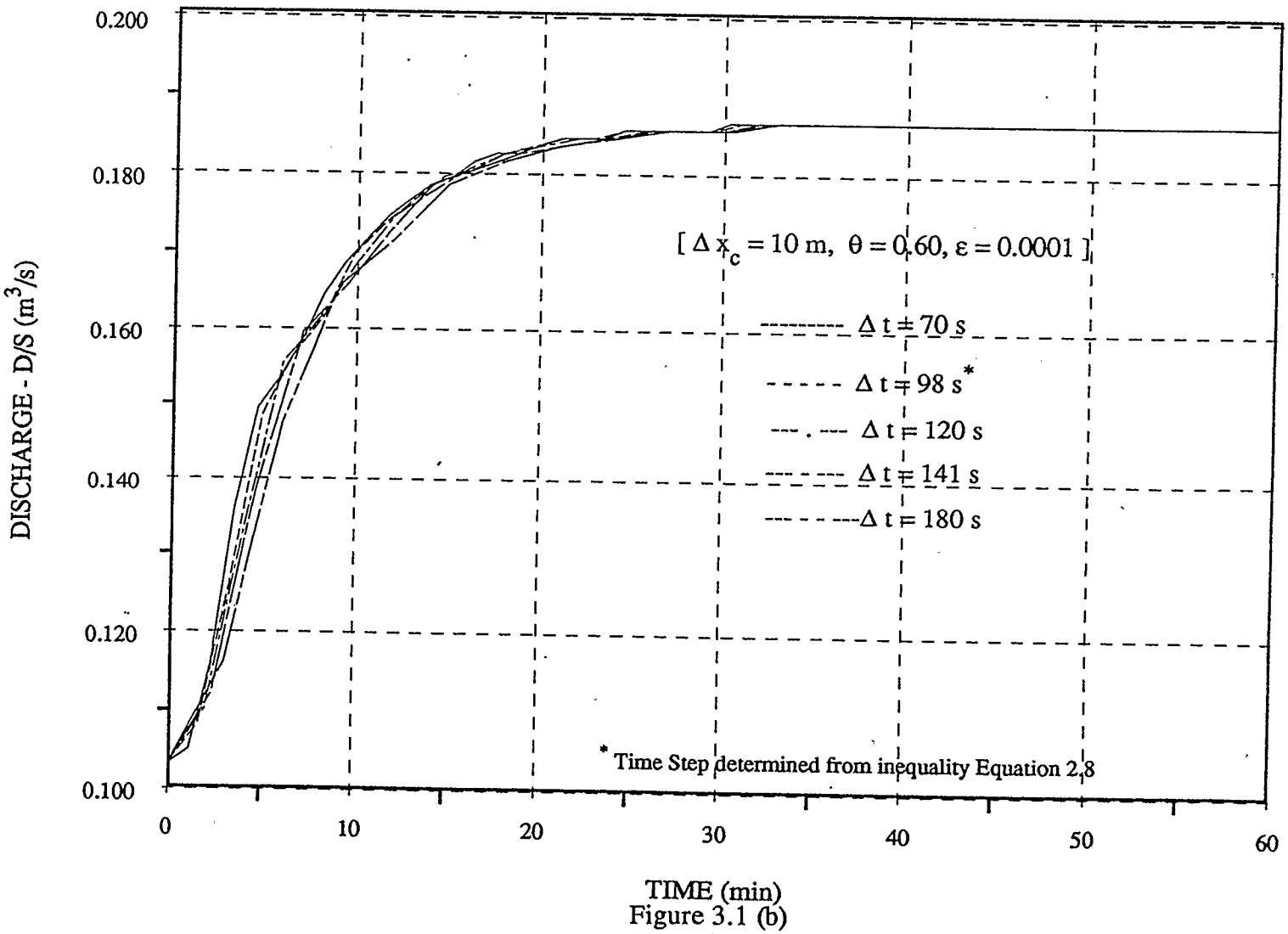

Figure 3.1 (b)

Comparisons of computed discharge hydrographs at the downstream boundary (D/S) for various values of time interval, Δt, for the abrupt increase in inlet flow from 0.103 to 0.186 m^3/s

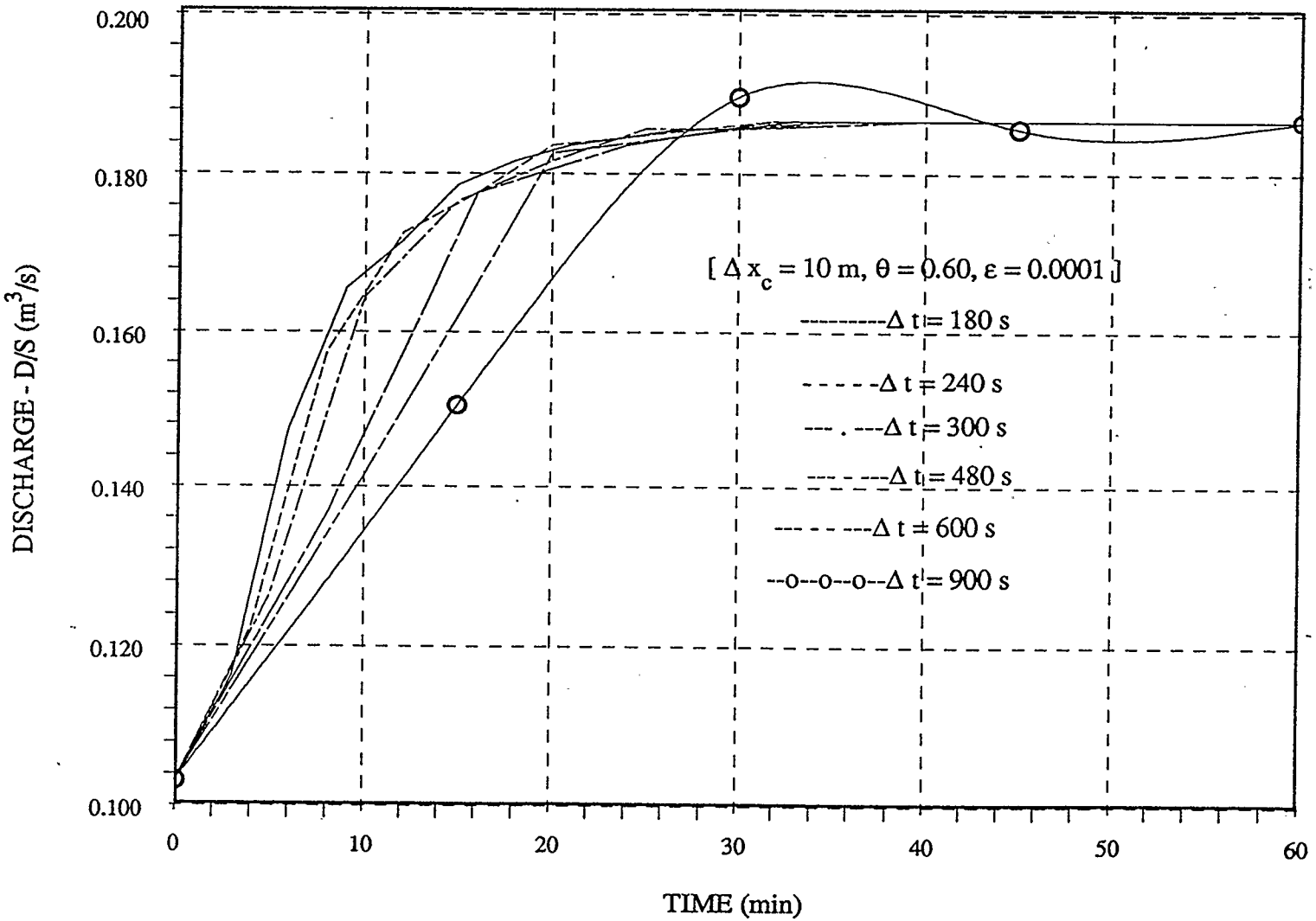

Figure 3.1 (c)

Comparisons of computed discharge hydrographs at the downstream boundary (D/S) for various values of time interval, Δt, for the abrupt increase in inlet flow from 0.103 to 0.186 m^3/s

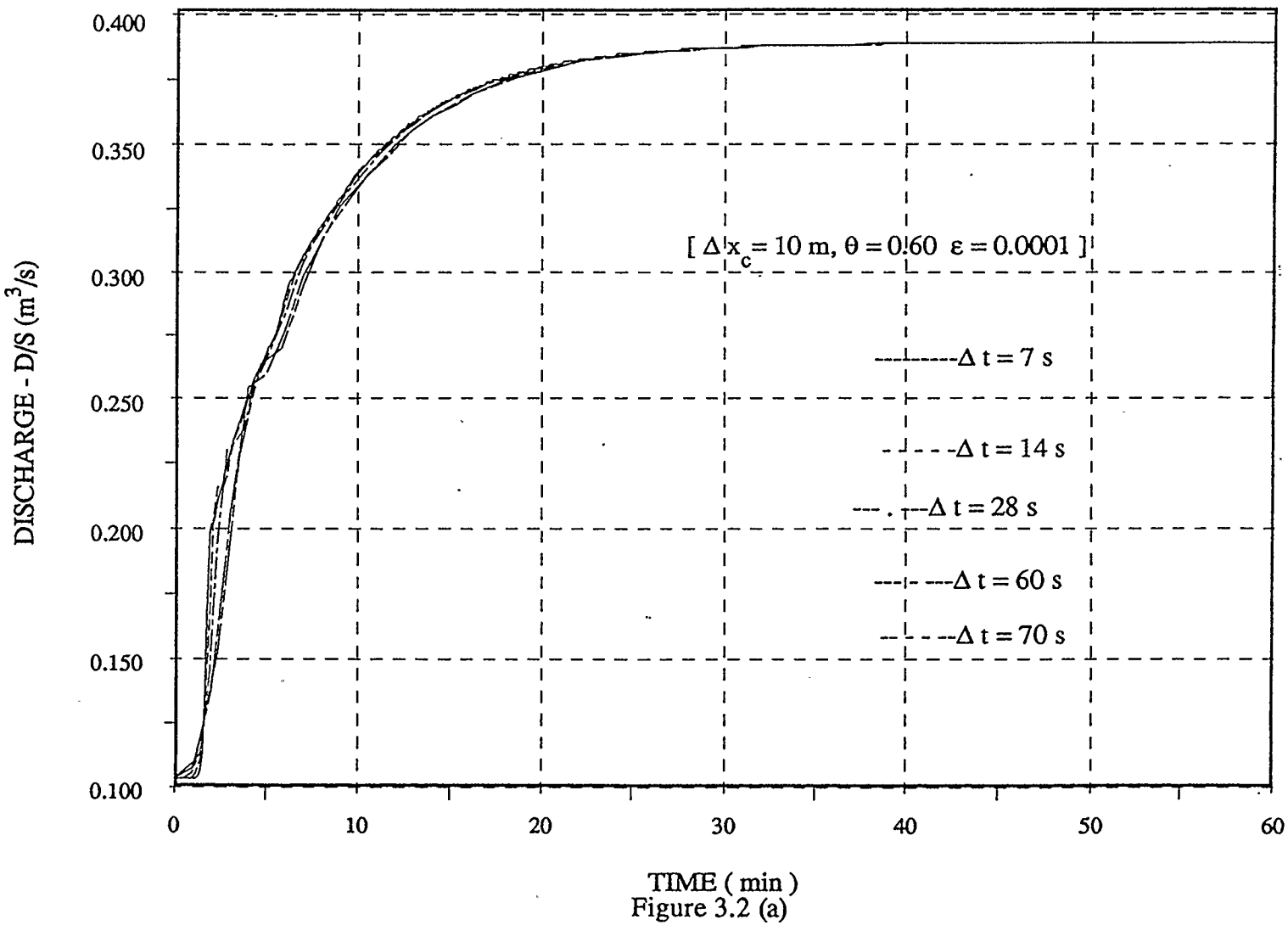

Figure 3.2 (a)

Comparisons of computed discharge hydrographs at the downstream boundary (D/S) for various values of time interval, Δt, for the abrupt increase in inlet flow from 0.103 to 0.387 m^3/s

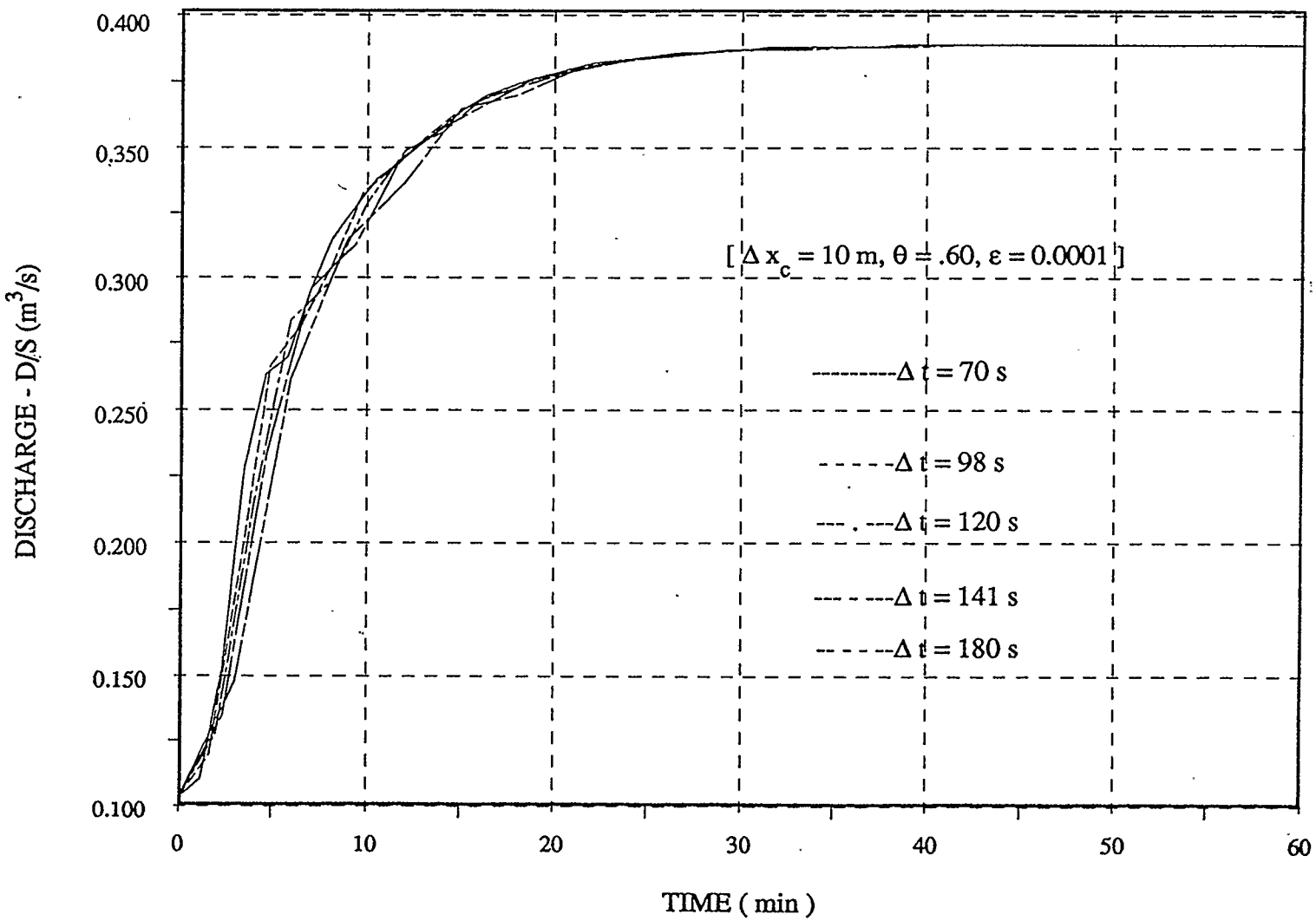

Figure 3.2 (b)

Comparisons of computed discharge hydrographs at the downstream boundary (D/S) for various values of time interval, Δt, for the abrupt increase in inlet flow from 0.103 to 0.387 m^3/s

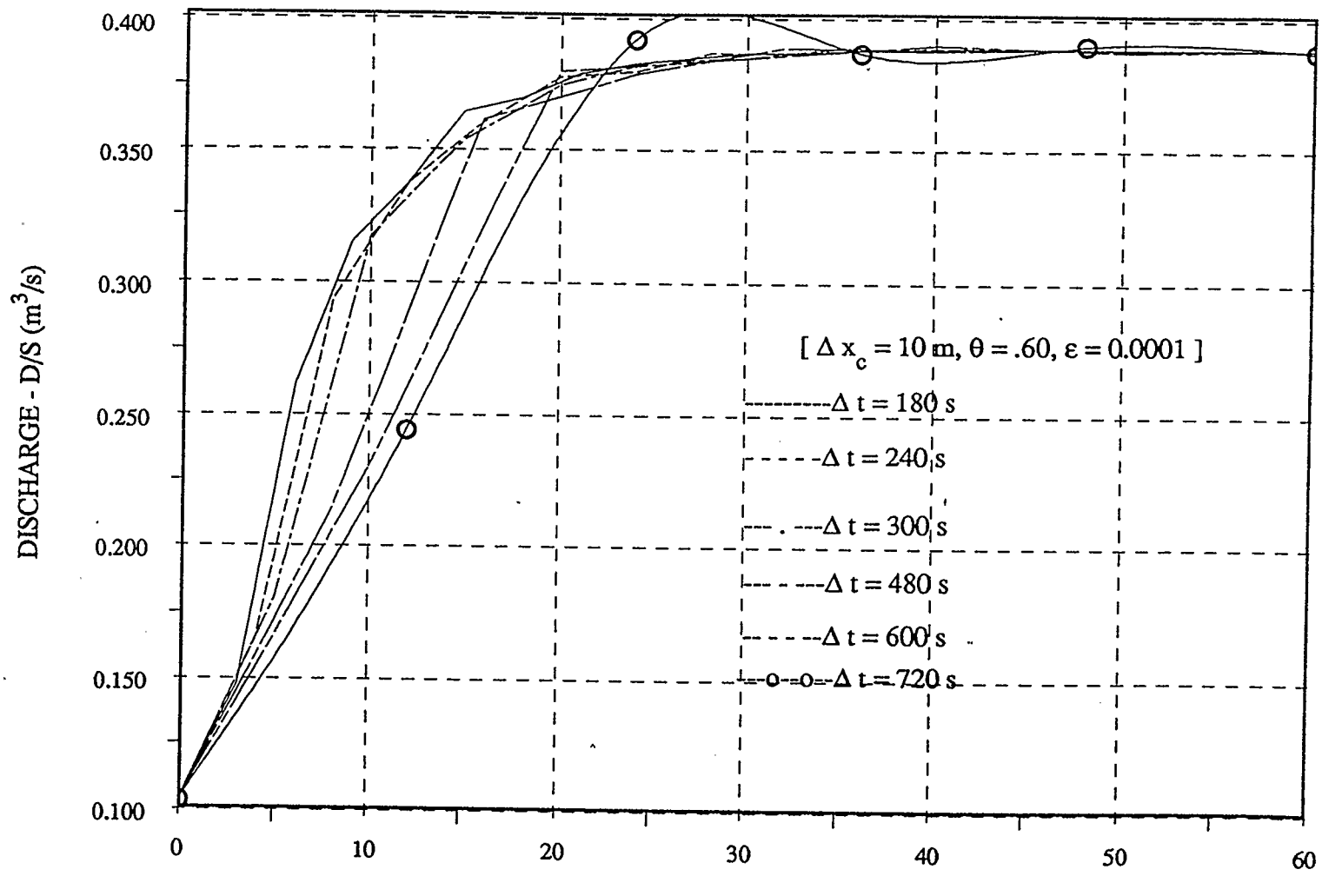

Figure 3.2 (c)

Comparisons of computed discharge hydrographs at the downstream boundary (D/S) for various values of time interval, Δt, for the abrupt increase in inlet flow from 0.103 to 0.387 m^3/s

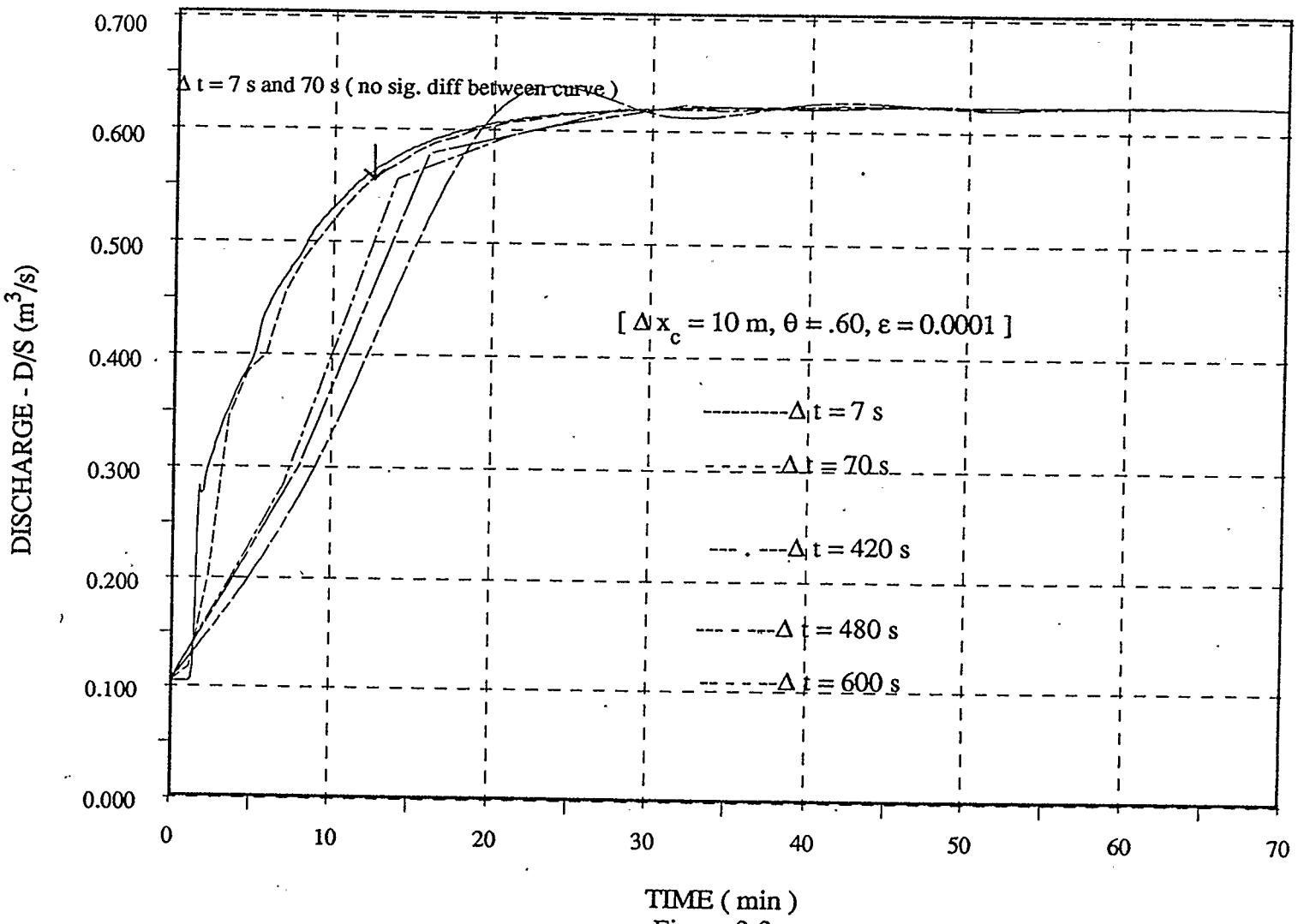

Figure 3.3

Comparisons of computed discharge hydrographs at the downstream boundary (D/S) for various values of time interval, Δt, for the abrupt increase in inlet flow from 0.103 to 0.618 m^3/s

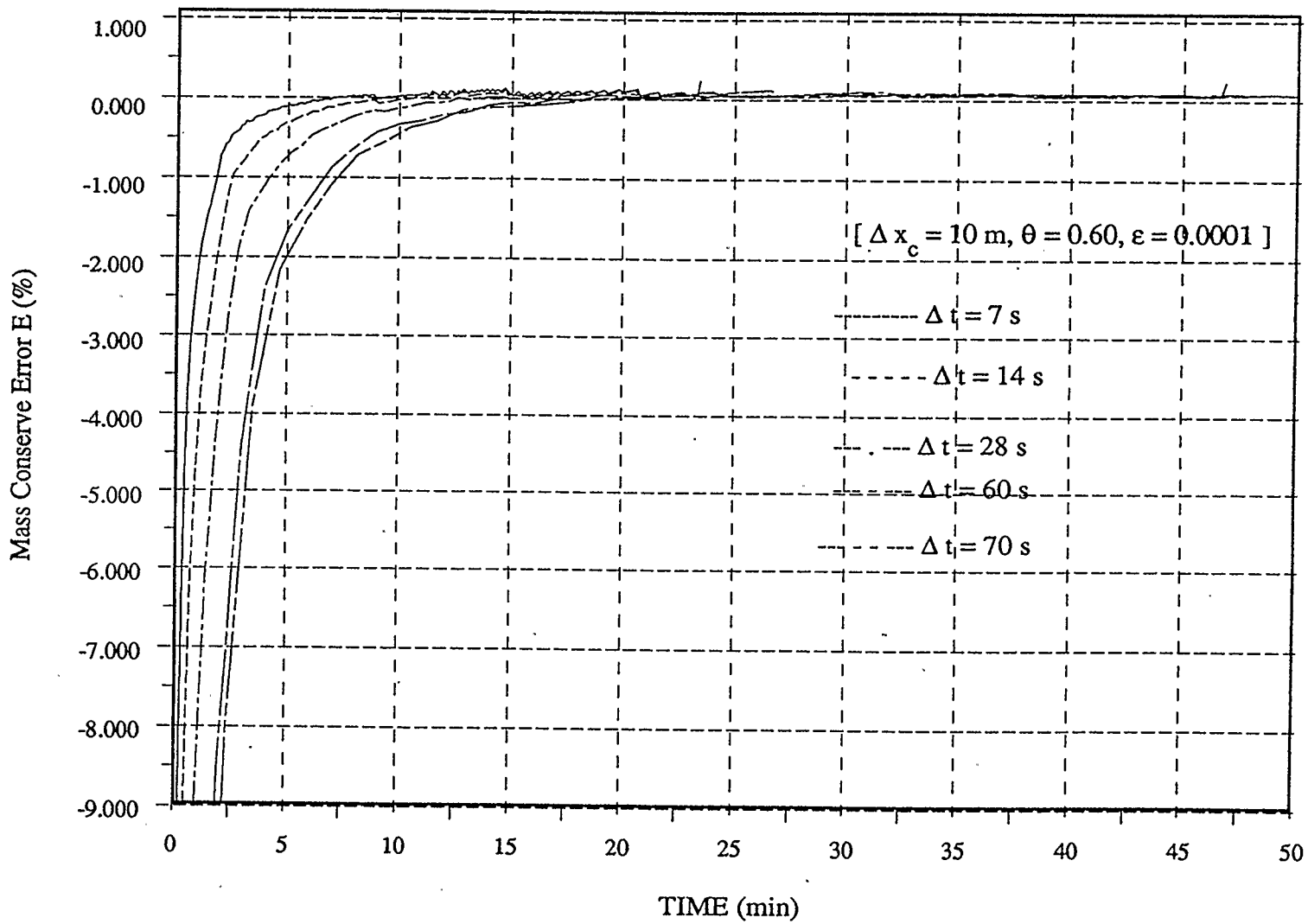

Figure 3.4 (a)

Comparisons of computed Mass Conservation Error (E %) for various values of time iinterval Δt, for the abrupt increase in inlet flow from 0.103 to 0.186 m^3/s

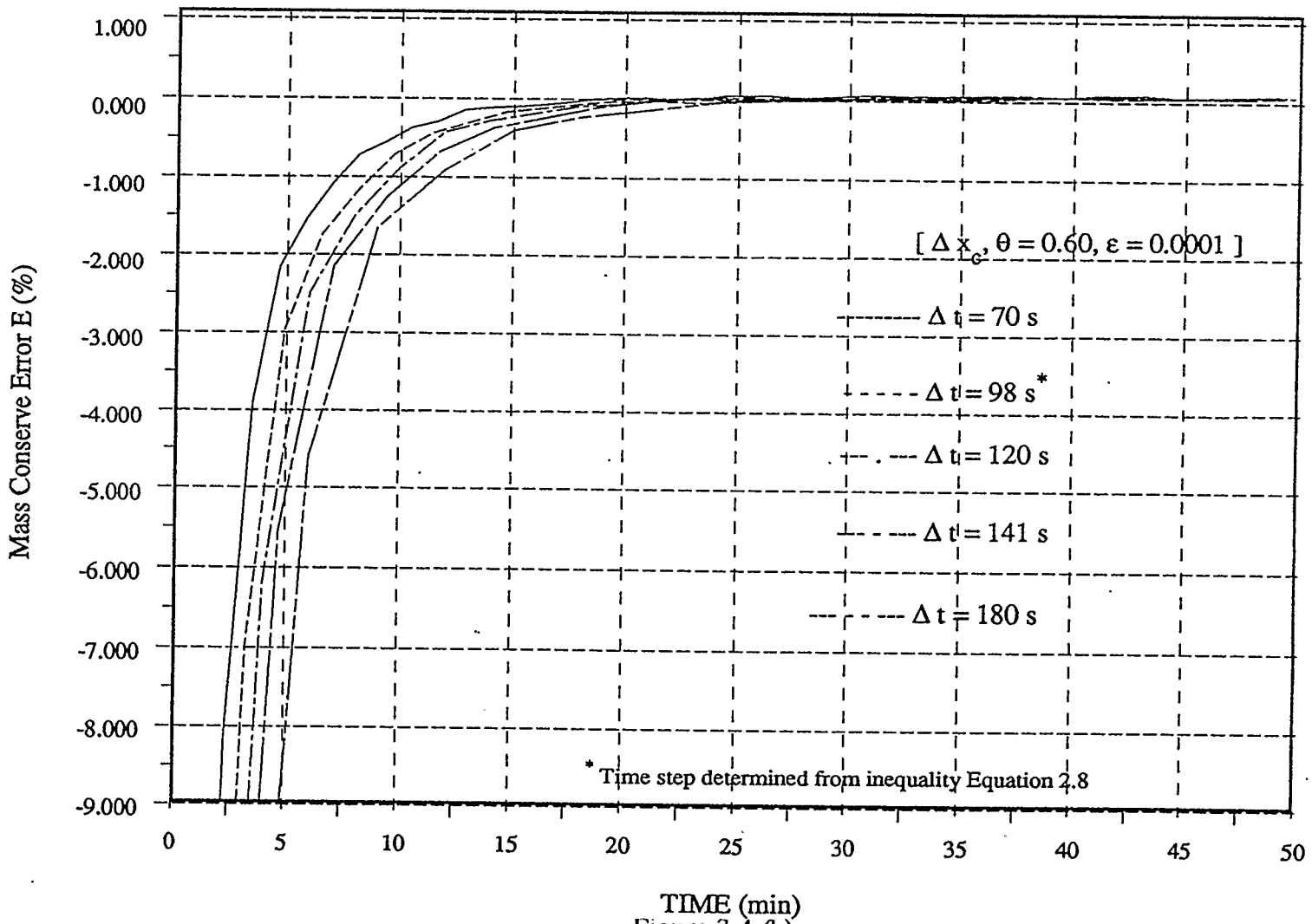

Figure 3.4 (b)

Comparisons of computed Mass Conservation Error (E %) for various values of time iinterval Δt, for the abrupt increase in inlet flow from 0.103 to 0.186 m^3/s

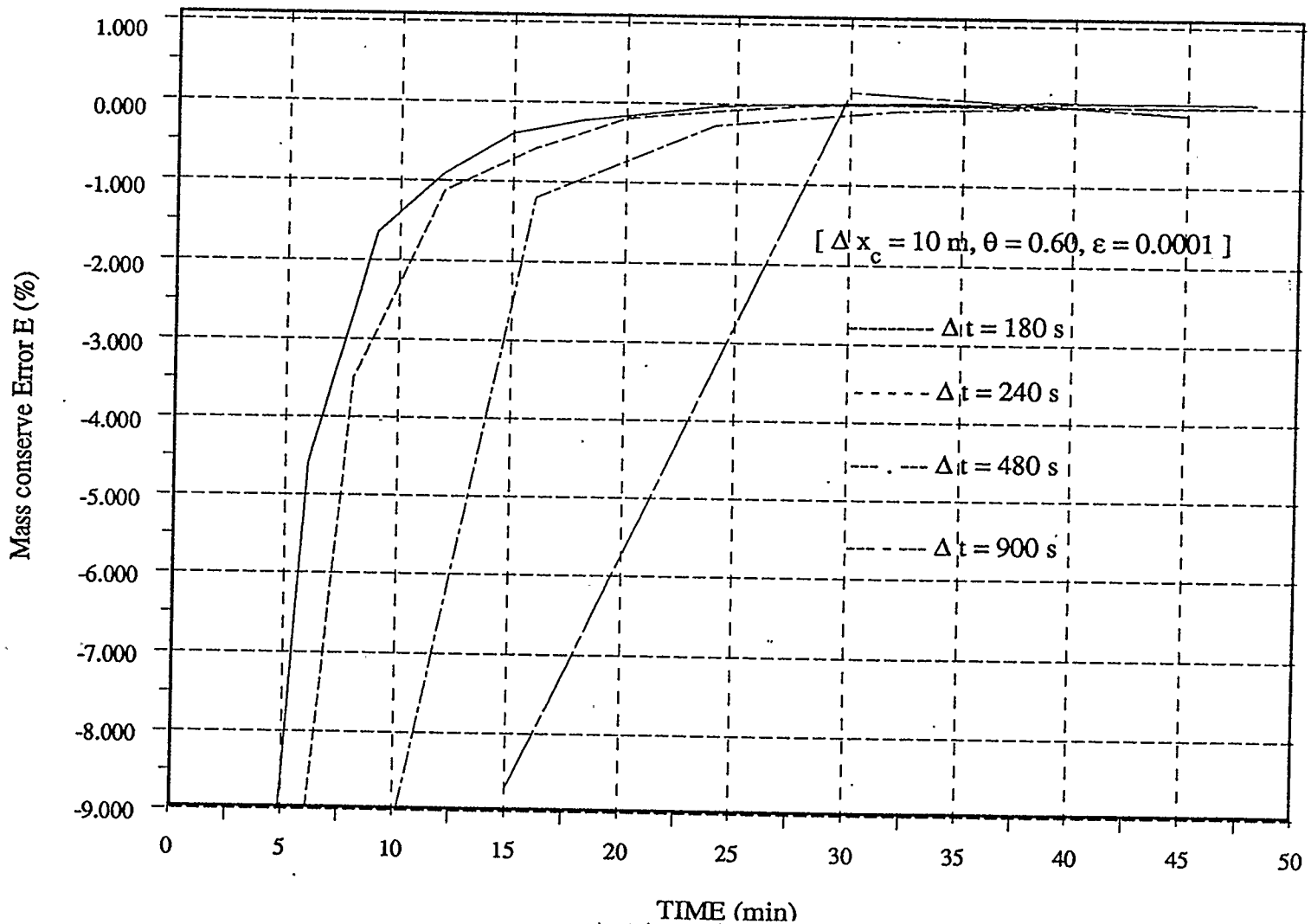

Figure 3.4 (c)

Comparisons of computed Mass Conservation Error (E %) for various values of time iinterval Δt, for the abrupt increase in inlet flow from 0.103 to 0.186 m^3/s

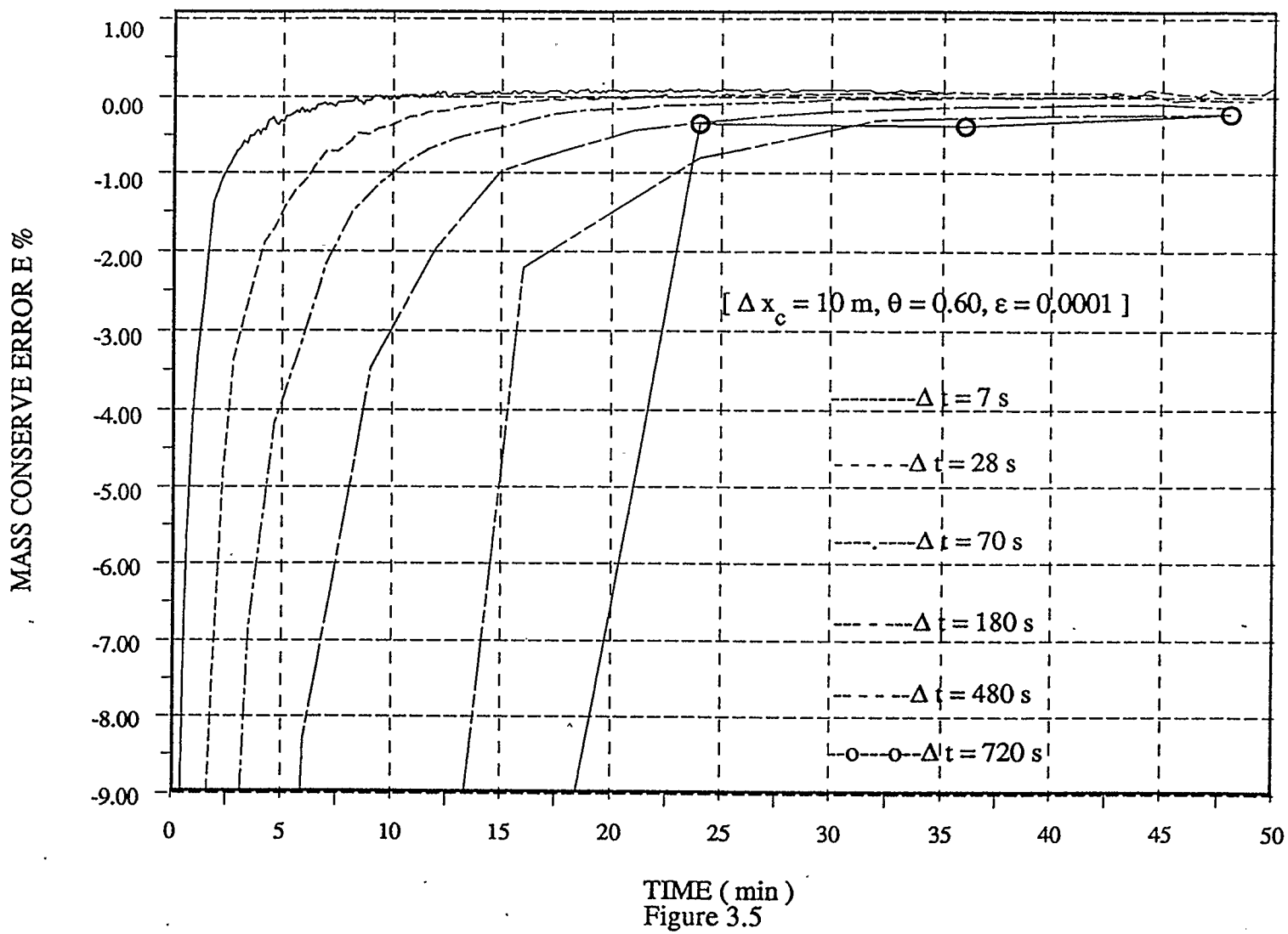

Figure 3.5

Comparisons of computed Mass Conservation Error (E %) for various values of time iinterval Δt, for the abrupt increase in inlet flow from 0.103 to 0.387 m^3/s

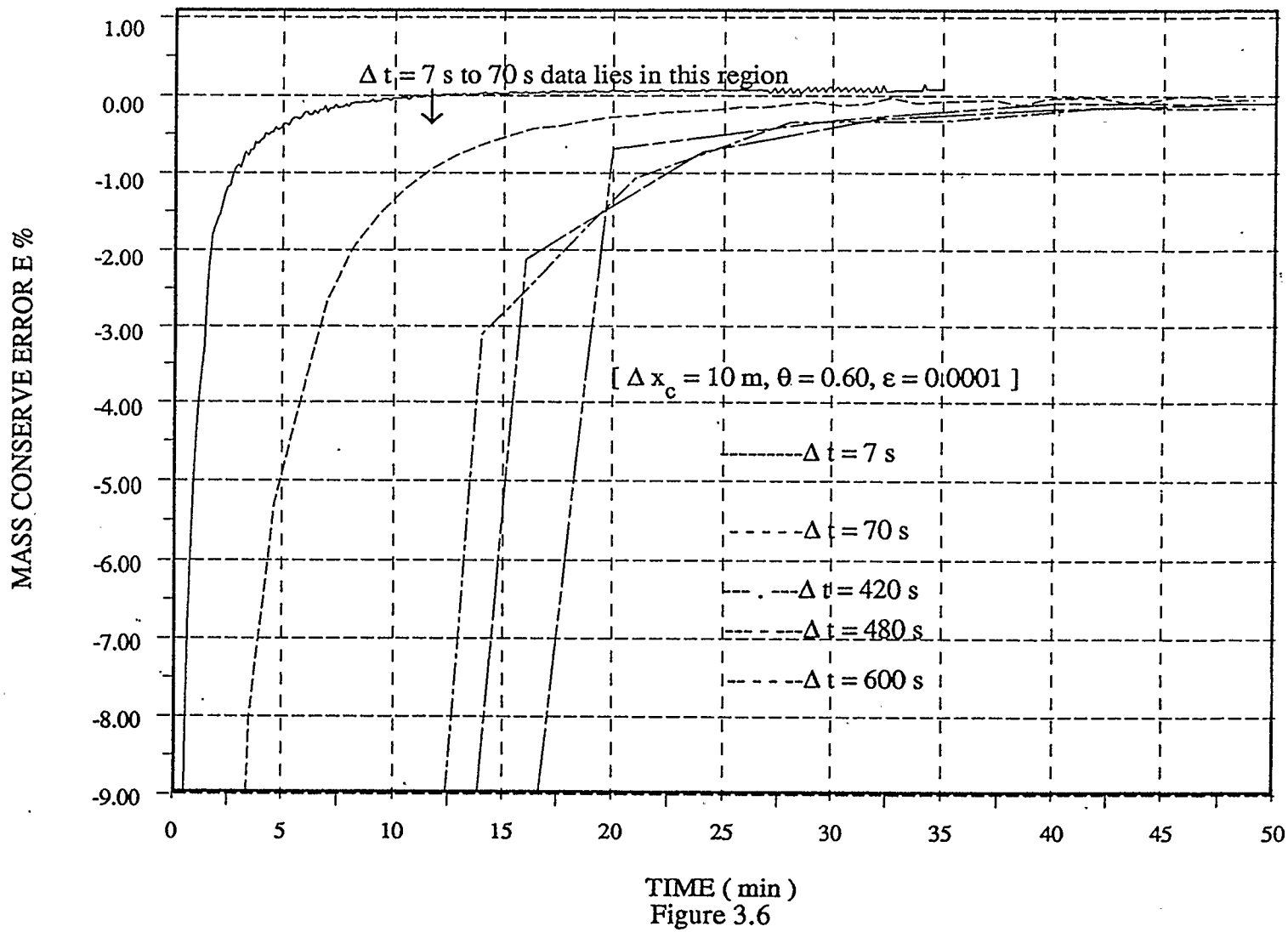

Figure 3.6

Comparisons of computed Mass Conservation Error (E %) for various values of time iinterval Δt, for the abrupt increase in inlet flow from 0.103 to 0.618 m^3/s

3.3). It was further noted that mass was not conserved and rapid loss was observed in the rapidly varied unsteady region, that is, before the time at which the downstream discharge was equal to the upstream inlet flow (Figures 3.4 to 3.6). The maximum Δt for stability decreased as the instantaneous upstream inlet rate increased. Figure 3.1(c) shows maximum Δt=900s for Q=0.106 m^3/s, for Q=0.387 m^3/s, maximum Δt=720s (Figure 3.2(c)) while for Q=0.618 m^3/s, maximum Δt=600s (Figure 3.3). However, it was noted that as Δt increased, the mass conservation errors increased (Figures 3.4 to 3.6). These results demonstrate that convergence considerations are more important than stability considerations. The computations satisfactorily converge for $\Delta t \approx 70s$ $(\Delta t/\Delta t_c \approx 10)$, whereas stable solutions may be obtained for much larger time increments.

TEST 2

In test 2, the time interval was set at Δt_c=7s, and the distance increment was varied. The flow at the channel inlet was abruptly increased from 0.103 to 0.387 m^3/s. The resulting discharge hydrographs are shown in Figures 3.7(a) and (b). The test using Δx=21m (i.e. $\Delta t/\Delta x \cdot C$=0.5) and for Δx=42m, 70m, 105m (i.e. $(\Delta t/\Delta x \cdot C)$ approaches 0) produced meaningless results, i.e. some numerical instabilities are exhibited (indicated by waves developed behind the main surge). When Δx was reduced to 5m, (i.e. $\Delta t/\Delta x \cdot C > 1$) sensible results were obtained. The resulting discharge hydrograph was approximately the same as when Δx_c=10m. No waves were observed behind the main surge (i.e. no numerical instabilities). The corresponding mass conservation error versus distance increment is shown in Figure 3.7(c). Note the similarities between the curves.

TEST 3

These numerical experiments were carried out to compare the value of $\Delta t/\Delta x \cdot C=1$ and the values of $\Delta t/\Delta x \cdot C > 1$ for each of ratios $\Delta t_c/\Delta x_c$, (recall C=1.485

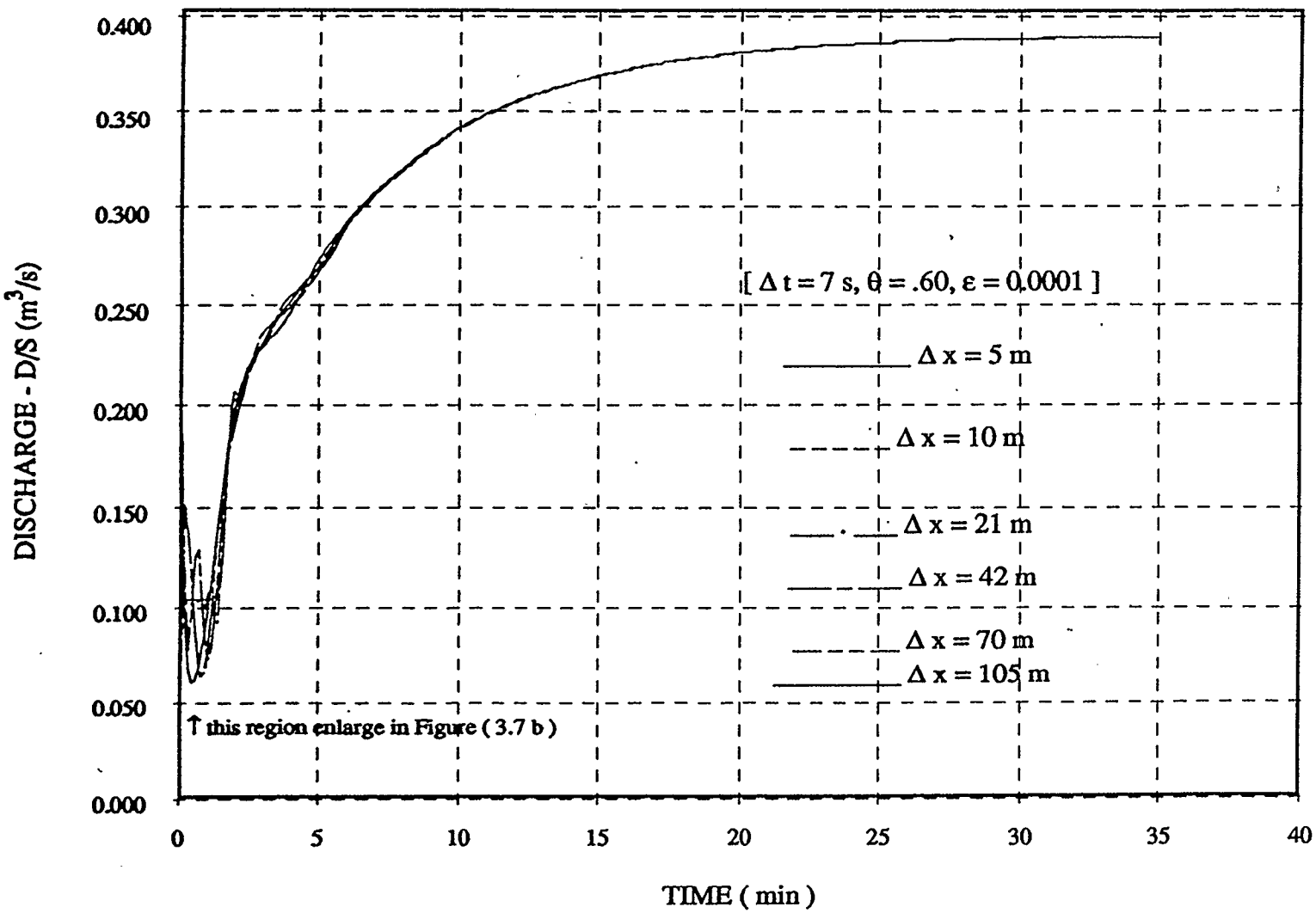

Figure 3.7 (a)

Comparisons of computed discharge hydrographs at downstream for various values of time iinterval Δt, for the abrupt increase in inlet flow from 0.103 to 0.387 m^3/s

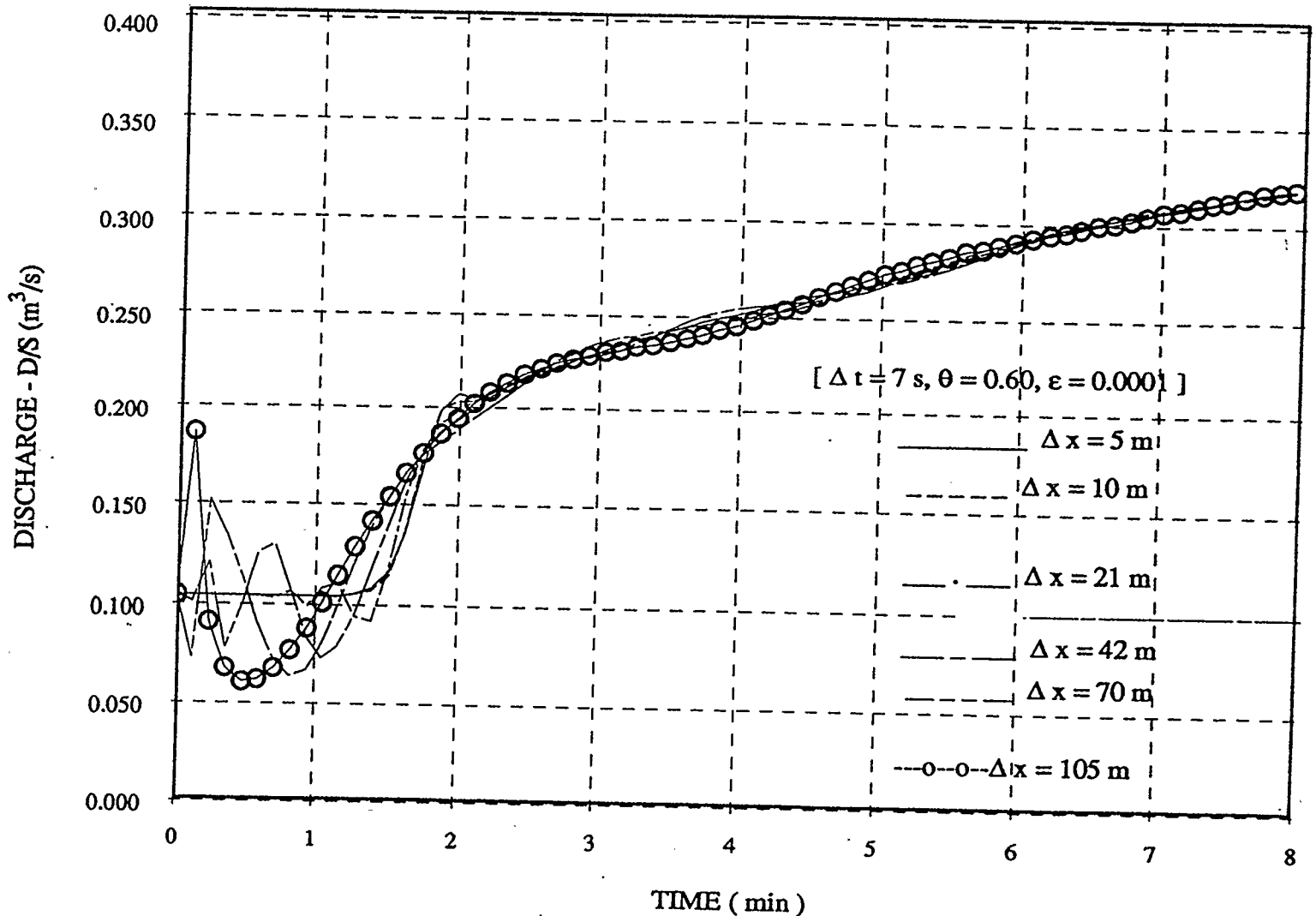

Figure 3.7 (b)

Enlargement of the initial part of Figure 3.7 (a) showing instabilities behind the main surge

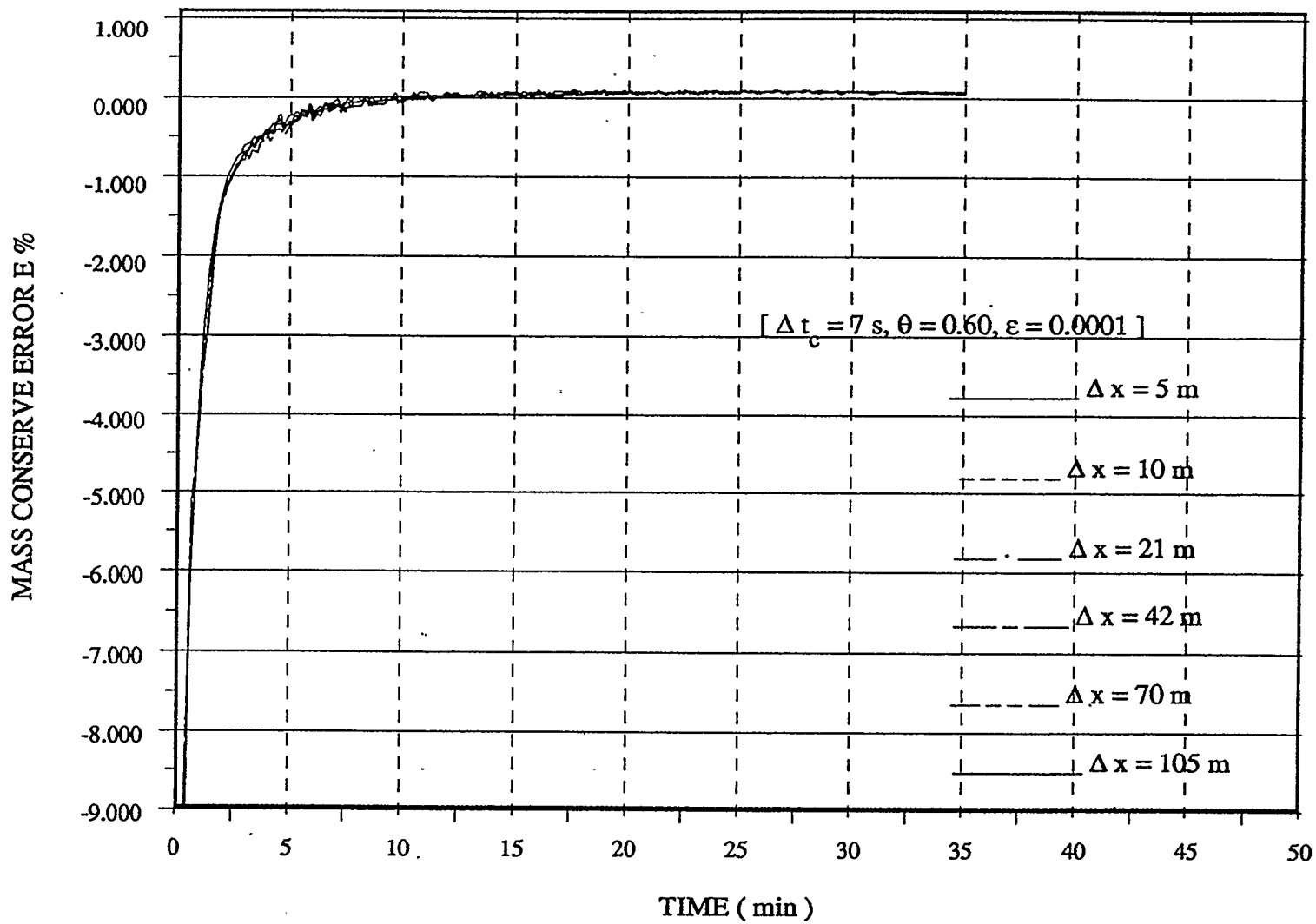

Figure 3.7 (c)

Comparison of computed Mass Conservation Error (E %) for various values of distance interval Δx, for the abrupt increase in inlet flow from 0.103 to 0.387 m^3/s

m/s). It may be observed, Figure 3.8 (a), (b) and (c), that when $\Delta t/\Delta x \cdot C = 1$, the results indicate a steep wave front which becomes more diffused when $\Delta t/\Delta x \cdot C > 1$.

TEST 4

These numerical experiments were conducted to compare the values of selected $\Delta t/\Delta x_c \cdot C = 1$. The resulting discharge hydrographs are plotted in Figure 3.9. The results indicate that for smaller $\Delta t_c/\Delta x_c$ ratios steeper wave fronts are obtained. In observing the corresponding mass conservation E (Figure 3.10) the smaller $\Delta t_c/\Delta x_c$ ratio exhibits less error. Clearly, as $\Delta x, \Delta t \rightarrow 0$, the solution is more convergent.

3.4.1.2 Abrupt Decrease in Flow

The second series of experiments in this section were conducted for variable Δt and Δx for an abrupt decrease in flow. In this series of experiments only one set of abrupt decrease of flow, from 0.387 to 0.103 m^3/s was used. The objective was to determine if the characteristics of the model results were similar to model results when the flow was abruptly increased. Channel conditions were the same as those used for the abrupt increase of inlet flow, except that the initial depth and discharge conditions at the outlet were set equal to $y_0 = 0.607$ m, and $Q_0 = 0.387$ m^3/s respectively. The numerical experiments were conducted as follows:

TEST 5

Numerical experiments were carried out for various values of time steps Δt in multiples of $\Delta t_c = 7s$ while the distance increment was held constant at 10 m, similar to test 1 (Section 3.4.1.1). Figure 3.11 (a), (b) and (c) shows the completed discharge hydrographs at the downstream end of the channel. Note that the behaviour of the model is similar to test 1; that is, there is flattening of the curves and forward displacement with increase in time step. In Figure 3.11(c) note that the approximate maximum value of Δt required to maintain stability is 1200 s. Recall that for an abrupt increase in flow the

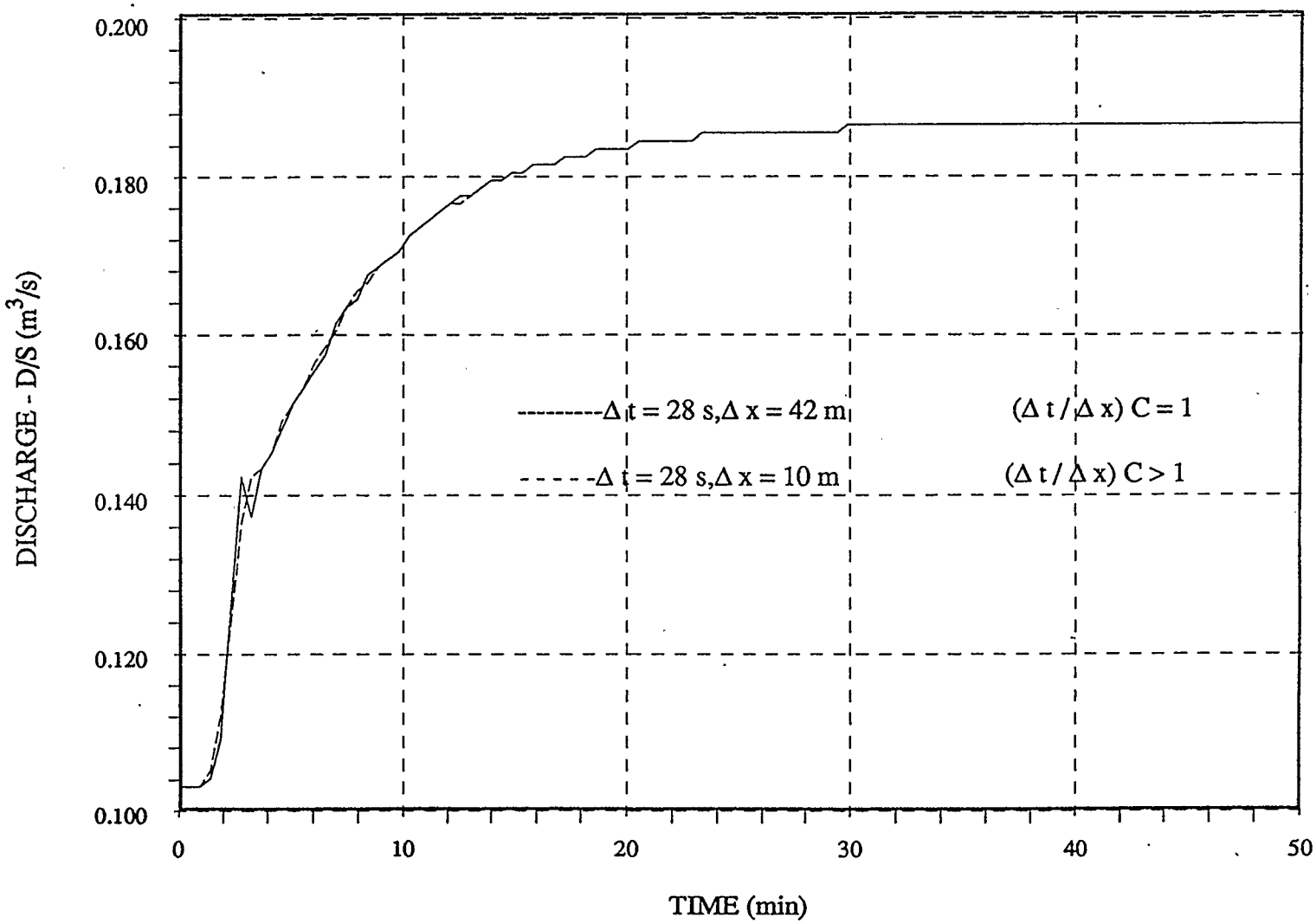

Figure 3.8 (a)

Comparison of computed discharge hydrographs at downstream boundary (D/S) between the value of time interval (Δt) and distance interval (Δx) satisfying the conditions (Δt / Δx) C=1 and (Δt / Δx)C > 1

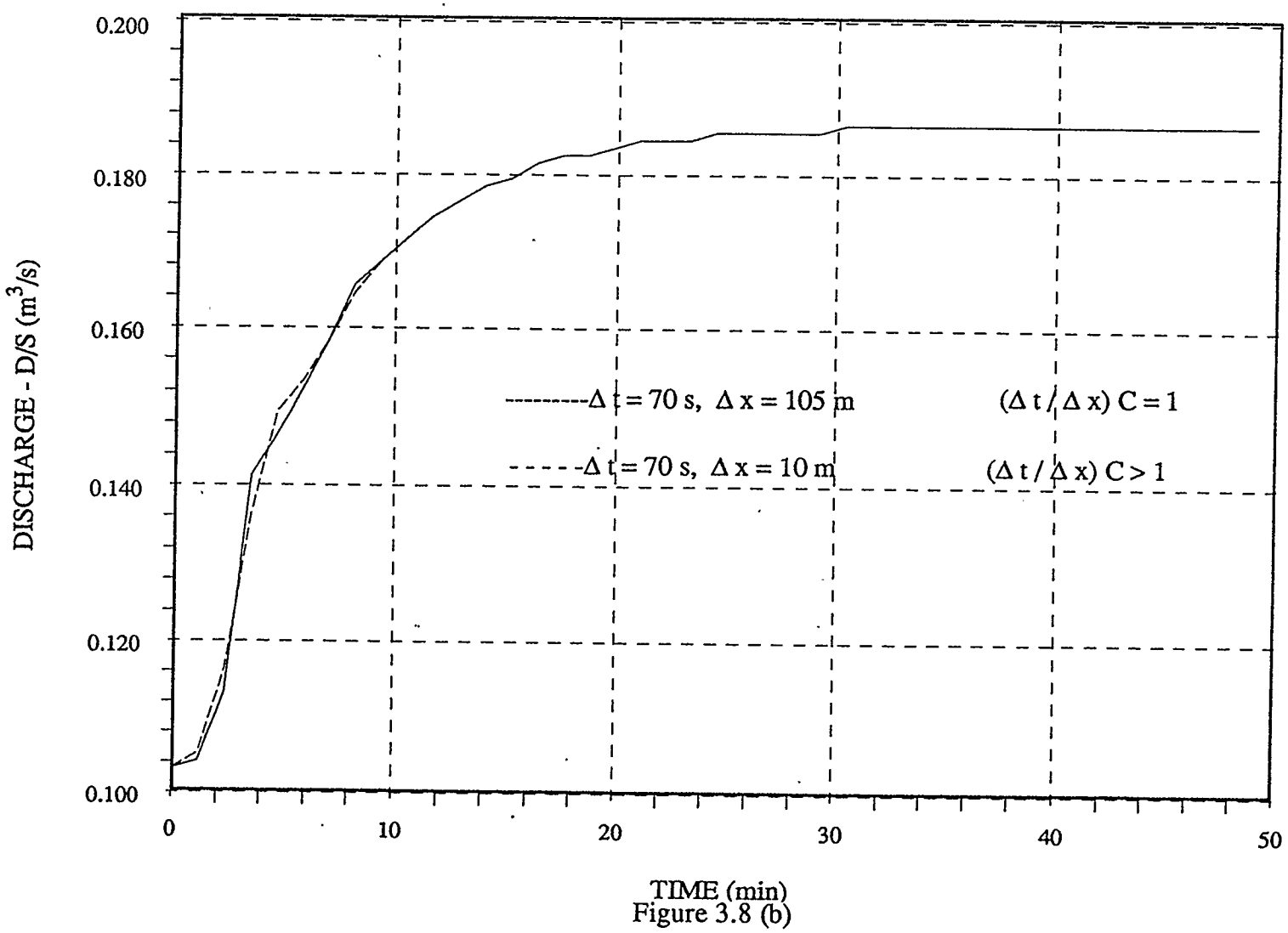

Figure 3.8 (b)

Comparison of computed discharge hydrographs at downstream boundary (D/S) between the value of time interval (Δt) and distance interval (Δx) satisfying the conditions $(\Delta t / \Delta x)\ C=1$ and $(\Delta t / \Delta x) C>1$

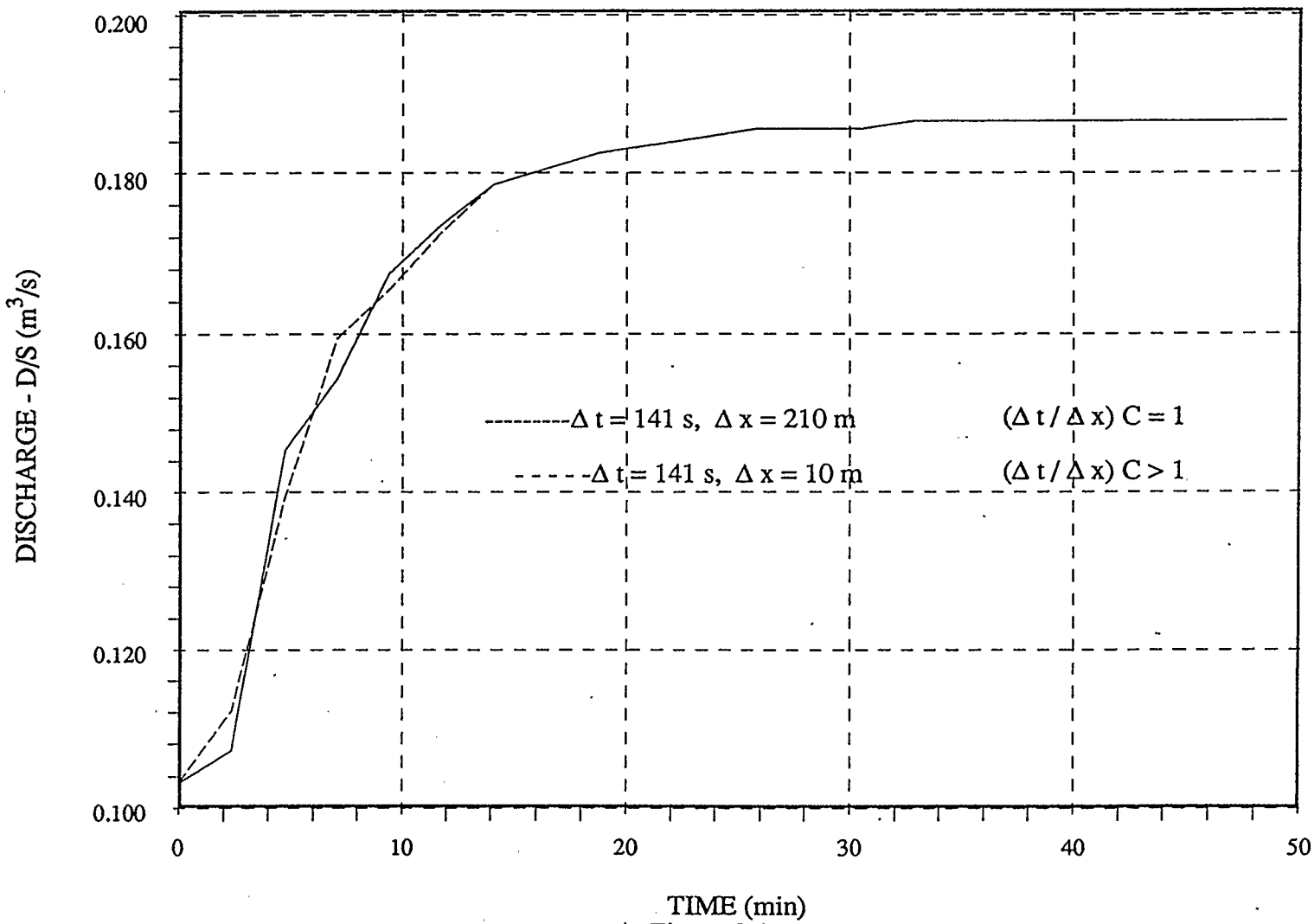

Figure 3.8 (c)

Comparison of computed discharge hydrographs at downstream boundary (D/S) between the value of time interval (Δt) and distance interval (Δx) satisfying the conditions (Δt / Δx) C=1 and (Δt / Δx)C > 1

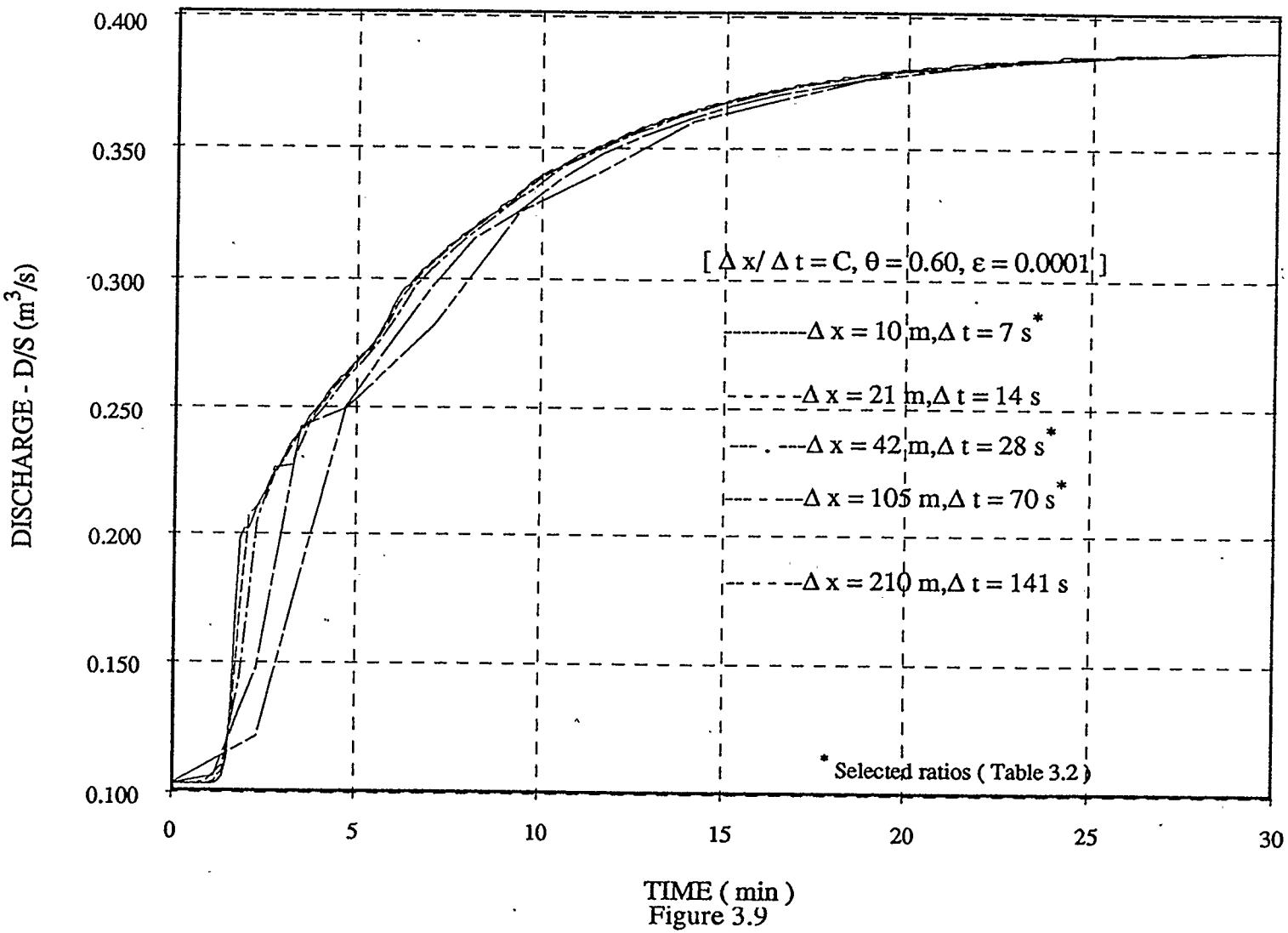

Figure 3.9

Comparison of computed discharge hydrographs at downstream boundary (D/S) between the value of time step (Δt), and distance interval (Δx) selected to satisfy the conditions (Δt / Δx)=C

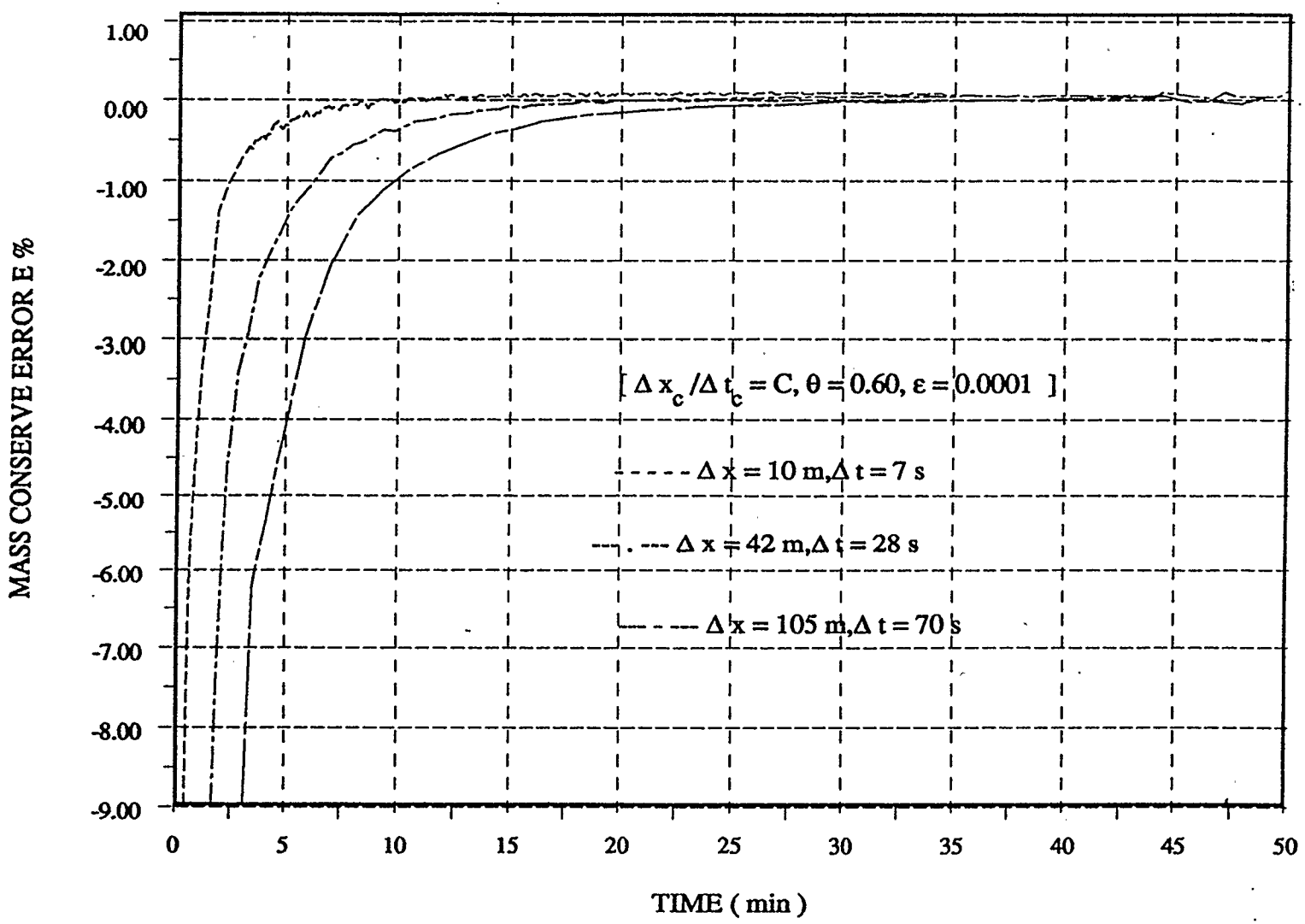

Figure 3.10

Comparison of computed Mass Conservation Error (E%) for various values of time interval Δt, and distance interval Δx, selected to satisfy the condition $(\Delta t / \Delta x)C=1$

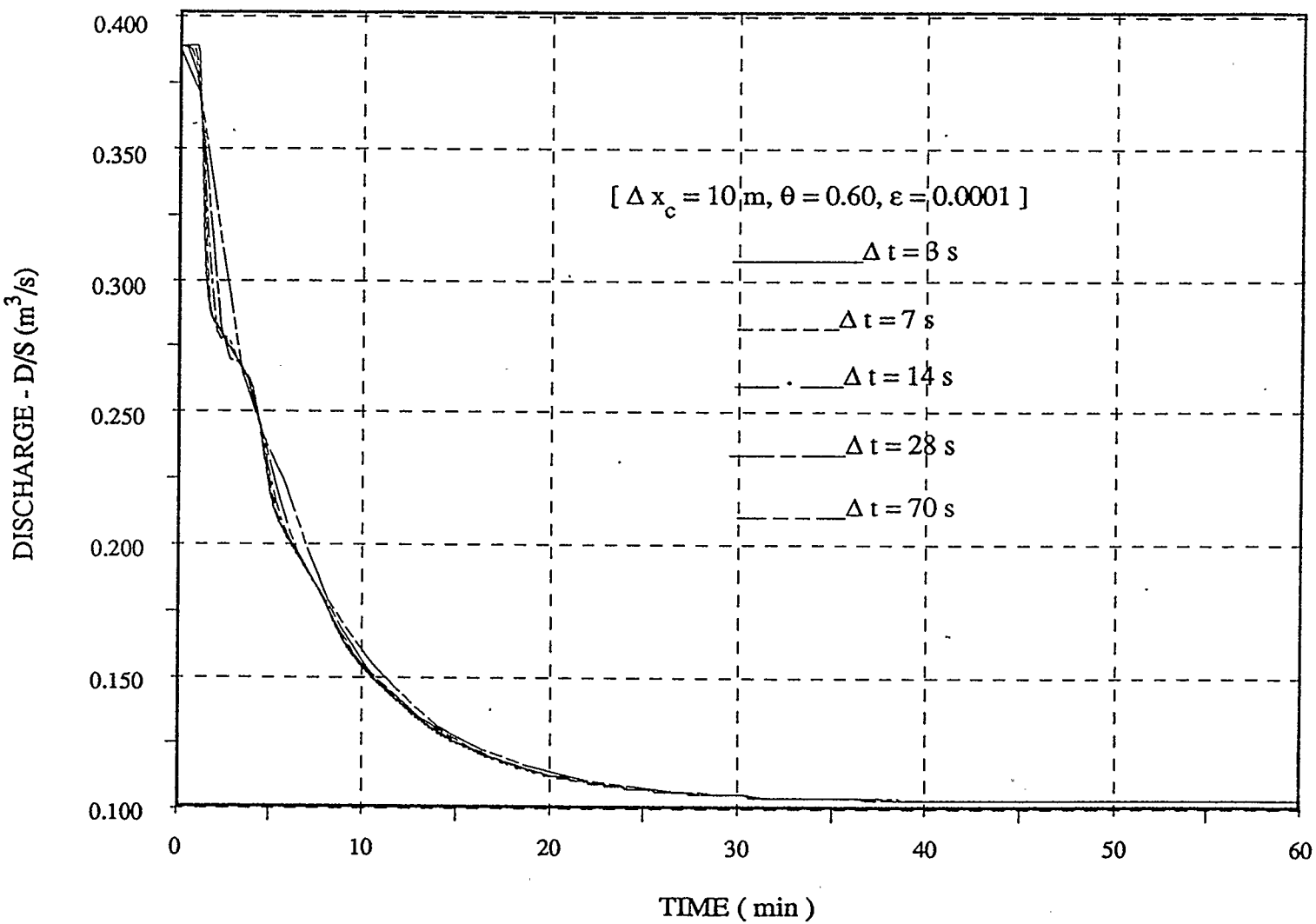

Figure 3.11 (a)

Comparison of computed discharge hydrographs at the downstream boundary (D/S) for various values of time step Δt, for the abrupt decrease in inlet flow from 0.387 to 0.103 m^3/s

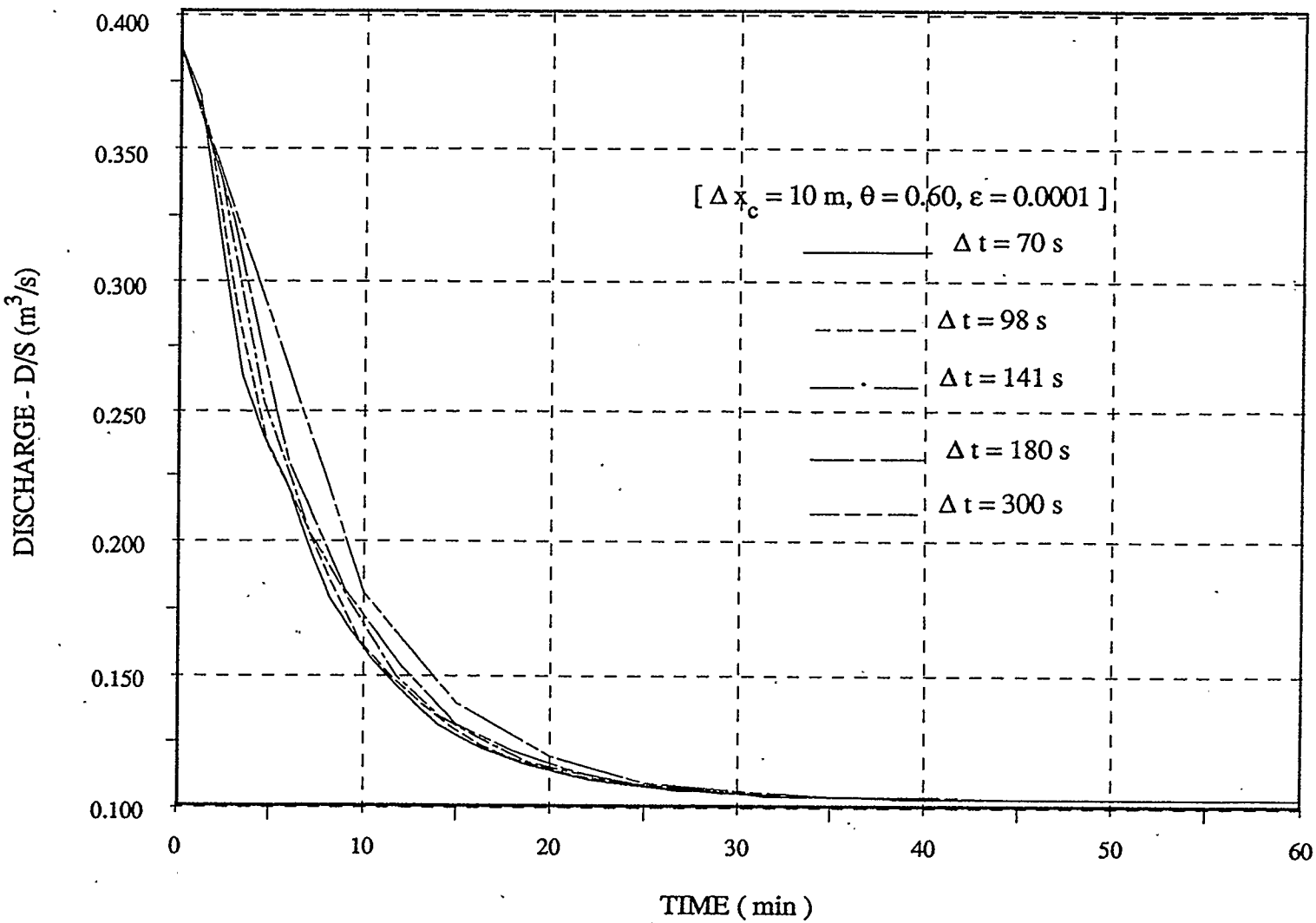

Figure 3.11 (b)

Comparison of computed discharge hydrographs at the downstream boundary (D/S) for various values of time step Δt, for the abrupt decrease in inlet flow from 0.387 to 0.103 m^3/s

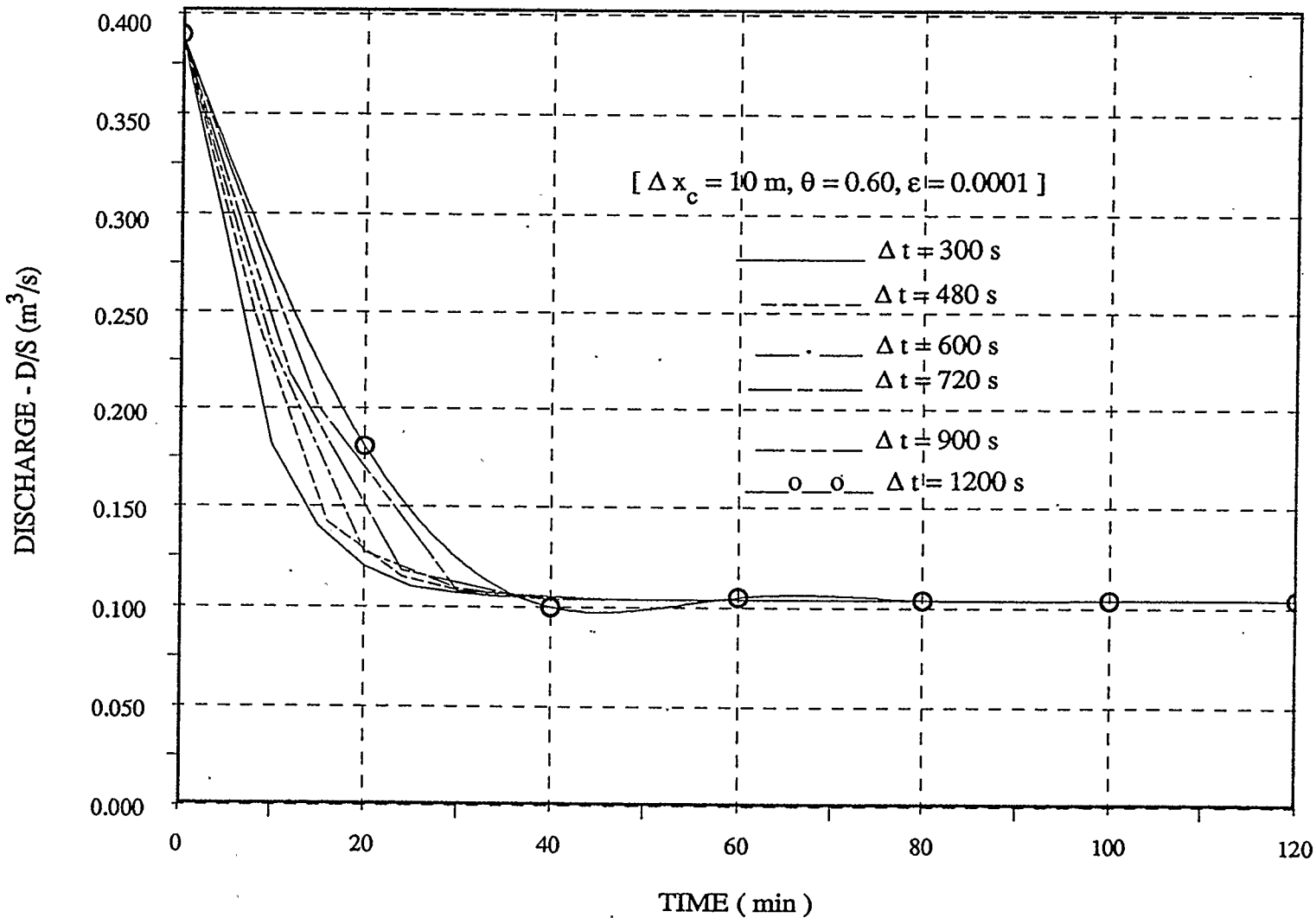

Figure 3.11 (c)

Comparison of computed discharge hydrographs at the downstream boundary (D/S) for various values of time step Δt, for the abrupt decrease in inlet flow from 0.387 to 0.103 m^3/s

observed maximum value is 720 s. However, the same approximate limit of $\Delta t \approx 70s$ was required to achieve convergence. Figure 3.12 shows the corresponding mass conservation error, E, computed for various values of Δt. Noted in Figure 3.12, E increased as the time increment increased similiar to results observed in test 1.

TEST 6

The numerical experiments were conducted for various distance increment, Δx, while maintaining the time interval constatnt at $\Delta t_c = 7s$ in a similar fashion to test 2 (section 3.4.1.1). The computed discharge hydrographs at the downstream end of the channel are shown in Figure 3.13. Similar instabilities to test 2 were observed with increase in Δx above 10m, (i.e. $\Delta t/\Delta x_c \cdot C$ approaches 0). For Δx smaller than $\Delta x_c = 10$ (i.e. $\Delta t_c/\Delta x \cdot C > 1$) the resulting discharge hydrographs were approximately the same as when $\Delta x_c = 10m$.

TEST 7

Numerical experiments were performed to compare simulations where $\Delta t/\Delta x \cdot C = 1$ to those where $\Delta t/\Delta x \cdot C > 1$. The computed discharge hydrographs at the downstream end of the channel for various values of time steps and distance interval are shown in Figure 3.14. It is noted that when parameters are selected to satisfy the condition $\Delta t/\Delta x \cdot C = 1$ the model produces steep curves (similar to test 3). When parameters were selected such that $\Delta t/\Delta x \cdot C > 1$ the scheme output is diffused (similar to test 3).

TEST 8

Numerical experiments were carried out for various combinations of time steps and distance interval which satisfy the condition $\Delta t/\Delta x \cdot C = 1$ similar to those listed in Table 3.2. The discharge hydrographs at downstream end are shown in Figure 3.15. Smaller values of Δt_c and Δx_c result in steeper output curves similar to test 4. Computed

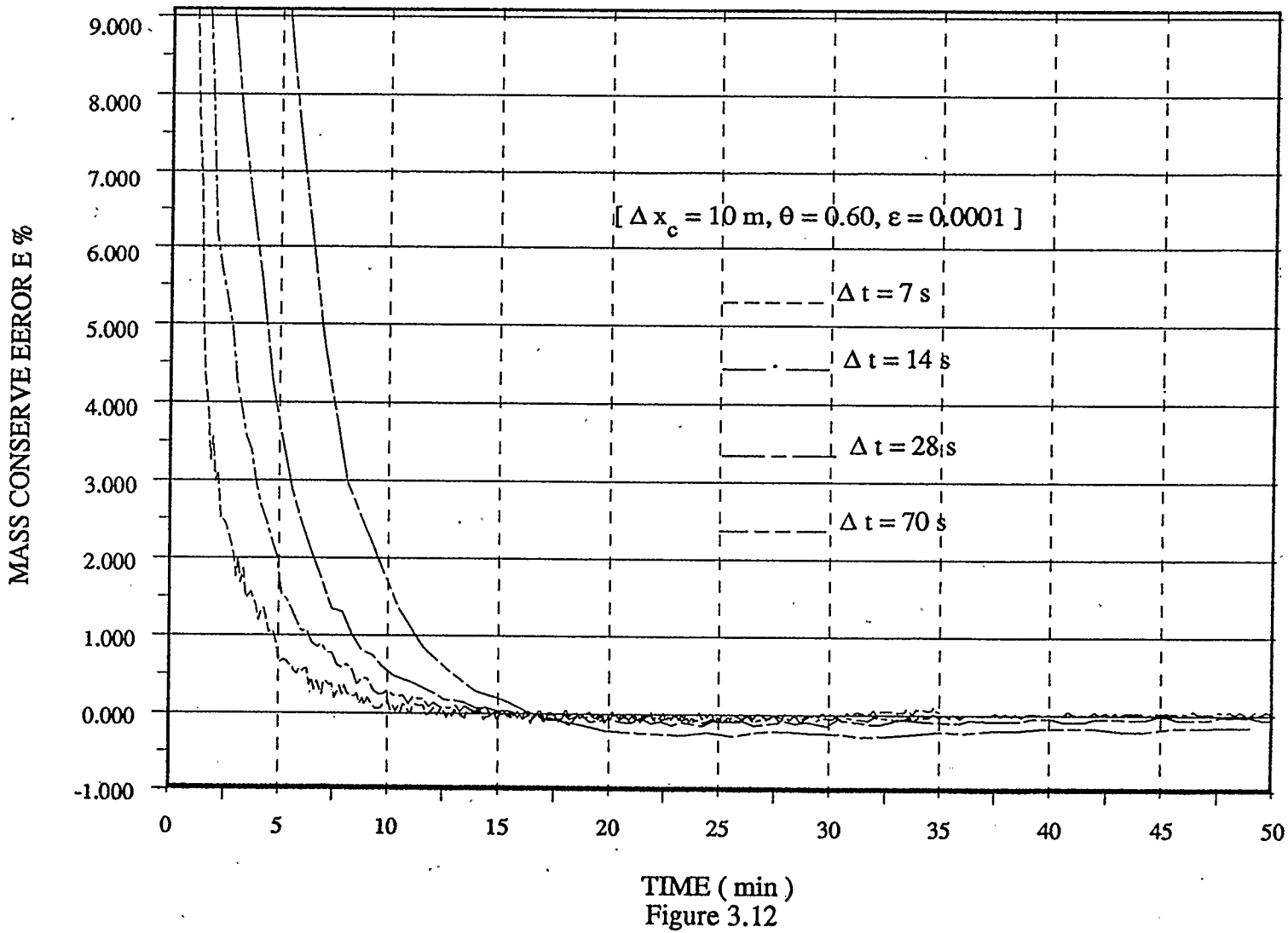

Figure 3.12

Comparison of computed Mass Conservation Error (E%) for various values of time step Δt, for the abrupt decrease in inlet flow from 0.387 to 0.103 m^3/s

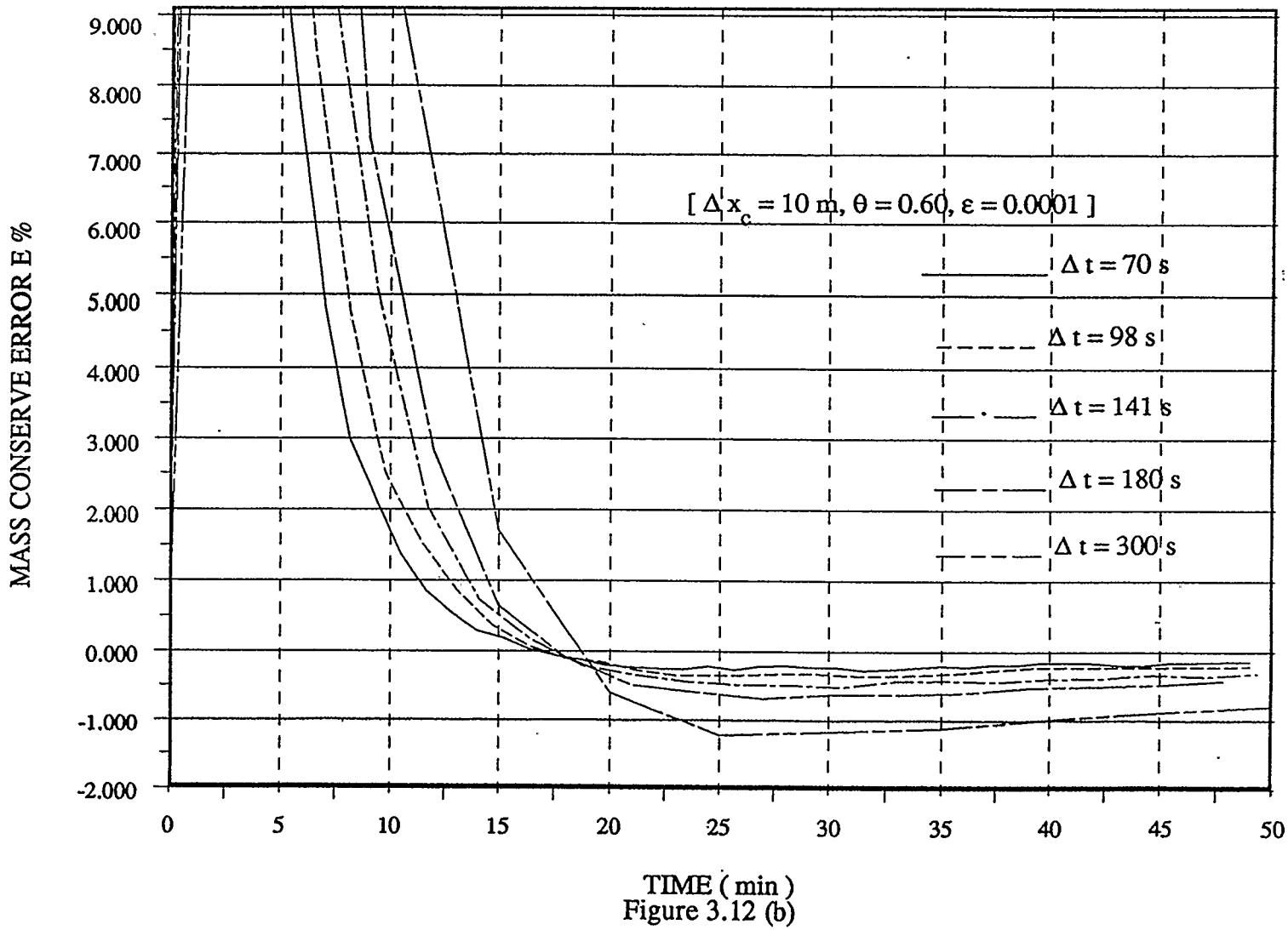

Figure 3.12 (b)

Comparison of computed Mass Conservation Error (E%) for various values of time step Δt, for the abrupt decrease in inlet flow from 0.387 to 0.103 m^3/s

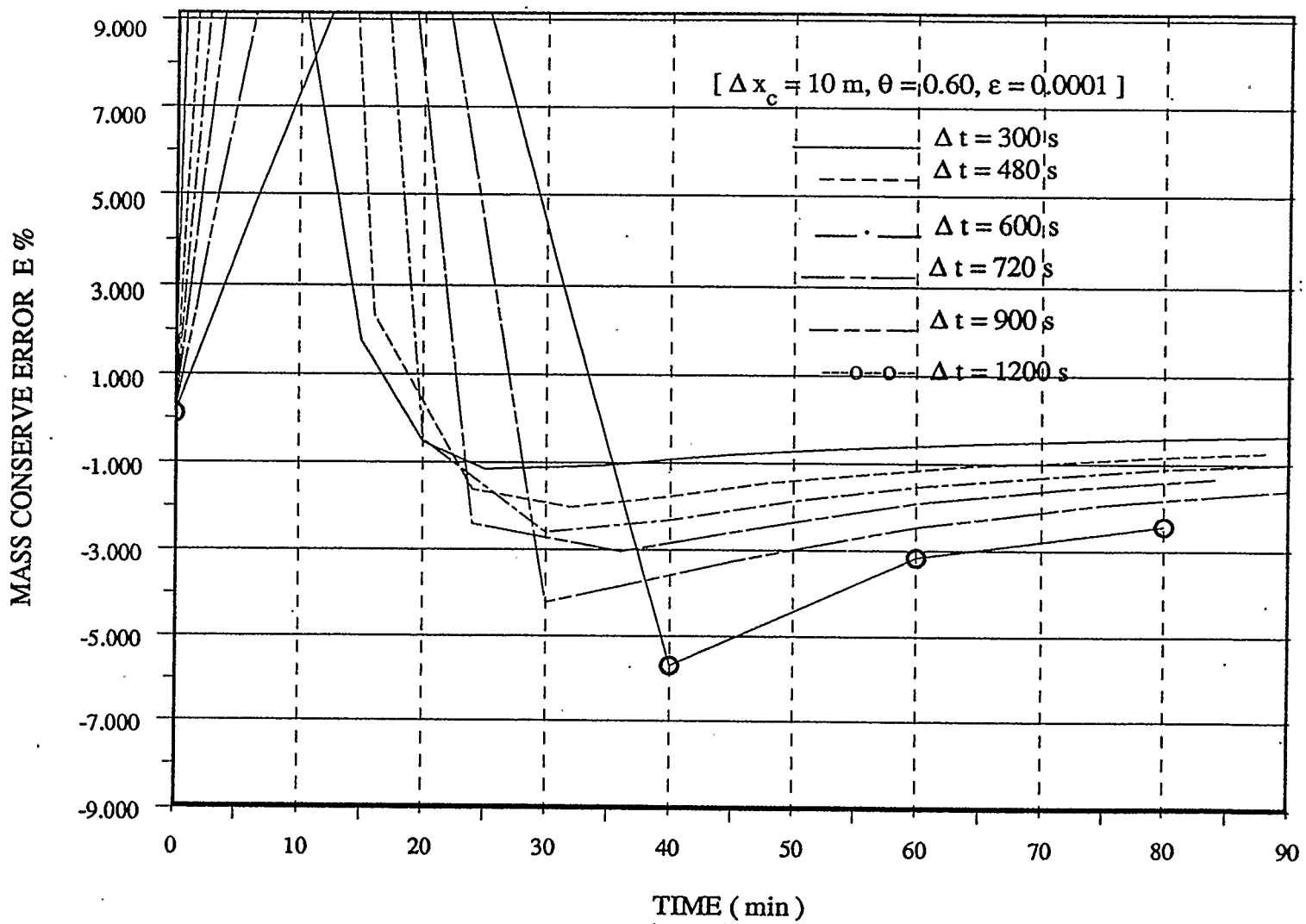

Figure 3.12 (c)

Comparison of computed Mass Conservation Error (E%) for various values of time step Δt, for the abrupt decrease in inlet flow from 0.387 to 0.103 m^3/s

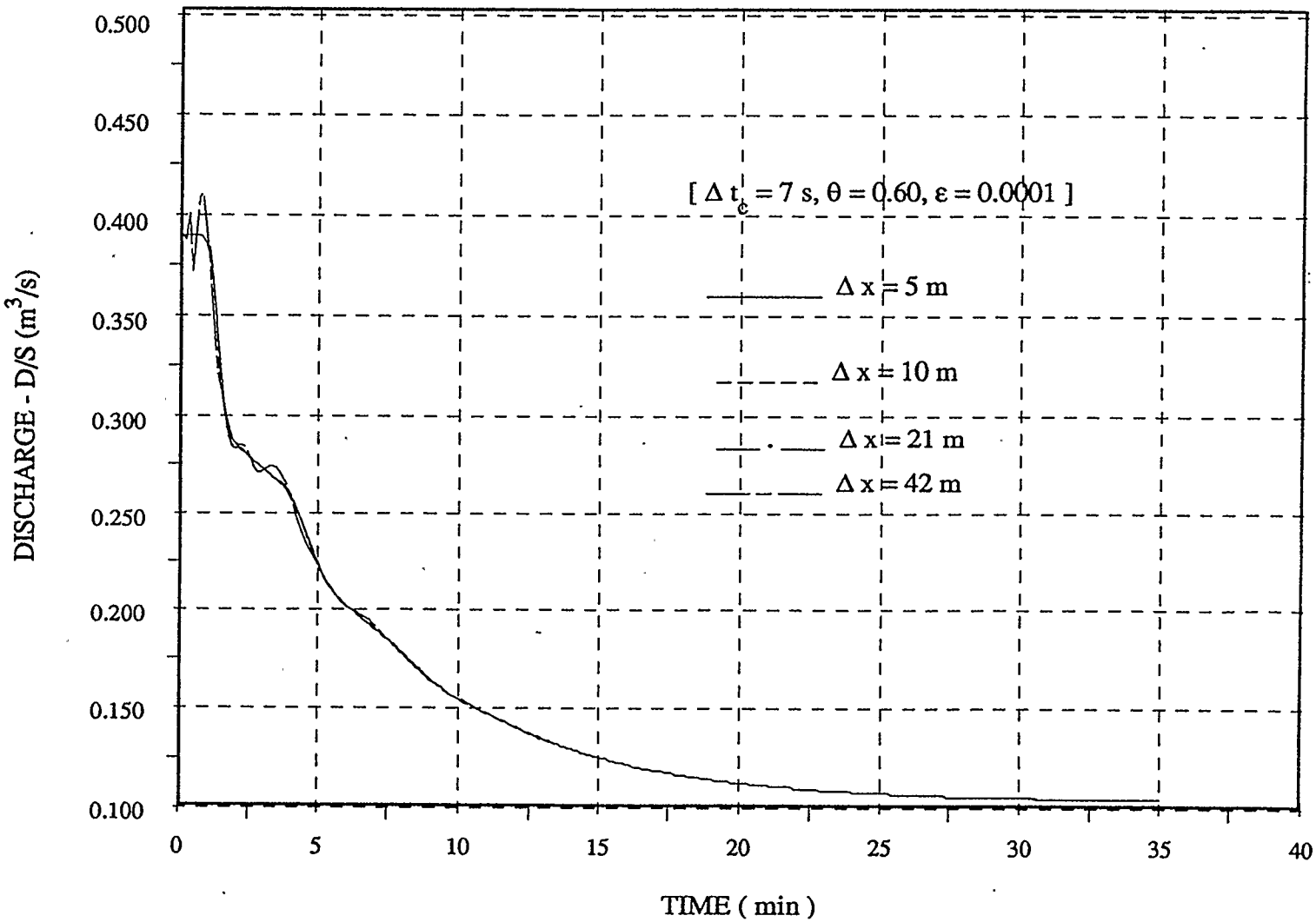

Figure 3.13

Comparison of computed discharge hydrographs at the downstream boundary (D/S) for various values of distance interval Δx, for the abrupt decrease in inlet flow from 0.387 to 0.103 m^3/s

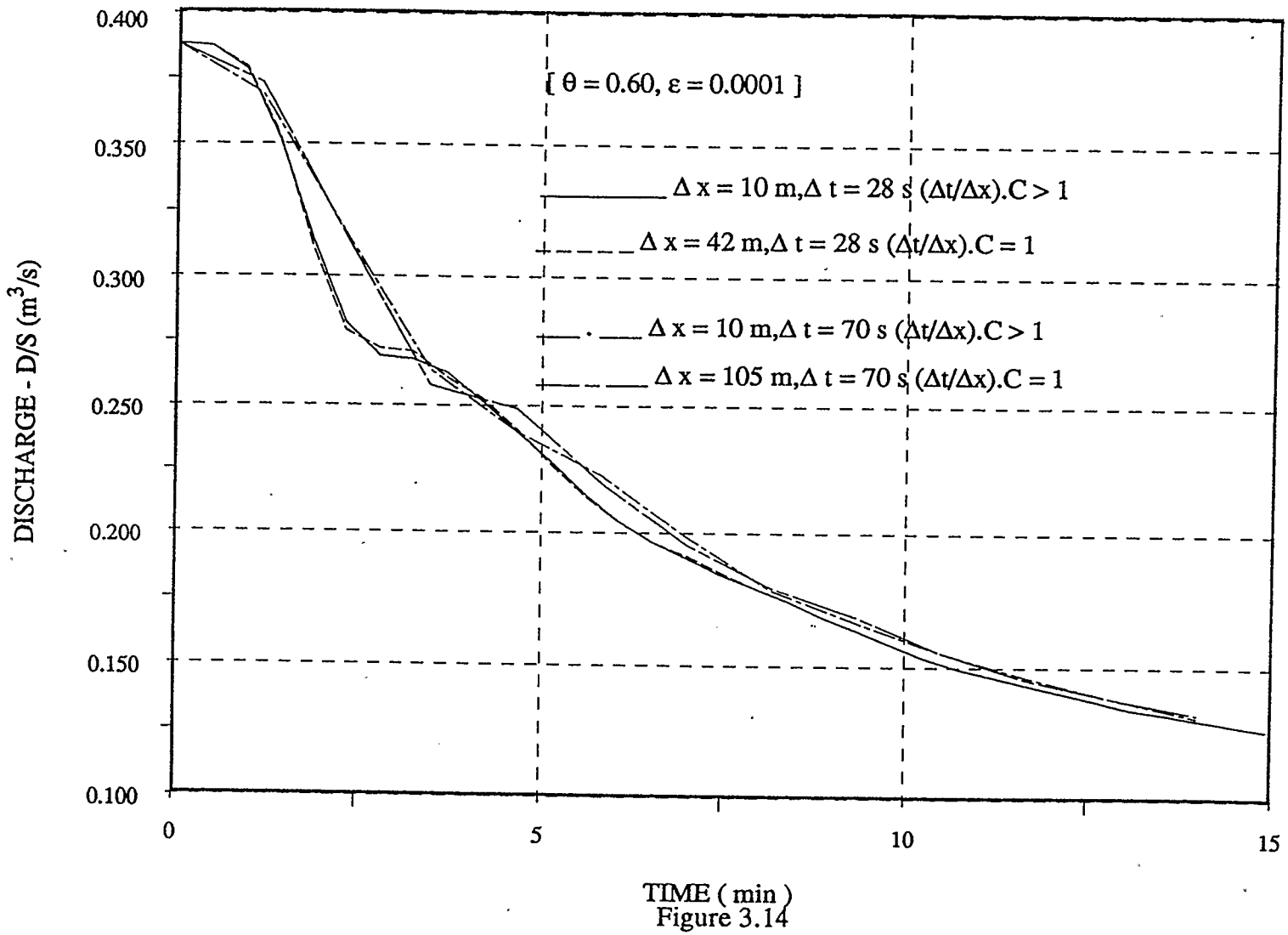

Figure 3.14

Comparison of computed discharge hydrographs at downstream boundary for values of time step(Δt) and distance interval (Δx) satisfying the conditions (Δt / Δx) C=1 and (Δt / Δx)C > 1 for the abrupt decrease in inlet flowfrom 0.387 to 0.103 m^3/s

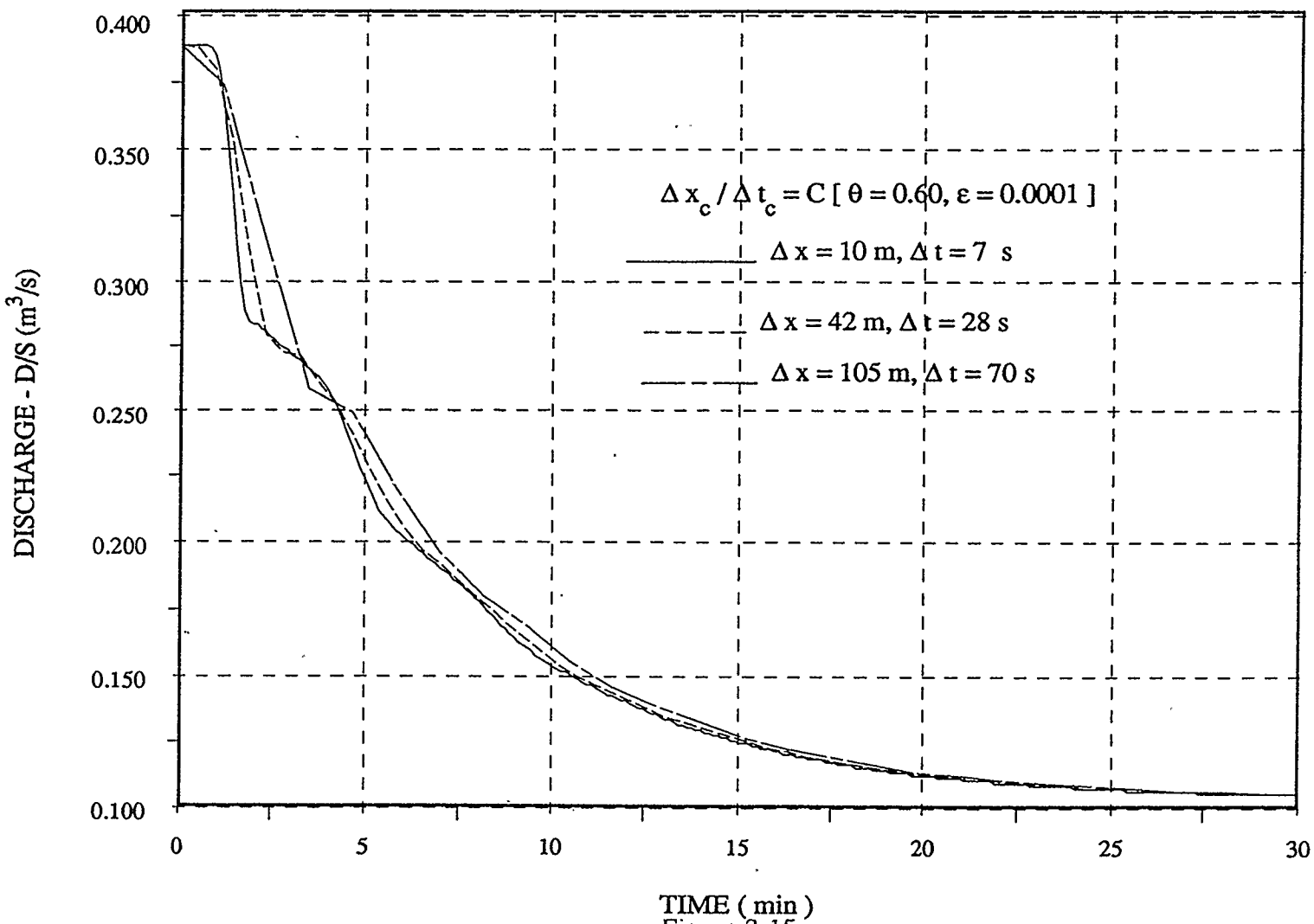

Figure 3.15

Comparison of computed discharge hydrographs at the downstream boundary (D/S) for various values of time steps and distance interval selected to satisfy the condition $(\Delta t / \Delta x)C = 1$ for the abrupt decrease in inlet flow from 0.387 to 0.103 m^3/s

values of mass conservation for different combinations of Δt_c and Δx_c are shown in Figure 3.16. Note that the mass conservation error tends to increase as the values of Δt_c and Δx_c increase.

3.4.2 VARIATION IN FINITE DIFFERENCE WEIGHTING PARAMETER

A series of numerical experiments were performed in order to evaluate the influence of the weighting factor θ (at $\theta=0.5$, the numerical procedures contained in the unsteady flow routing subroutine is said to be fully centred and is theoretically stable. At θ greater than 0.5 the calculations are said to be unconditionally stable). The numerical experiments were conducted for two cases: one with $\Delta x_c=10$m, another with $\Delta x_c=105$m. In both cases, the time intervals, Δt, were set for condition $\Delta t/\Delta x \cdot C=1$ (see Table 3.2). Also, in both cases, the discharge at the channel inlet was abruptly increased from 0.103 m^3/s to 0.618 m^3/s. Other channel conditions were maintained constant as described in Section 3.2. The simulation was repeated for values of θ between 0.5 and 1.0. The resulting discharge hydrographs at the outlet of the channel are plotted in Figures 3.17(a) and (b) and the corresponding mass conservation error in Figures 3.18(a) and (b).

The following observations may be made:

1. The surge celerity and general shape of the curve is not affected by variation of θ;

2. The use of $\theta=0.5$ for surge flow results in a steeper curve front, but a significant numerical instability and greater mass conservation error E after the passage of the surge. These characteristics are more pronounced for larger distance increments.

3. The use of $\theta=1$ results in diffused surge but no numerical stability.

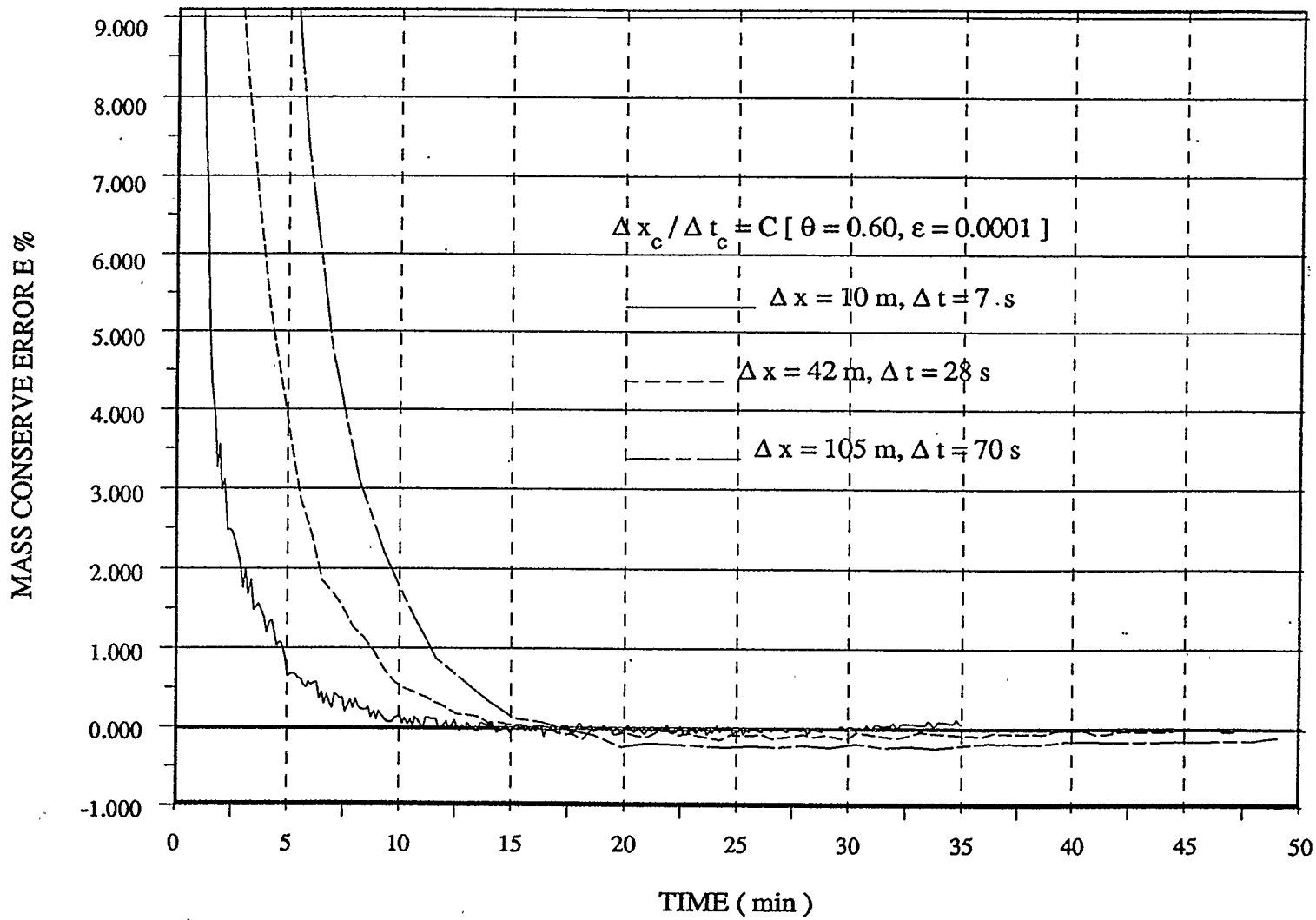

Figure 3.16

Comparison of computed Mass Conservation Error (E %) for various values of time steps and distance interval selected to satisfy the condition $(\Delta t / \Delta x)C=1$ for the abrupt decrease in inlet flow from 0.387 to 0.103 m^3/s

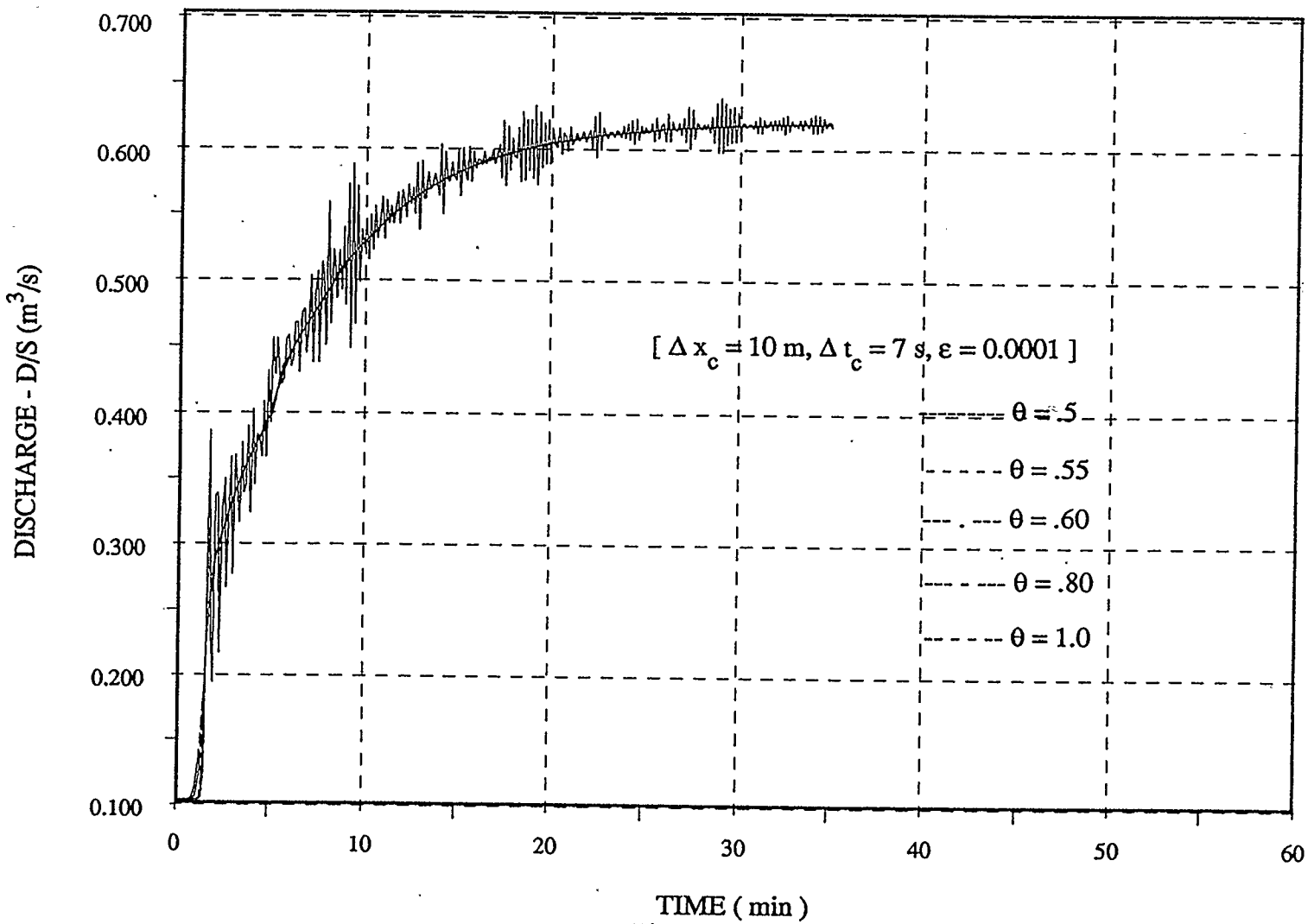

Figure 3.17 (a)

Comparison of computed discharge hydrographs at the downstream boundary (D/S) for various values of weighting factor θ, and for time step $\Delta t = 7$ s and distance interval $\Delta x = 10$ m satisfying $(\Delta x / \Delta t) = C$

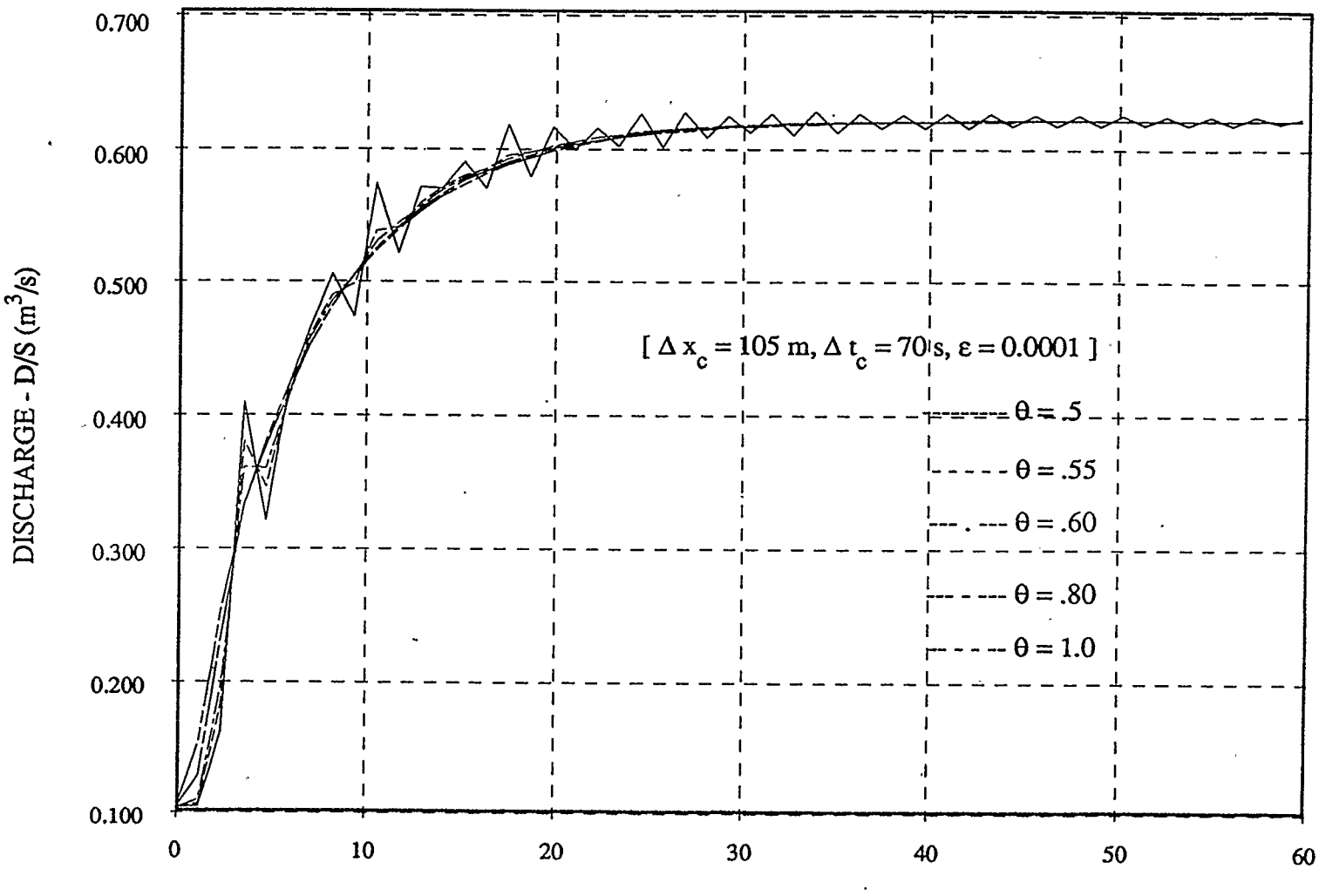

Figure 3.17 (b)

Comparison of computed discharge hydrographs at the downstream boundary (D/S) for various values of weighting factor θ, and for time step $\Delta t = 70$ s and distance interval $\Delta x = 105$ m satisfying $(\Delta x / \Delta t) = C$

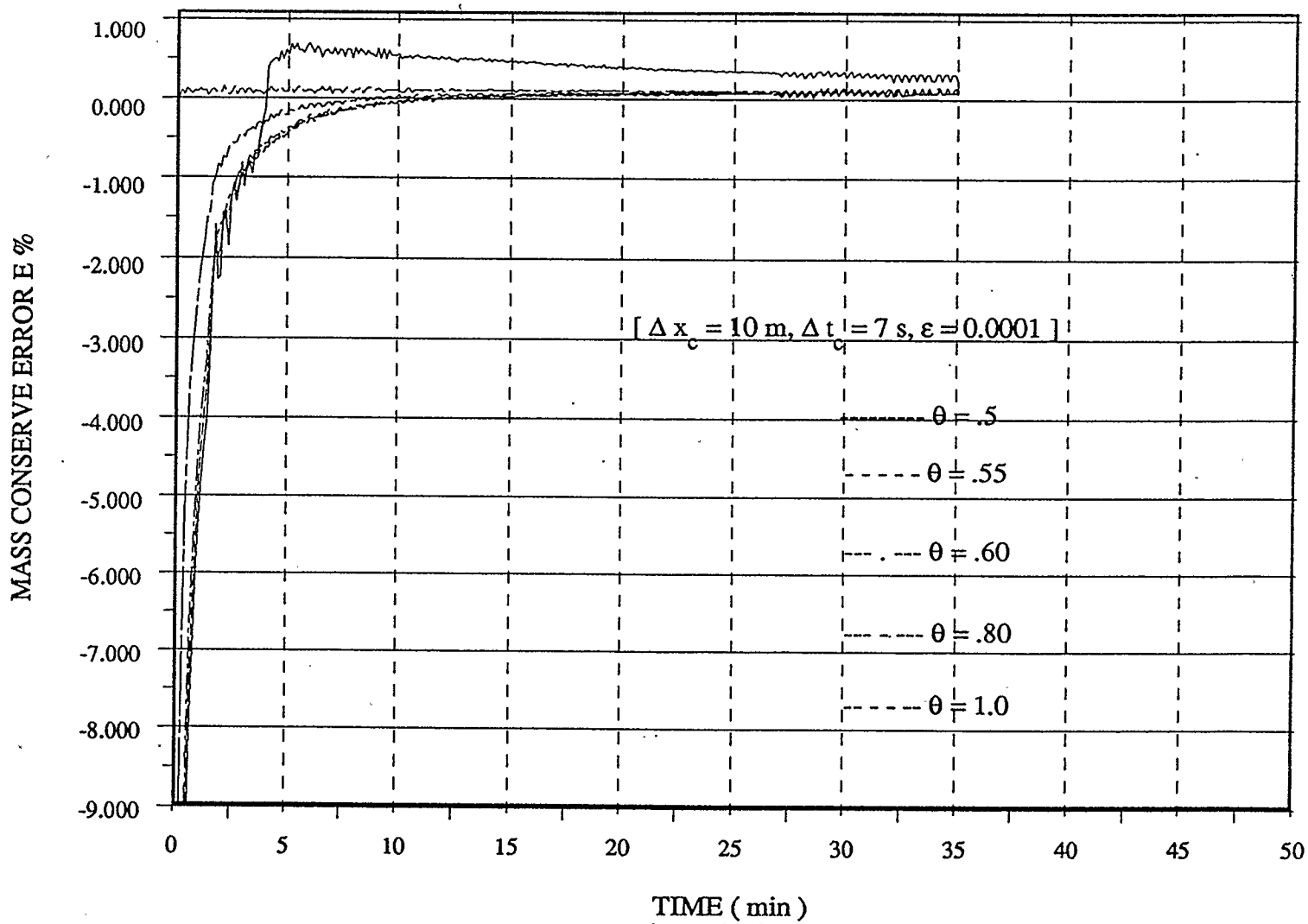

Figure 3.18 (a)

Comparison of Mass Conservation Error (E%) for various values of weighting factor θ, and for time step $\Delta t = 7$ s and distance interval $\Delta x = 10$ m satisfying $(\Delta t / \Delta x) = C$

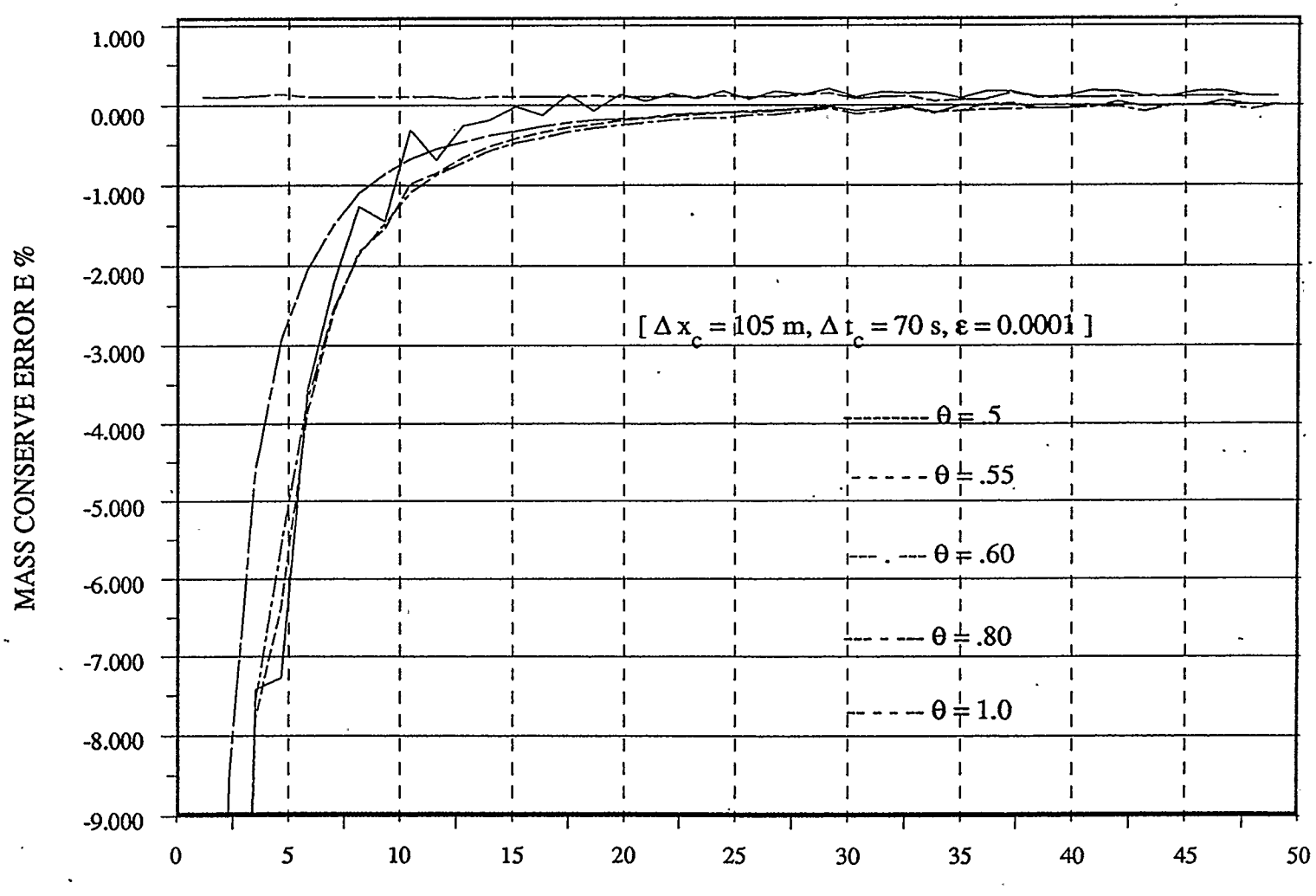

Figure 3.18 (b)

Comparison of Mass Conservation Error (E%) for various values of weighting factor θ, and for time step $\Delta t = 70$ s and distance interval $\Delta x = 105$ m satisfying $(\Delta t / \Delta x) = C$

4. The use of $\theta=0.6$ (as suggested by Chaudhry and Contractor (1973) for simulation of steeper flow fronts and smaller resistance coefficients) results in solutions with little or no numerical instabilities and well defined steep surge fronts. However, the value of $\theta=0.55$ exhibits fairly similar characteristics in surge front and mass conservation error E as when $\theta=0.6$, but, slightly more numerical instabilities and changes in E after the passage of the surge, especially for smaller distance $\Delta x=10$m.

5. The increase of θ from 0.5 to 1.0 results in flattening of the surge curve and lesser mass conservation error; however, this effect may not be considered a significant error in view of the error induced by varying Δt (as shown in Figure 3.6)

3.4.3 VARIATION IN CONVERGENCE CRITERION IN NEWTON ITERATION METHOD, ε

A series of numerical experiments were performed in order to determine the influence of convergence criterion, ε. Two cases were considered: $\Delta t/\Delta x \cdot C=1$ and $\Delta t/\Delta x \cdot C > 1$. For the former case $\Delta x=10$m and $\Delta t=7$s (which was previously found to have a steeper surge front and small mass conservation error E) and the latter case $\Delta x=10$m and $\Delta t=70$s (which was previously found to be the approximate upper limit for convergence). In both cases, the value of the weighting coefficient θ was set equal to 0.6 to ensure the numerical stability of computations and well-defined profile of the steep surge fronts (i.e. no numerical computation results were achieved). In both cases, the discharge at the channel inlet was abruptly increased from 0.103 m^3/s to 0.387 m^3/s and the other channel conditions were described in Section 3.2. The simulation was repeated for values of ε between 0.00001 and 1.0. The resulting discharge hydrographs at the outlet of the reach are shown in Figures 3.19 (a) and 3.20 (b) for the conditions $\Delta t/\Delta x \cdot C=1$ and $\Delta t/\Delta x \cdot C > 1$, respectively. When ε was set equal to 1.0, numerical computation did

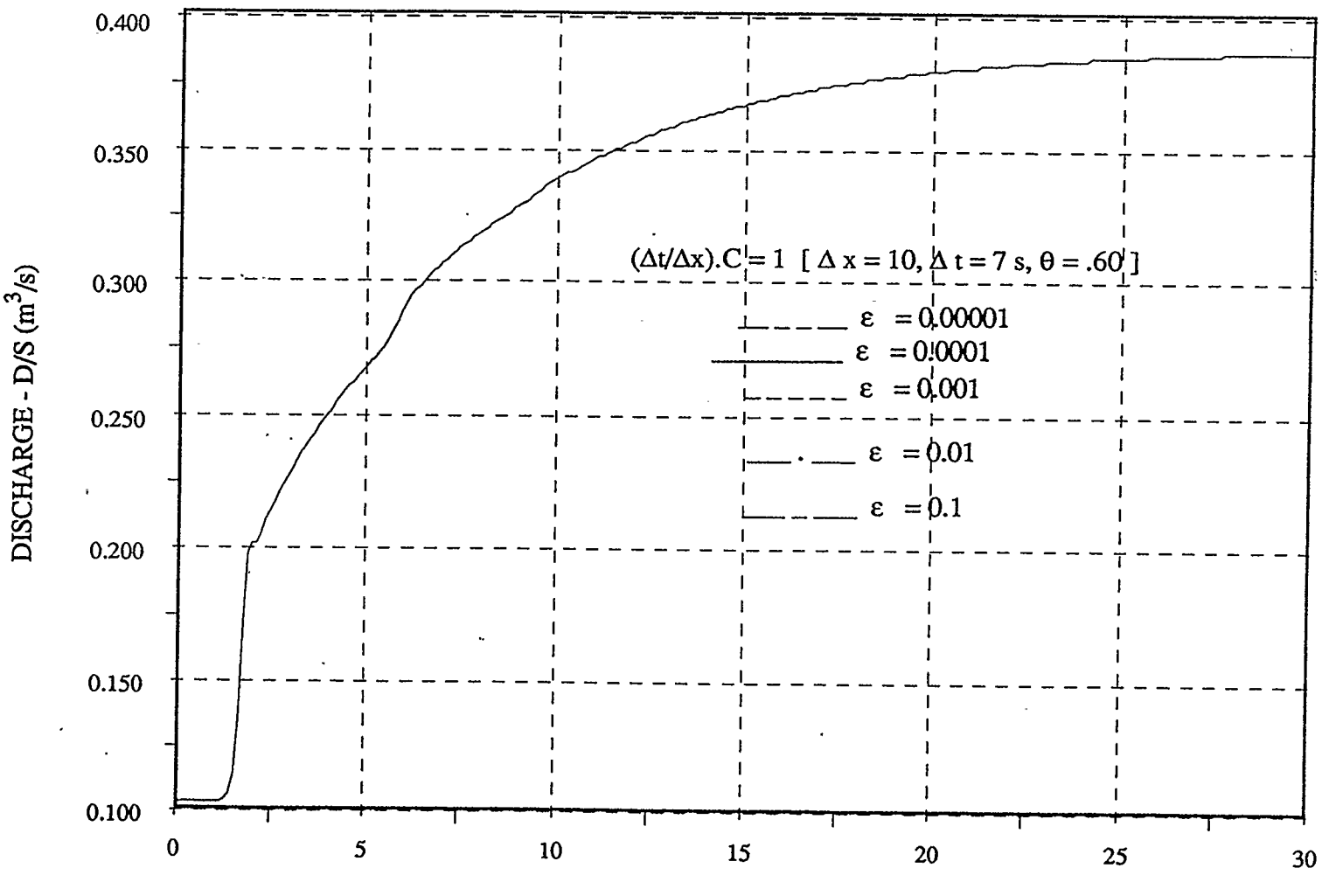

Figure 3.19 (a)

Comparison of computed discharge hydrographs at the downstream boundary (D/S) for various values of Convergence criterion parameter ε, and for time step $\Delta t = 7$ s and distance interval $\Delta x = 10$ m satisfying $(\Delta x / \Delta t) = C$

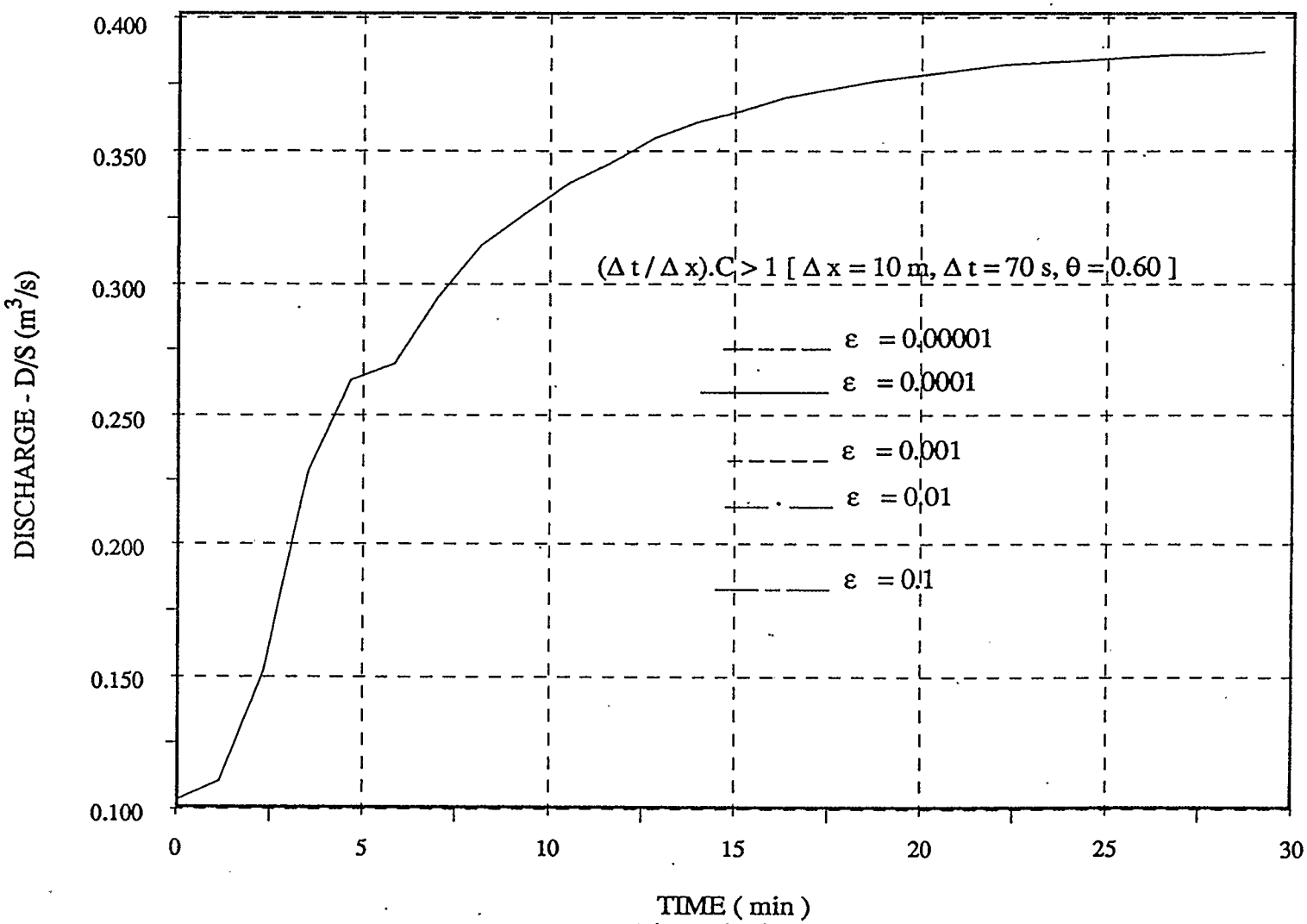

Figure 3.19 (b)

Comparison of computed discharge hydrographs at the downstream boundary (D/S) for various values of Convergence criterion parameter ε, and for time step $\Delta t = 70$ s and distance interval $\Delta x = 10$ m satisfying $(\Delta x / \Delta t) = C$

not proceed (i.e. no numerical computation results (or outputs) were achieved). Otherwise variation in ε appeared to have no effect.

3.5 SUMMARY OF RESULTS

The numerical computation properties of the weighted four-point implicit scheme for the solution of the St. Venant equations have been analyzed. A summary of the results of the numerical experiments are as follows:

1. When values of time and distance interval are selected such that the term $\Delta t/\Delta x \cdot C \approx 1$, simulations can be expected to be stable and convergent and provide a more accurate representation of the flow profile. However, if values of distance increment are selected much greater than Δx_c, serious instabilities may result.

2. The time interval must be chosen sufficiently small to ensure adequate detail of the flow is provided to the numerical model.

3. The maximum value of time interval which would ensure solution stability decreases as the relative change in abrupt increase or decrease in flow increases, convergence considerations withstanding.

4. The magnitude of the time interval had a much greater impact on solution convergence than either distance interval or weighting factor.

5. The maximum value of time interval which would ensure solution stability appears to be less for flow increases as compared to decrease in flow of similar magnitude.

6. A value of weighting coefficient approaching 0.6 permits stable, convergent and accurate representation of the wave profile of abruptly varying flow.

Weighting coefficients approaching 0.55 may be successfully used for changes in flow which are not abrupt.

7. If values of time and distance interval are selected such that the term $\Delta t/\Delta x \cdot C = 1$, the convergence criteria appears to have a negligible effect on solution results.

CHAPTER 4: VERIFICATION AND CALIBRATION

4.1 GENERAL DESCRIPTION

Once the numerical solution technique, i.e. the weighted four-point implicit scheme, is verified for the range of flow conditions based on convergence and stability criterion, a working implicit numerical model is available for simulating the prototype system.

Verification infers the evaluation of the mathematical relations used by the model to describe relevant hydraulic processes (including methods to manipulate and/or solve the equations) by comparing model results to observed results obtained from adequately controlled experimental programs. In the verification process, parameters needed to characterize the model hydraulics are specified and model output is compared to experimental observations. Once the mathematical relations used by the model have been verified, calibration of the model is possible. Calibration is the reverse of the verification process. In the calibration process, hydraulic control parameters are determined by repeated comparisons of model output to observed field conditions. Control parameters are mainly the flow and channel parameters assumed to influence the spatial and the temporal distribution of water in the channel including channel length, L, channel bottom slope S_o, cross-sectional area A, surface width B, rate of lateral inflow (q) or outflow (-q), frictional resistance S_f, wind resistance S_w, and the momentum correction factor β). Note that in development of the unsteady flow equation for the idealized prismatic channel it was assumed the factors $S_w=0$ and $\beta=1$. In this part of the study, preliminary results of verification of the implicit numerical model to an adequately controlled experimental program are presented. The experimental program data set is that of Treske (1980), measured in a straight rectangular channel (see Appendix C). Another series of simulations of the idealized Treske's channel using this implicit numerical model were conducted,

verified unsteady channel routing characteristics withstanding, in order to see how sensitive the model is to varying hydraulic control parameters.

The various implicit numerical modelling and simulation studies were made possible using the ICSS Model (Appendix D and ref. Manz, 1985).

4.2 VERIFICATION OF NUMERICAL MODEL

Simulations were carried out using the Treske data set (Treske, 1980) which was carefully evaluated and reported in Appendix C. The channel used by Treske was rectangular in cross-section, prismatic and 210 m long. The channel was 1.25 m wide.

The resistance coefficient was assumed constant along the entire reach. Two values of n were considered. The first, n=0.0120, was suggested by Treske. The second, n=0.0117, was determined based on calibration studies performed or described in Section 4.3.1.2. The channel bottom slope is 0.00019. The observed depths and flow rates at the upstream and downstream boundaries of the channel as they varied with time are listed in Table C.2 in Appendix C.

The computational parameters selected were:

- $\Delta t = 1$ min,
- $\Delta x = 5$ m,
- $\theta = 0.55$, and;
- $\varepsilon = 0.0001$.

The time interval is the same as the time interval between observations. According to numerical considerations discussed in Chapter 3 the maximum distance would be 90 m. However, a sensitivity analysis using distance intervals of 5, 23.33, 42, 70 and 105 m indicated that best results were obtained using the 5 m interval. The weighting factor used

could be lower using the distance interval and very little damping of predicted hydrograph could be expected. The convergence was selected to provide information on depth and flow rates with expected computational error less than on tenth of a millimeter or litre per second.

4.2.1 ACCURACY ASSESSMENT

The accuracy of predicted flow conditions was evaluated using the root mean square of the difference between observations, and predicted estimate, relative peak error, and system performance, defined as follows.

Root mean square error (S) is defined by the equation,

$$(S)_r = \left[\frac{\sum_{i=1}^{n} (M_i - C_i)^2}{n} \right]^{1/2} \tag{4.1}$$

Relative root mean square error (RS) is defined by the relation,

$$(RS)_r = \frac{(S)_r}{M_p} \times 100 \tag{4.2}$$

Relative error of the peak (Pe) of the hydrographs is defined by the relation,

$$(P_e)_r = 100 \cdot \left(1 - \frac{C_p}{M_p} \right) \tag{4.3}$$

where:

n = total number of hydrograph values being computed

C = depth or discharge computed values

M = depth or discharge measured values

C_p = maximum (peak) value of C

M_p = maximum value of M

r = subscript denoting the locations along the channel reach the hydrograph values are being computed, for example:

r = u denotes upstream end of reach, or

r = d denotes downstream end of reach.

A measurement of the ability of the model to predict flow conditions and specific location over a given time period, is called system performance (P), and can be mathematically written as

$$(P)_r = (1-(e)_r^2) \cdot 100 \tag{4.4}$$

$$\text{in which } (e)_r^2 = \frac{\sum_{i=1}^{n} (M_i - C_i)^2}{\sum_{i=1}^{n} (M_i)^2} \tag{4.5}$$

and r = denotes the location in the channel reach where hydrographs are being compared; e^2 is a scale-free measure of total relative error which is equal to the sum of the squares of the prediction errors divided by the sum of the square of the required values at a particular location in the reach over a specified time period.

4.2.2 NUMERICAL EXPERIMENT RESULTS

The numerical model output such as the flow depth at the upstream and downstream boundaries and the discharge at the downstream boundary as a function of time, were compared with measured data.

A summary of model output errors in terms of time of peak (phase shift), magnitude of peak flow and depth, and peak error P_e% (Equation 2.9) is shown in Table 4.1. Table 4.2 shows the summary of deviations of model output from the measured hydrographs in terms of root mean square (S) and model system performance variable P (see Section 4.2.1). The computed and measured depth hydrographs at upstream (u/s) and downstream

Table 4.1
Summary of Model Output Errors in terms of Phase Shift and Peak Errors in the Verification Procedure

MODEL	Peak Y (u/s)	Pe (%) Y (u/s)	Peak Y (d/s)m	Pe % Y (d/s)	Peak Q (d/s) m^3/s	Pe % Q (d/s)	phase shift[1] (min)	Froude No.
OBSERVED	.296	n/a	0.299	n/a	0.185	n/a	2.5	0.07-0.14
IMPLICIT MODEL	0.295	0.68	0.294	1.35	0.155	1.9	2.5	0.07-0.14
IMPLICIT MODEL[2]	0.292	1.35	0.295	1.35	0.155	1.9	2.5	0.07-0.14

[1]: Time between inflow and outflow peaks
[2]: Results when n=0.0117 is used in simulation

(d/s) boundaries are shown in Figures 4.1 and 4.2 respectively, while the discharge hydrographs at both boundary locations are shown in Figure 4.3.

The model was found to have underestimated the peak discharge at the downstream boundary by 1.9%. The peak depth was underestimated by 14% for both upstream (u/s)

Table 4.2
Summary of Deviation of Model Output from Measured Values in Terms of Root Mean Square (S) and System Performance Variable (P) in the Verification Procedure

MODEL	S for Y (u/s) m	S for Y (d/s) m	S for Q (d/s) m^3/s	P for Y (u/s) %	P for Y (d/s) %	P for Q (d/s) %
IMPLICIT MODEL	0.0027	0.0022	0.0015	99.9878	99.9922	99.9837
IMPLICIT MODEL [1]	0.0020	0.0021	0.0015	99.9932	99.9928	99.9843

[1] Results when n=0.0117 is used in simulation

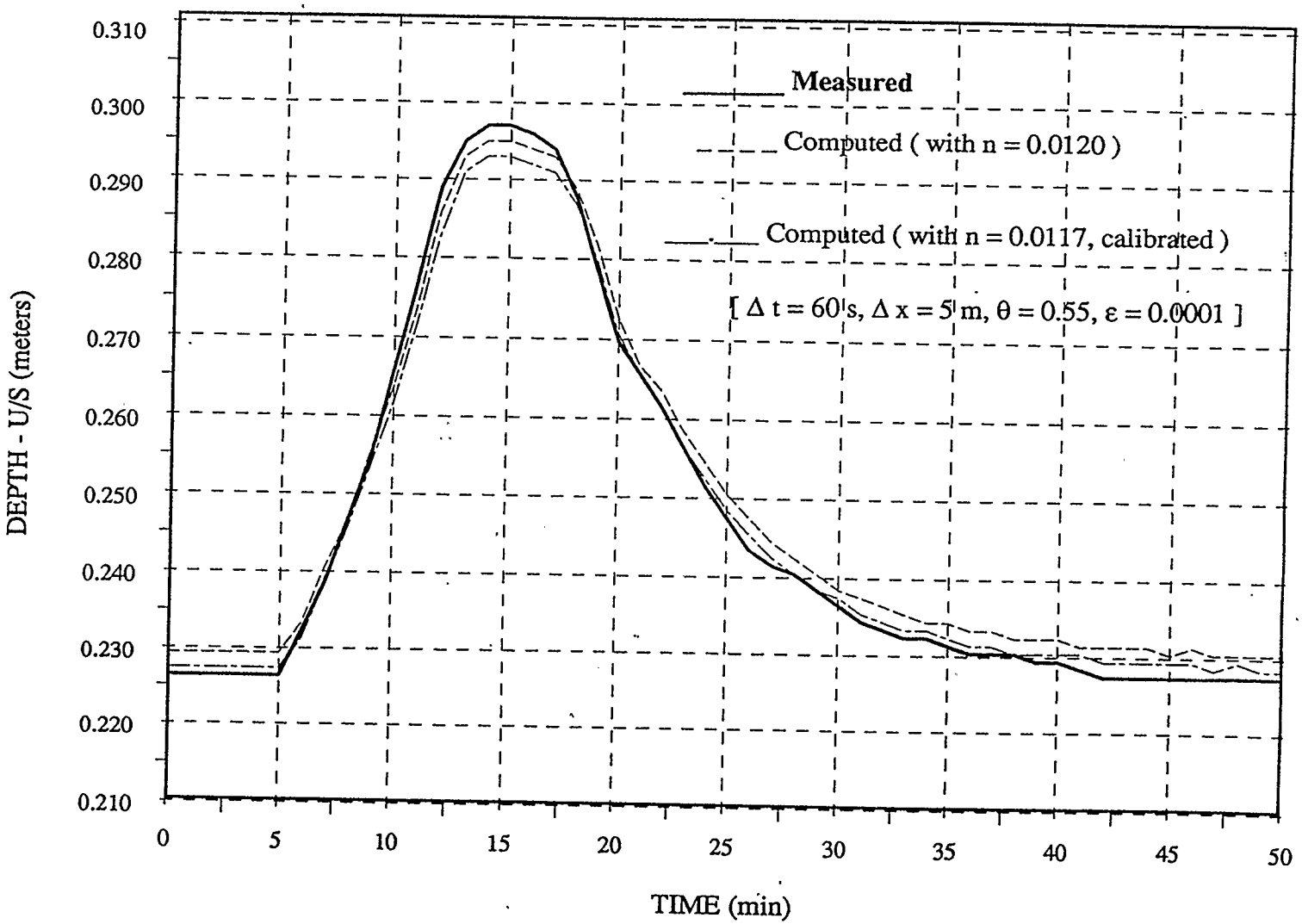

Figure 4.1

Measured and Computed Depth Hydrographs at the Upstream Boundary of Channel Reach in the Verification Procedure

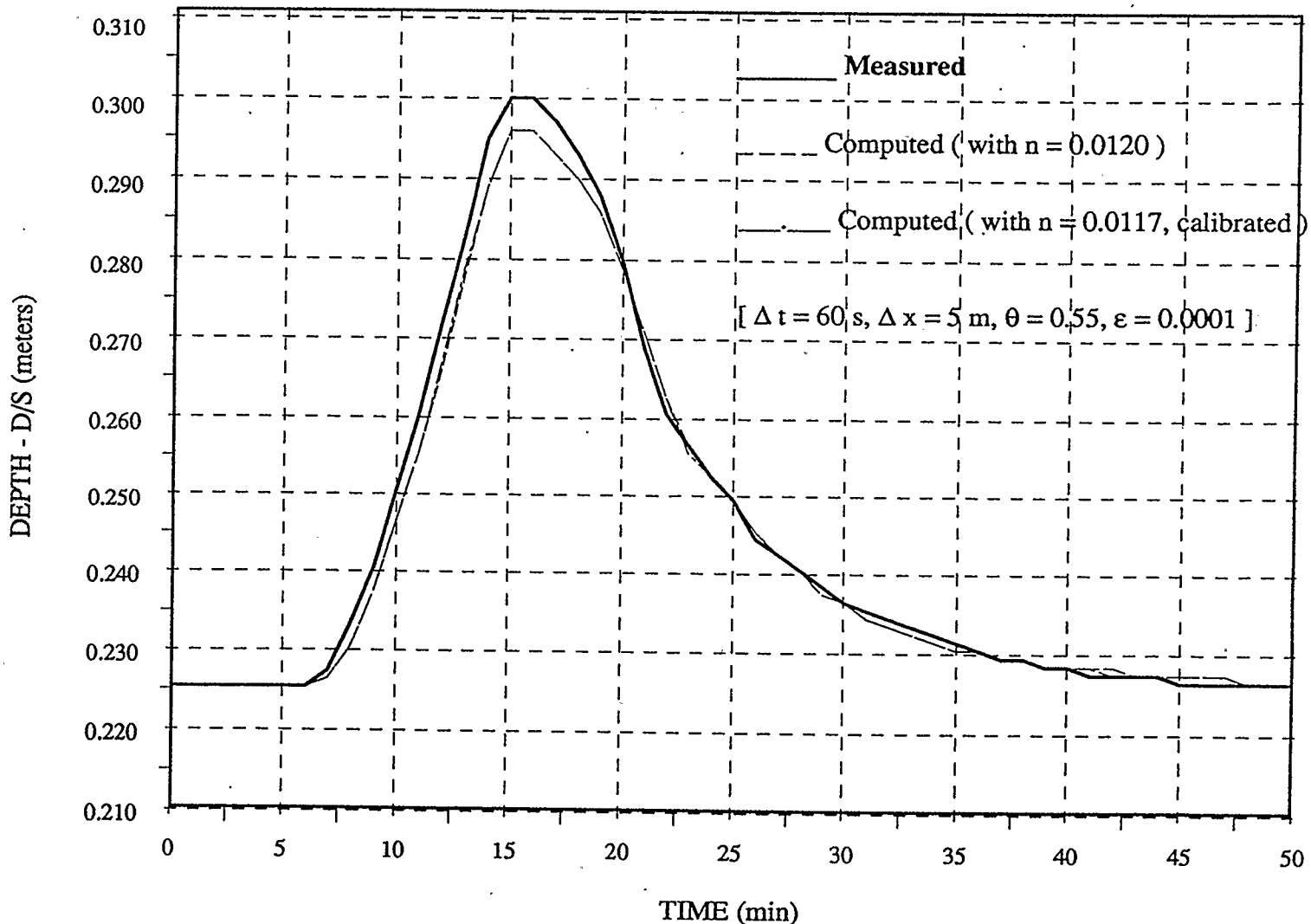

Figure 4.2

Measured and Computed Depth Hydrographs at the Downstream Boundary of Channel Reach in the Verification Procedure

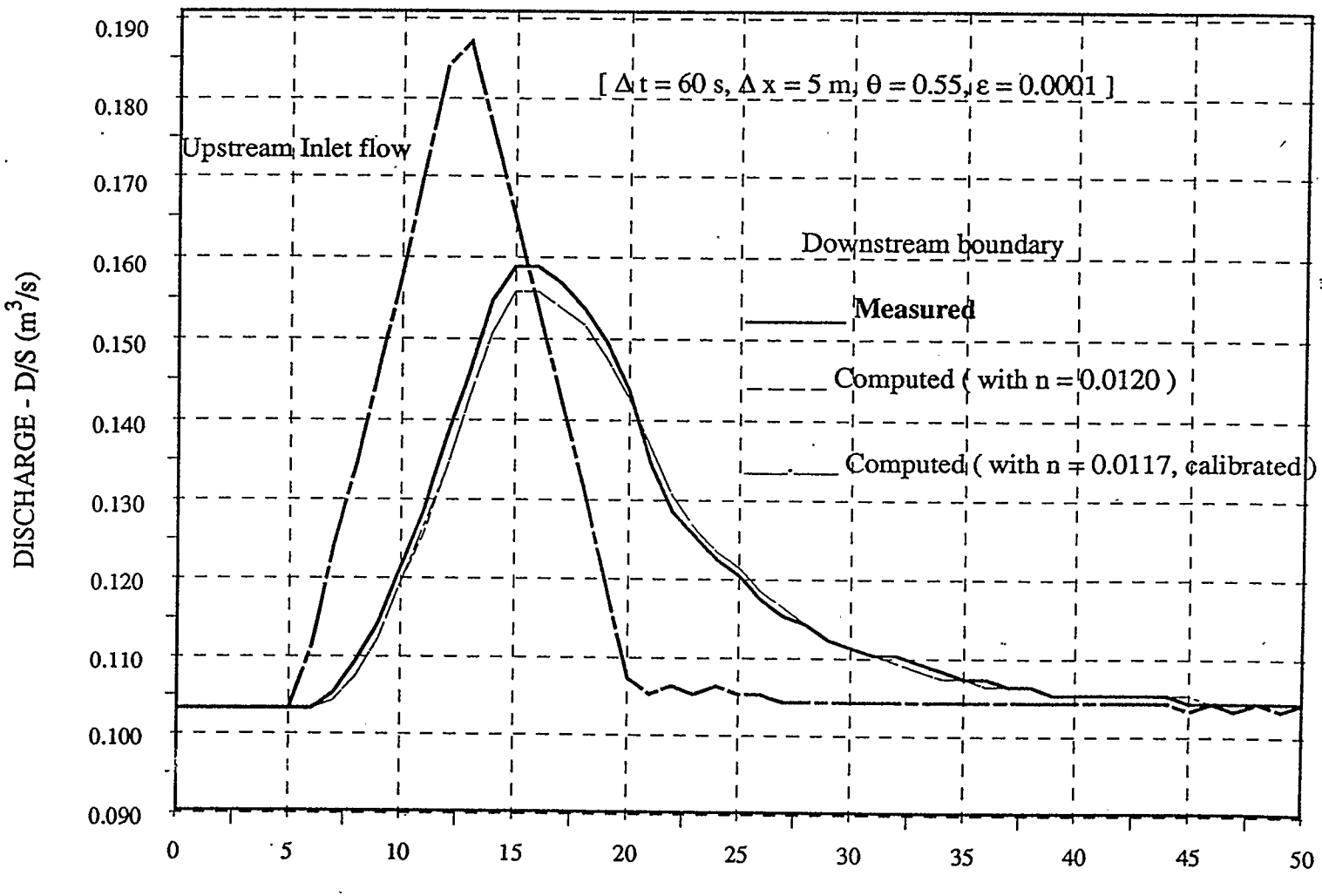

Figure 4.3

Measured and Computed Discharge Hydrographs at the Downstream Boundary and Measured Discharge Hydrographs at the Upstream Boundary of the Channel

and downstream (d/s) locations when n=0.0117 and at the downstream boundary when n=0.0120. However, when n=0.0120 a low 0.7% error was observed at the upstream boundary. The simulated and observed times to peak for discharge hydrographs (i.e. phase shifts) were found to be identical for both values of n. This would indicate that the model predicted the actual travel time rather closely. Figure 4.3 shows that the computed discharge curve is damped slightly and displaced forward in time. Therefore, as observed in Section 3.2.1, the computational time step should be reduced to allow the model to more precisely follow the inflow hydrograph and to more accurately predict the output.

The model satisfactorily simulated Treske's observations as indicated by the high system performance P>99.9% and very low deviations, S when n=0.012 or 0.0117, although it shows a lower performance P when n=0.012 (Table 4.2). The good agreement is verification that the mathematical and numerical formulations of the model are sound within the limitation of a simple prismatic channel at low Froude numbers.

4.3 SENSITIVITY ANALYSIS OF HYDRAULIC CONTROL PARAMETERS

For a particular channel, assuming that any noise (or error) originating from the numerical solution is duplicated in the calibration procedure, the quality of simulation is largely function of three control parameters; resistance coefficient, n (describing the channel roughness), channel bottom slope S_o and cross-section area A of the flow. To evaluate the relative significance of these parameters on the quality of the simulation, a series of simple numerical experiments was performed. The hydraulic control parameters selected for this study which characterize Treske's channel hydraulic components (some of them assumed, some measured) are referred in this study as the standard channel parameters (STD).

4.3.1 VARIATION IN RESISTANCE COEFFICIENT, MANNING'S N

Various techniques of determining the flow resistance coefficient, n value, from measurable prototype data have appeared in several publications (Baltzer and Lai (1968); Fread and Smith (1978), Schaffranek et al (1981) (referred in ref. French, 1978)).

It is a common practise to consider the resistance coefficient n as constant in a particular reach (when evaluated indirectly through the use of measurable prototype data or estimated). The acceptance of the constant n is due to the complexities associated with handling a friction factor with variable values and also the estimation of these values in the different sections of the reach.

The objectives of this study are to demonstrate the effects of error in estimation of resistance coefficient, n, on model output error and demonstrate a simple but efficient trial and error method to determine the optimum n value. Accuracy assessment is performed using Equations (4.1), (4.2), (4.3) and (4.4) to evaluate errors between predicted and measured depths.

4.3.1.1 NUMERICAL EXPERIMENTS

Three series of numerical experiments were performed. They consisted of:

1. Examination of the sensitivity and variation of resistance coefficient on error in predicting depth hydrographs at the upstream and downstream boundary and the discharge hydrograph at the downstream boundary.
2. Demonstration of the technique for calibrating model for variable resistance coefficient, using comparisons of observed and predicted depth hydrographs at the upstream and downstream boundary.
3. Examination of the sensitivity of variation of resistance coefficient on downstream depth hydrograph from channels of varying length.

4.3.1.2 RESULTS

The impact of the variation of resistance coefficient, n, on the depth at the upstream and downstream ends of the channel is shown in Figures 4.4 and 4.5 respectively. Additional more-detailed information is illustrated in Figure B.1(a) to (e) and Figure B.2(a) to (e) in Appendix B. Variations of the downstream depth hydrograph and discharge hydrograph were found to be similar. It was clearly unnecessary to present both types of information. The downstream depth hydrograph information was chosen to illustrate relationship to the upstream depth hydrograph. It is clear that variation in n has a much more significant effect on depth hydrograph at the upstream boundary than at the downstream boundary. The upstream depth hydrograph exhibits significant inverse relationship to n without observable phase shift. The downstream depth hydrograph exhibits very little change in response to variation of n except for minor phase shifts which increase slightly with n.

The model calibration procedure for consideration where n is the unknown variable was performed using a series of experiments in which n was varied from 0 to 0.0360, (Treske suggested the value of n to be 0.0120). For each experiment the quality of the predicted depth hydrographs at the upstream and downstream boundary was evaluated using the root mean square error and system performance as defined by equations (4.1) and (4.4) and phase shift. These results are tabulated in Table 4.3 and plotted in Figures 4.6 and 4.7. From examination of the figures, it is evident that the root mean square error and system performance are particularly sensitive to analysis of depth hydrographics at the upstream boundary. The downstream depth hydrographs exhibited very little or no sensitivity. The best n value was determined to be 0.0117 and not 0.0120 as suggested by Treske. Visual examination of the upstream and downstream depth hydrographs with variation of n as shown in Figures 4.8(a) and (b) and 4.9(a) and (b) would not have permitted as refined an estimate of n.

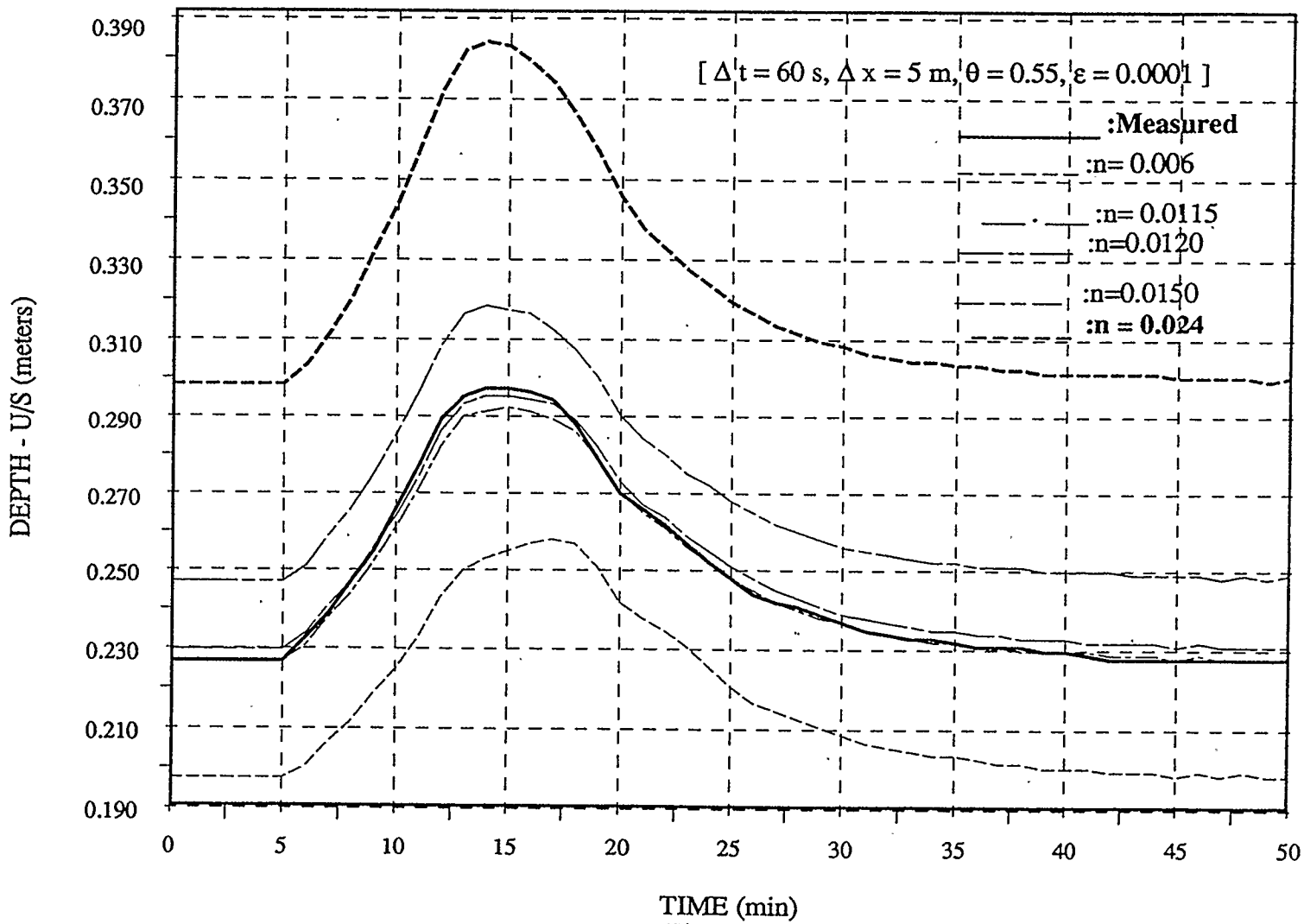

Figure 4.4

Measured and Computed Depth Hydrographs at Upstream Boundary of the Channel Reach for Varying Resistance Coefficient

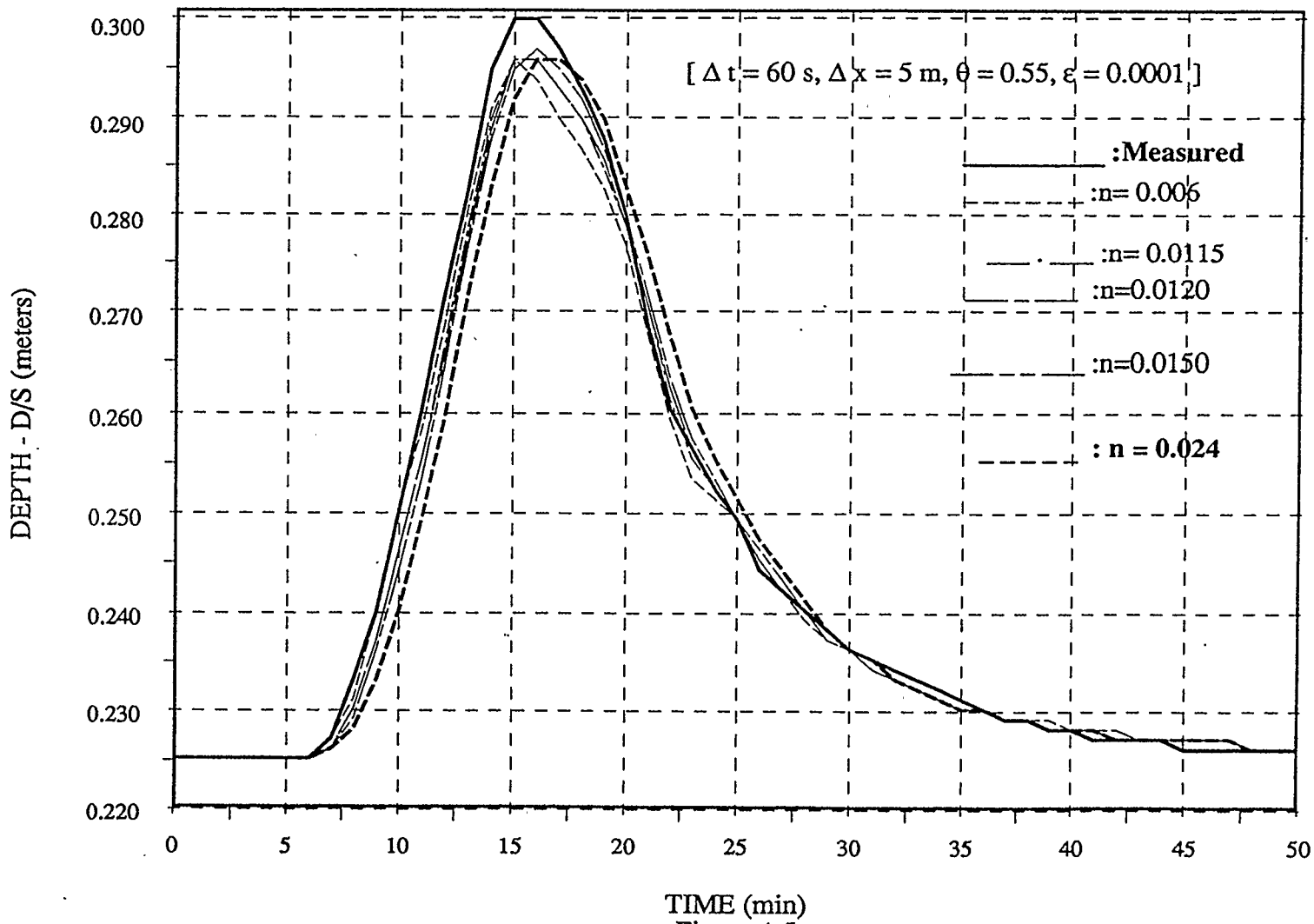

Figure 4.5

Measured and Computed Depth Hydrographs at Downstream Boundary of the Channel Reach for Varying Resistance Coefficient

Table 4.3
Summary of Deviation of Model Output from Measured Values in Terms of Root Mean Squares (S) and System Performance Variable (P) and phase shift for various values of Resistance Coeficient n in the Calibration Procedure

n	PHASE SHIFT*	S_u m (RS_u %)	S_d m (RS_d %)	P_u %	P_d %
0.0000	2.0	0.0469 (15.86)	0.0026 (0.86)	96.3776	99.9890
0.0030	2.0	0.0426 (14.39)	0.0024 (0.79)	97.0177	99.9907
0.0060	2.0	0.0313 (10.58)	0.0021 (0.71)	98.3877	99.9924
0.0090	2.5	0.0159 (5.36)	0.0019 (0.63)	99.5864	99.9941
0.0100	2.5	0.0103 (3.49)	0.0020 (0.67)	99.8249	99.9933
0.0105	2.5	0.0075 (2.52)	0.0020 (0.66)	99.9083	99.9936
0.0110	2.5	0.0047 (1.59)	0.0019 (0.65)	99.9636	99.9937
0.0115	2.5	0.0024 (0.80)	0.0020 (0.68)	99.9908	99.9931
0.0117	2.5	0.0021 (0.69)	0.0021 (0.69)	99.9932	99.9928
0.0120	2.5	0.0027 (0.92)	0.0022 (0.72)	99.9878	99.9922
0.0125	2.5	0.0052 (1.75)	0.0021 (0.71)	99.9561	99.9927
0.0130	3.0	0.0081 (2.73)	0.0021 (0.71)	99.8929	99.9926
0.0140	3.0	0.0139 (4.69)	0.0024 (0.81)	99.6832	99.9903
0.0160	3.0	0.0260 (8.78)	0.0027 (0.91)	98.8902	99.9877
0.0180	3.0	0.0382 (12.89)	0.0030 (1.00)	97.6043	99.9852
0.0200	3.0	0.0501 (16.92)	0.0034 (1.15)	95.8758	99.9803
0.0220	3.0	0.0620 (20.93)	0.0038 (1.29)	93.6899	99.9754
0.0240	3.5	0.0735 (24.84)	0.0043 (1.40)	91.1102	99.9690
0.0360	4.5	0.1393 (47.05)	0.0066 (2.19)	68.1179	99.9284

* Phase shift equal to time (min) between peak inflow and outflow: Actual phase shift for Treske's experiment is 2.5 min. If computed phase shift (ph_c) is: (a) $ph_c < 2.5$ than, advance in phase; (b) $ph_c = 2.5$ than, no phase shift; (c) $ph_c > 2.5$ than, lag in phase.

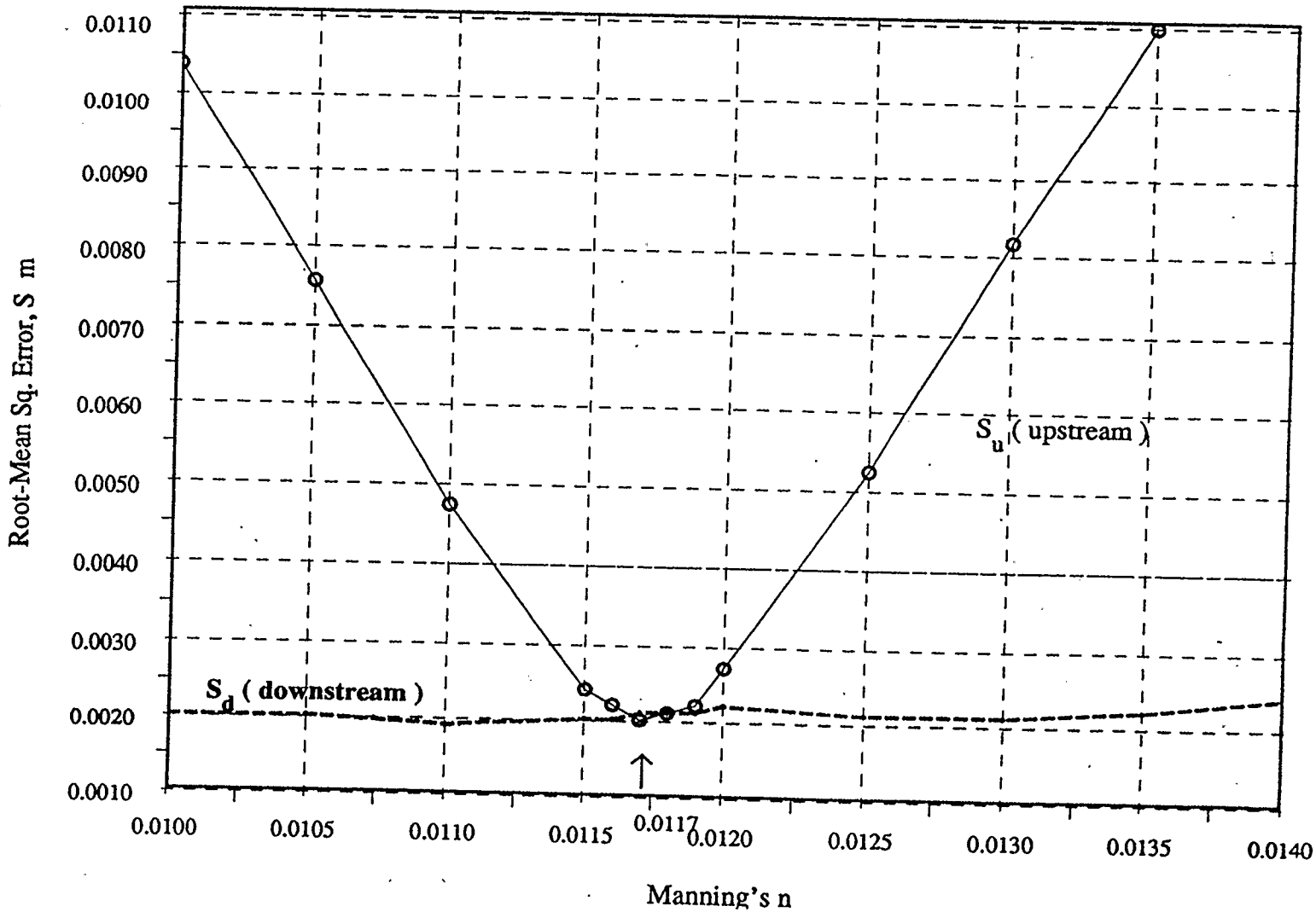

Figure 4.6

Root mean Square Error of Depth Hydrographs at the Upstream and Downstream Boundary as a Function of Resistance Coefficient

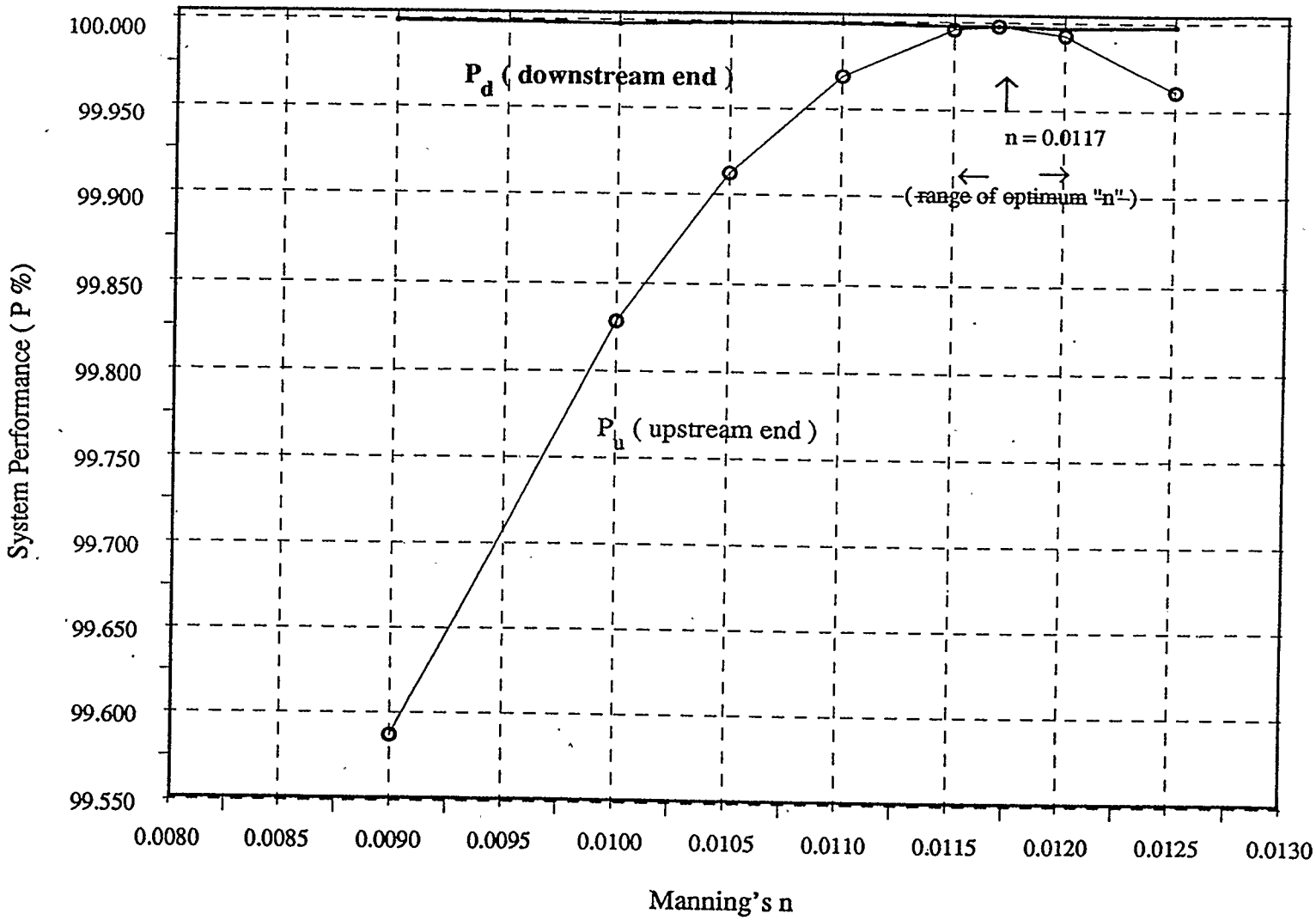

Figure 4.7
System Performance Evaluated using Depth Hydrographs at the Upstream and Downstream Boundary as a Function of Resistance Coefficient

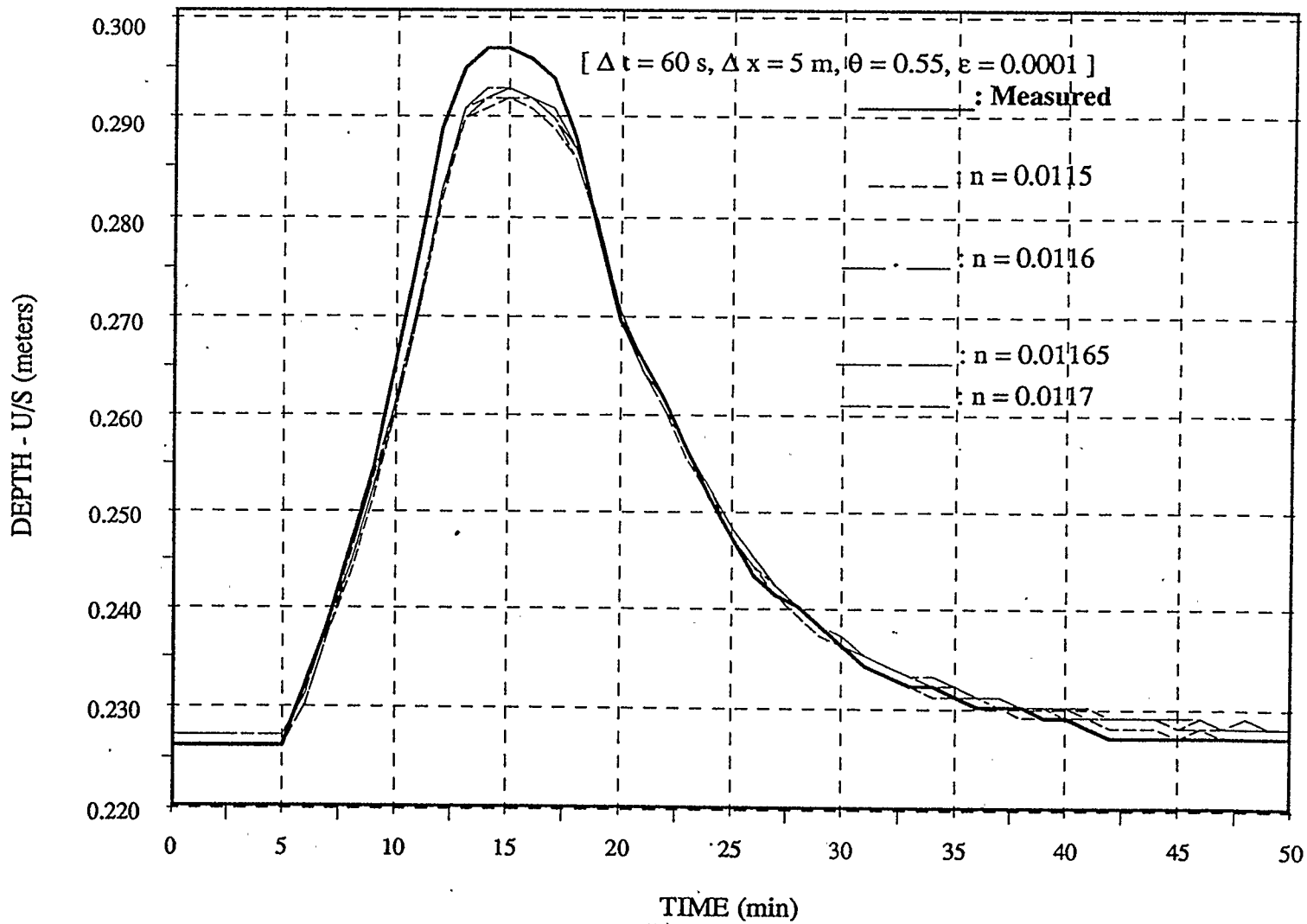

Figure 4.8 (a)

Measured and Computed Depth Hydrographs at Upstream Boundary of the Channel Reach for Varying Resistance Coefficient ($0.0115 \leq n \leq 0.0117$)

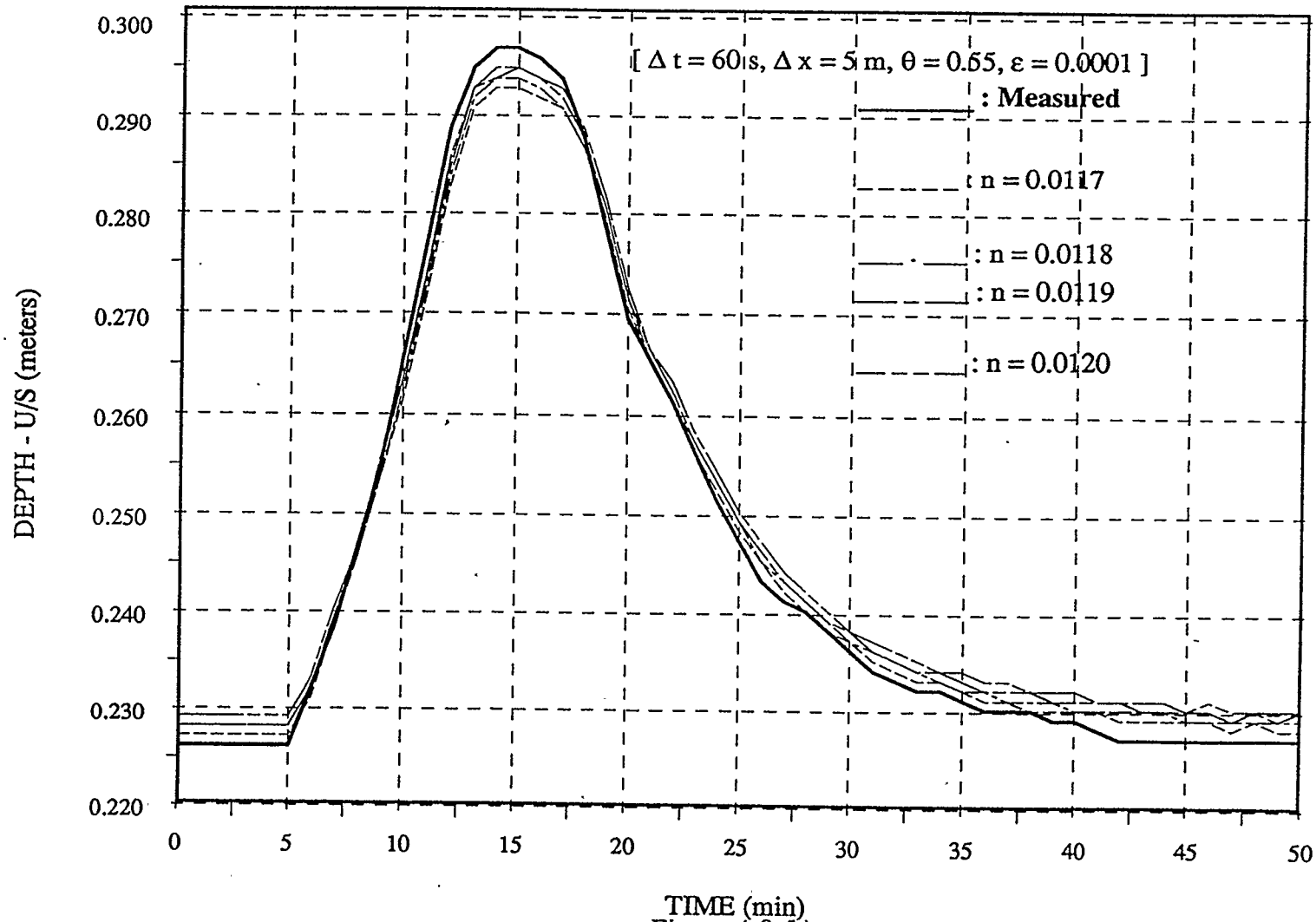

Figure 4.8 (b)

Measured and Computed Depth Hydrographs at Upstream Boundary of the Channel Reach for Varying Resistance Coefficient ($0.0117 \leq n \leq 0.0120$)

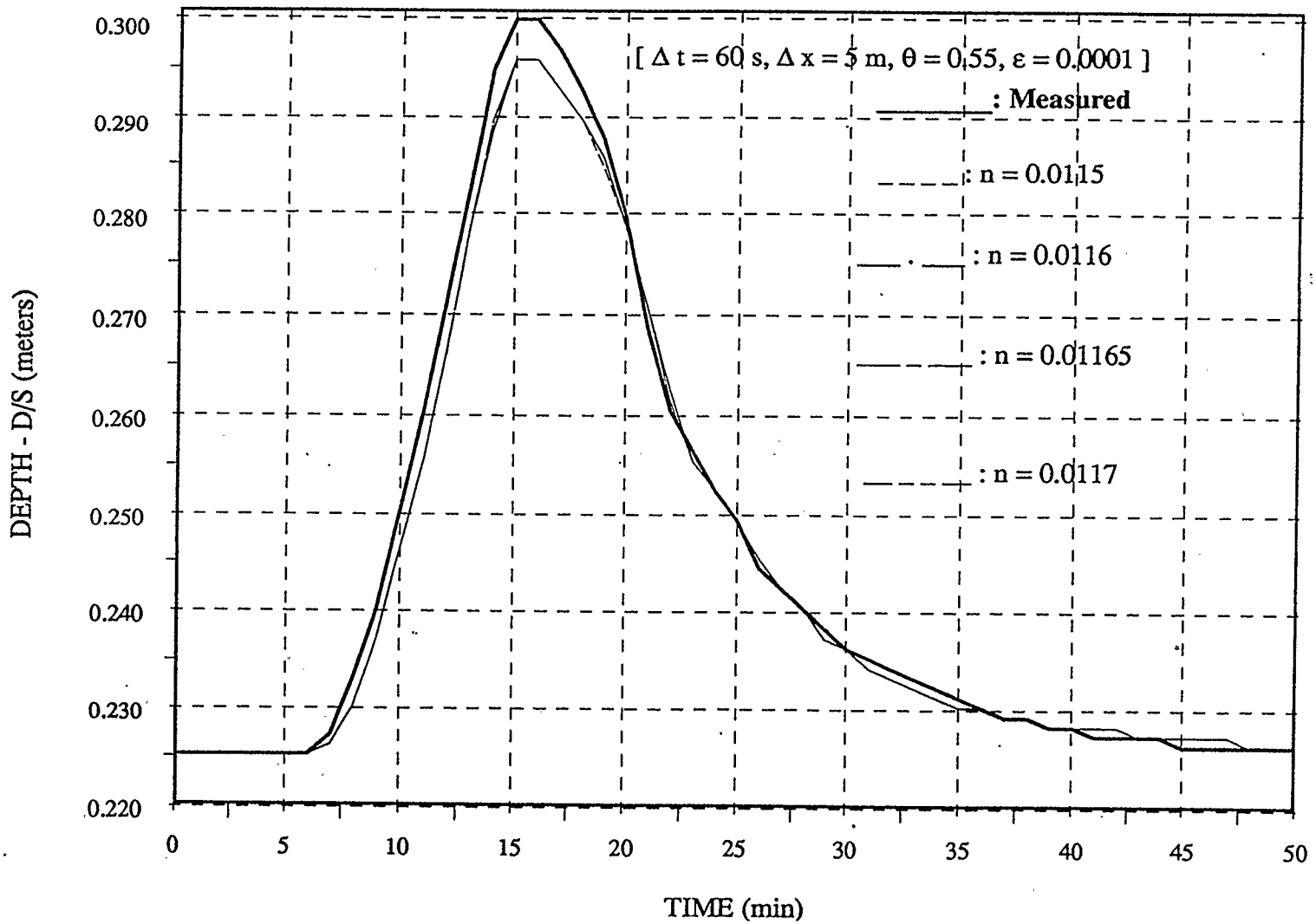

Figure 4.9 (a)

Measured and Computed Depth Hydrographs at Downstream Boundary of the Channel Reach for Varying Resistance Coefficient ($0.0115 \leq n \leq 0.0117$)

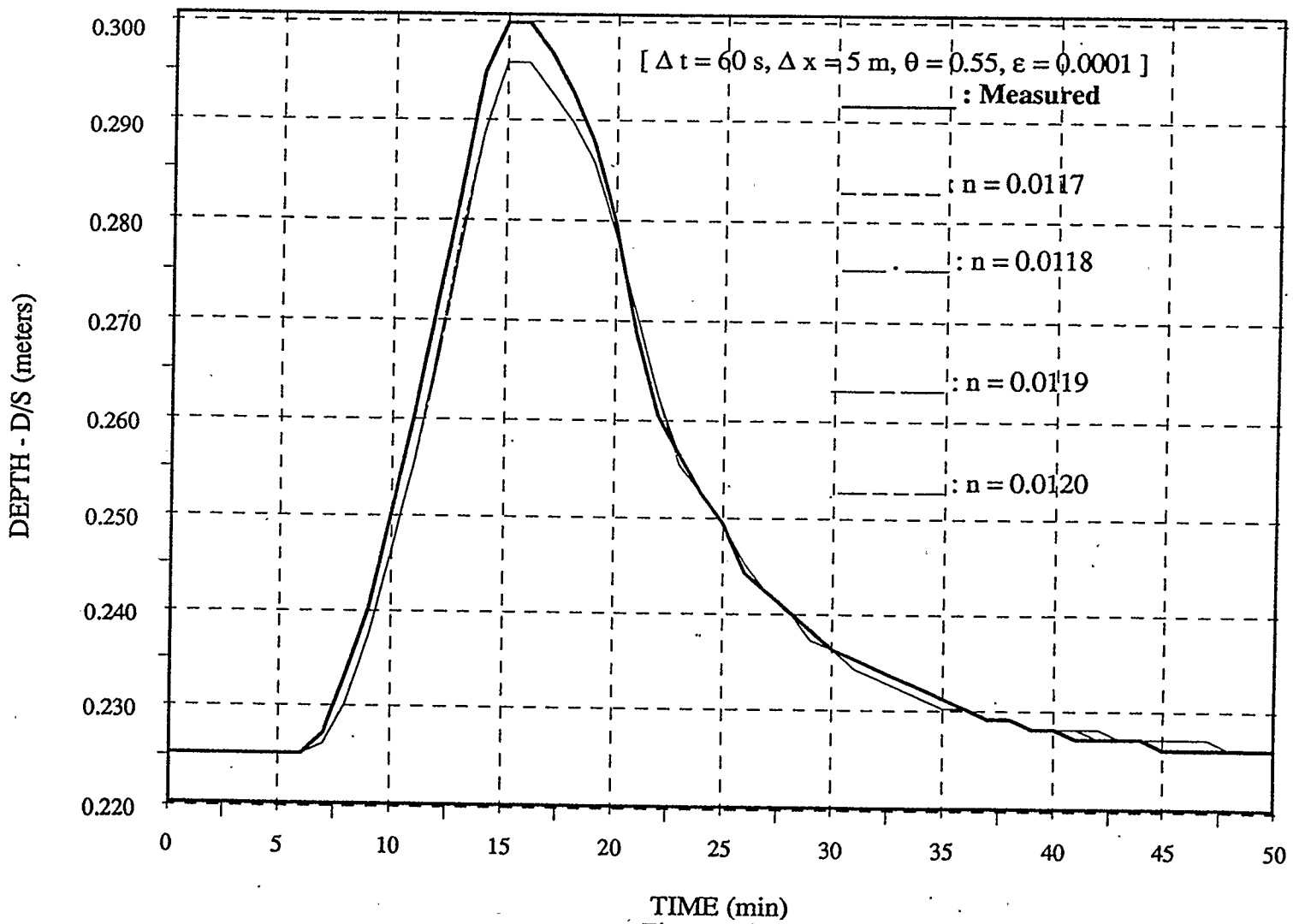

Figure 4.9 (b)

Measured and Computed Depth Hydrographs at Downstream Boundary of the Channel Reach for Varying Resistance Coefficient ($0.011 \leq n \leq 0.0120$)

The impact of the variation of resistance coefficient on the downstream depth hydrograph for channels of varying lengths are shown in Figures 4.5 and 4.10(a), (b) and (c). Figure 4.5 shows results for standard Treske channel (210 m), Figure 4.10(a), (b) and (c) show results for channels 150%, 180% and 200% of the standard Treske channel. It may be observed that with increasing channel length, increases in n result in greater dampening and phase shift effects.

4.3.2 VARIATION IN CHANNEL BOTTOM SLOPE (S_o)

The channel bed slope is a measure of the reach geometry. It is common practise to neglect error in the channel bottom slope term and its effect is compensated, as far as possible, by adjustment of the resistance coefficient (using Manning's n or Chezy's C). The reasons for the error in bottom slope are that natural or artificial channels are very flat and irregular along the channel length. The problems in estimating the bottom slope may be attributed to data errors, surveying inaccuracies, vertical displacement of gauging structures and recorder malfunction or improper use. In the case of Treske's channel, bottom slope was easily and accurately determined using the channel bed elevations at upstream and downstream ends and reach length (L=210 m). Adjustment of resistance coefficient alone permitted adequate calibration of the model.

The objectives of this study are to demonstrate the effects of error in estimation of channel bottom slope.

4.3.2.1 NUMERICAL EXPERIMENTS

The value of the bed slope, S_o, was varied from 0.0 (flat) to 0.0019 by adjusting the bed elevation at upstream end of the channel reach. Other channel conditions remain constant as specified in Table C.1 (Appendix C). A value of Manning's n=0.012 was used.

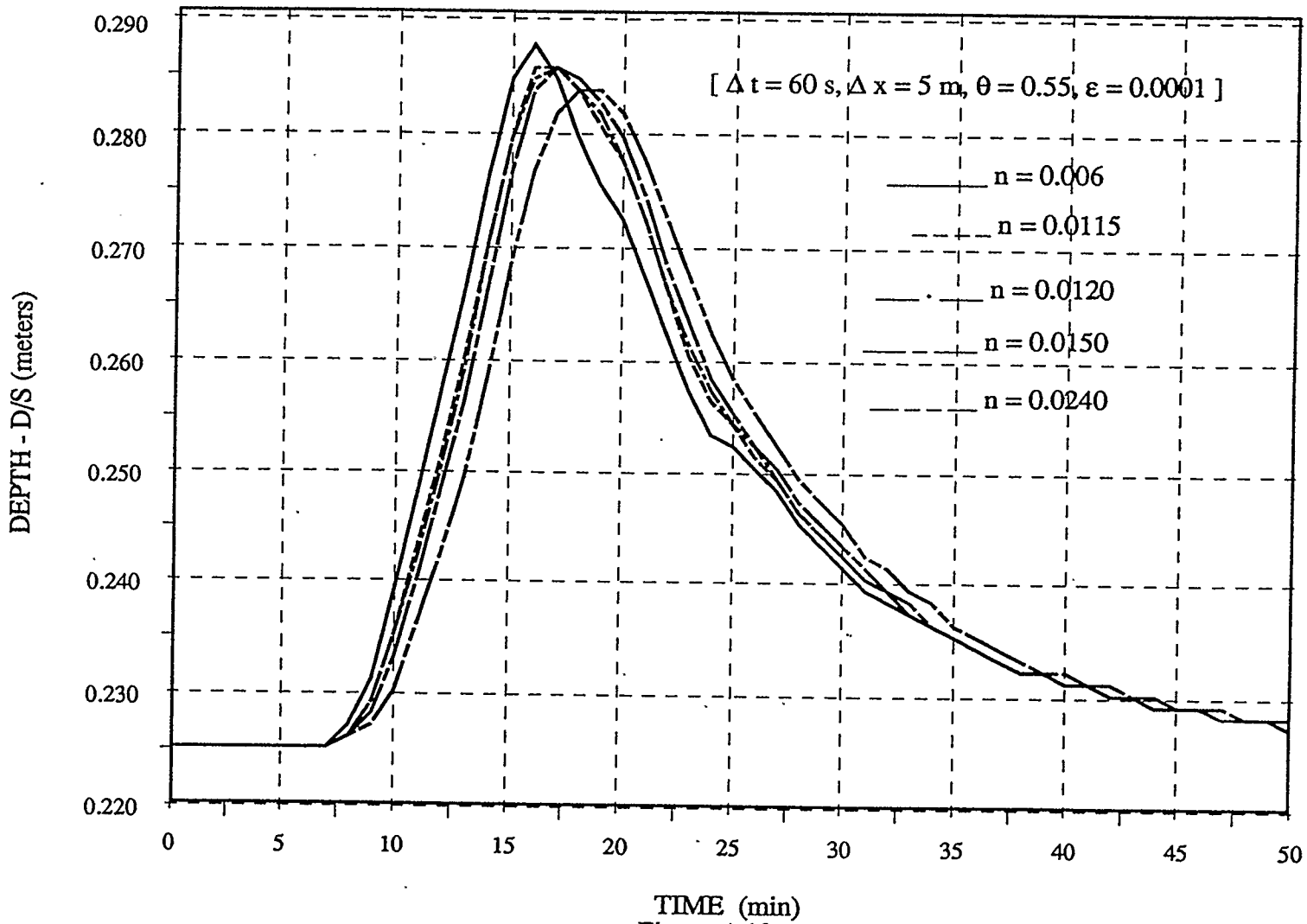

Figure 4.10 (a)
Computed Depth Hydrographs at Downstream Boundary of the Channel Reach Length, L=315m (1.50 x 210) for Varying Resistance Coefficient

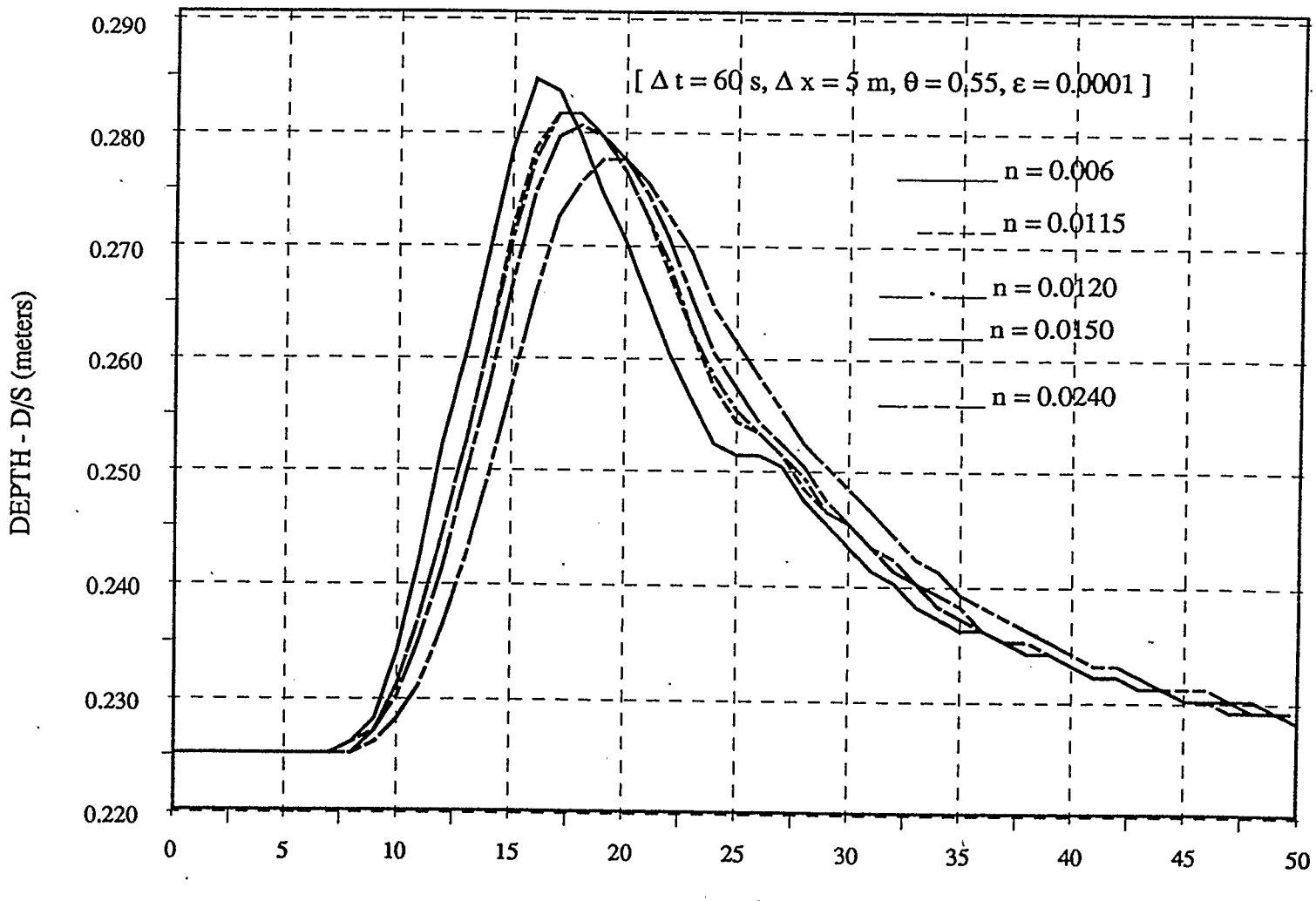

Figure 4.10 (b)

Computed Depth Hydrographs at Downstream Boundary of the Channel Reach Length, L=378m (1.80 x 210) for Varying Resistance Coefficient

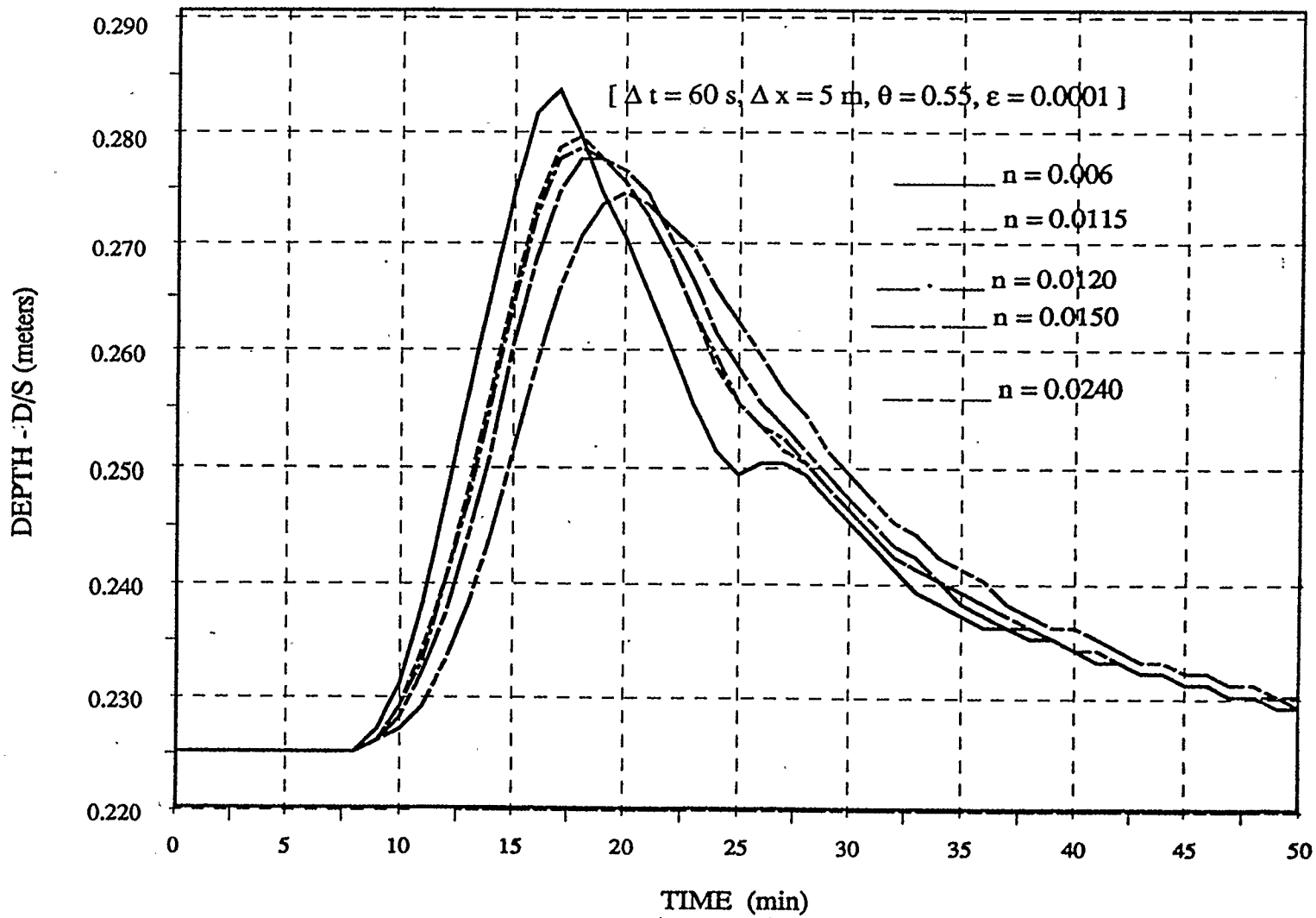

Figure 4.10 (c)

Computed Depth Hydrographs at Downstream Boundary of the Channel Reach Length, L=420m (2.0 x 210) for Varying Resistance Coefficient

4.3.2.2 RESULTS OF NUMERICAL EXPERIMENTS

The effect of varying channel bottom slop on discharge hydrographs at the downstream boundary and the depth hydrograph of the upstream boundary are shown in Figures 4.11 and 4.12 (recall that the depth and discharge hydrograph at the downstream are similar). In addition, more detailed information is illustrated in Figures B.3(a) to (e) and B.4(a) to (e). It may be noted that variation in channel bottom slope had a relatively minor effect on the characteristics of the downstream discharge hydrograph when compared to the significant effect on the upstream depth hydrograph. As expected, maximum upstream depths were observed for very flat slopes and maximum downstream depths (and discharge) were observed for steep slopes. Variation in channel slope does not affect phase shift of the hydrographs at either the upstream or downstream boundary.

4.3.3 VARIATION IN CROSS-SECTION AREA (A)

It is important to note that the form of the St. Venant equation used in the preceding and following experiments can only be used to consider prismatic channels. If applied to non-prismatic channels serious errors in estimation may result (see Halliwell and Ahmed, 1973). The objective of this series of experiments is to investigate the effect of variations in estimation of channel geometry, in this case channel width, b, on model prediction of depth and discharge hydrographs.

4.3.3.1 NUMERICAL EXPERIMENTS

The value of channel width, b, was varied from 0.625 m to 2.50 m, that is, from one-half of standard width to twice standard width. Three values of Manning's n equal to 0.0105, 0.0120 and 0.0135 were considered.

4.3.3.2 RESULTS OF NUMERICAL EXPERIMENTS

The effects of varying channel width on the depth hydrograph at the upstream boundary and the depth and discharge hydrograph at the downstream boundary are shown

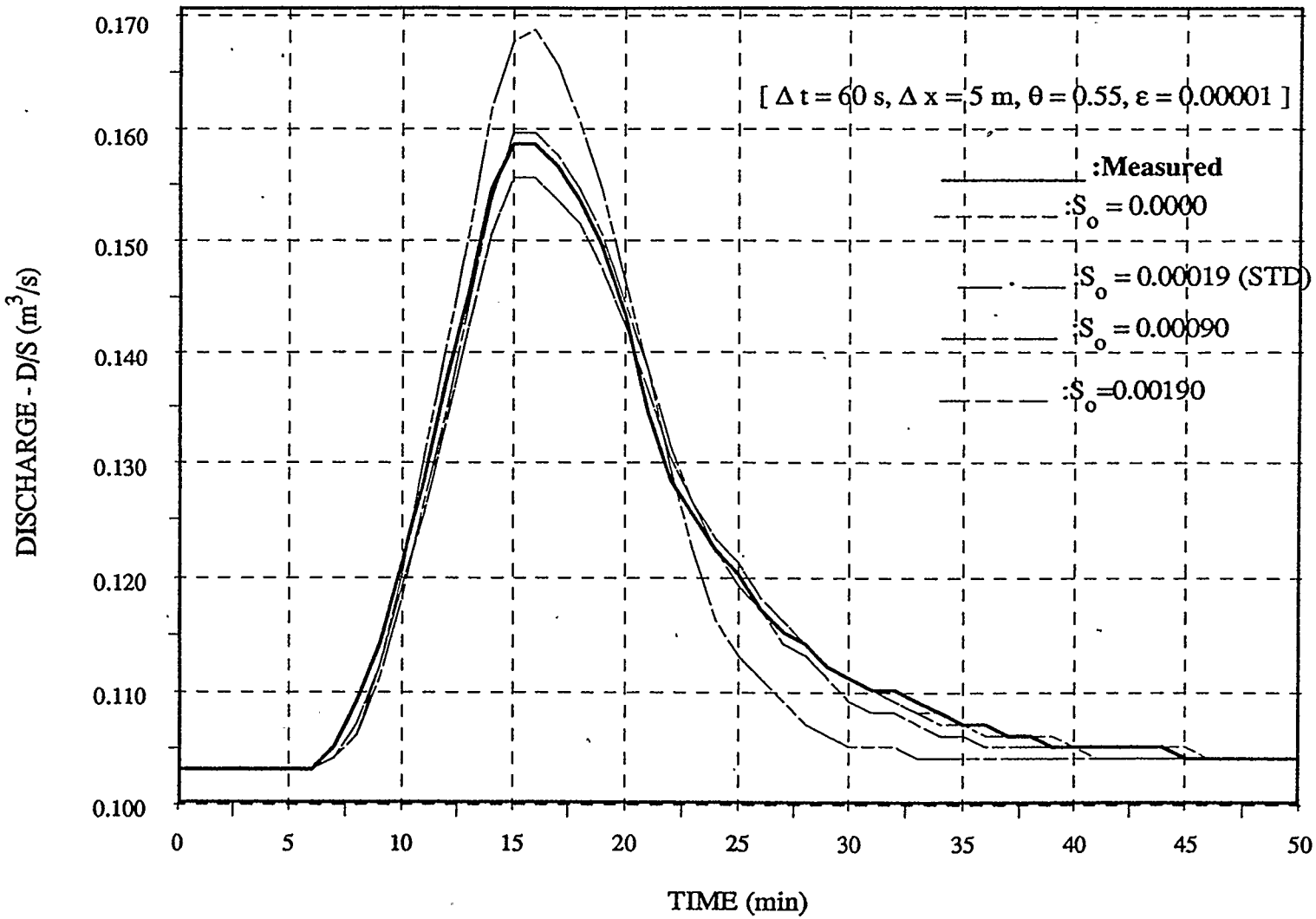

Figure 4.11
Measured and Computed Discharge Hydrographs at Downstream Boundary of the Channel Reach for Varying Channel Bottom Slope

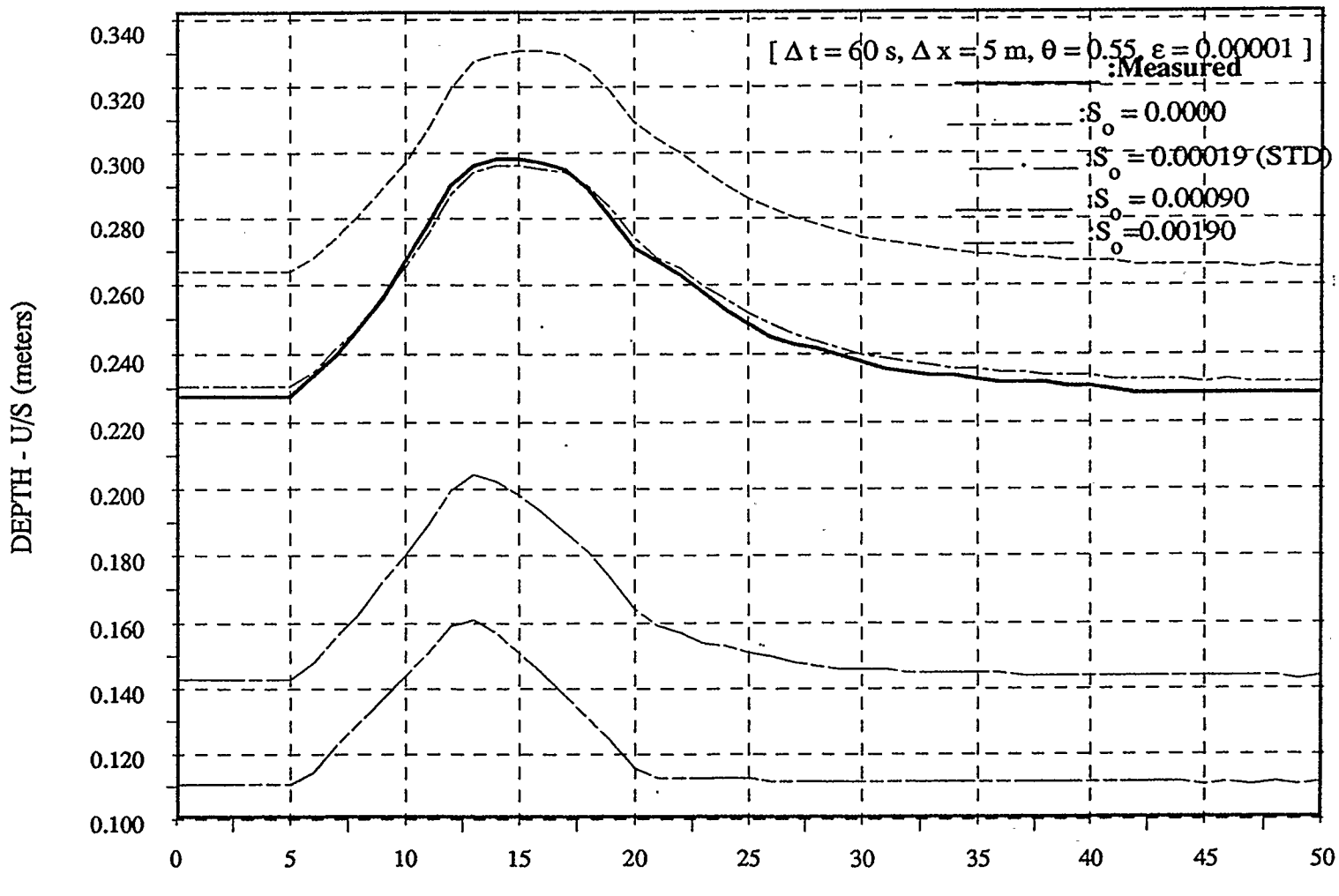

Figure 4.12
Measured and Computed Depth Hydrographs at Upstream Boundary of the Channel Reach for Varying Channel Bottom Slope

in Figures 4.13, 4.14 and 4.15 respectively for n=0.0120. (Note that the depth and discharge hydrographs at the downstream reach are similar; however, the effect of variations in bottom width is relatively more pronounced in the depth hydrograph.) It may be noted that variation in bottom width has a much greater effect on upstream depth than downstream depth; however, both upstream and downstream depth hydrographs varied similarly to changes in bottom width. That is, when bottom width increased, both hydrographs tended to dampen. Only the downstream hydrograph exhibited a lagging phase shift and then only when the error was very large.

The effect of incremental variations in channel width on the upstream and downstream depth hydrographs for values of Manning's n equal to 0.0105 are shown in Figure B.5(a) to (d) in Appendix B. Hydrographs for Manning's n=0.0120 are shown in Figure B.6(a) to (d). Similarly, hydrographs for Manning's n=0.0135 are shown in Figures B.7 (a) to (d). Careful examination of these results indicates that errors in estimation of channel width can be compensated for by varying the resistance coefficient. This is particularly evident in the upstream depth hydrograph.

4.4 SUMMARY OF RESULTS

The numerical simulation properties of a computer model which employed the weighted four point implicit method of solution of the unsteady open channel flow equation have been investigated in two parts, verification and calibration.

The verification process employed high quality experimental data obtained by Treske (1980). The model, when using appropriate hydraulic control parameters and boundary conditions, successfully predicted the measured flow conditions and may be considered verified.

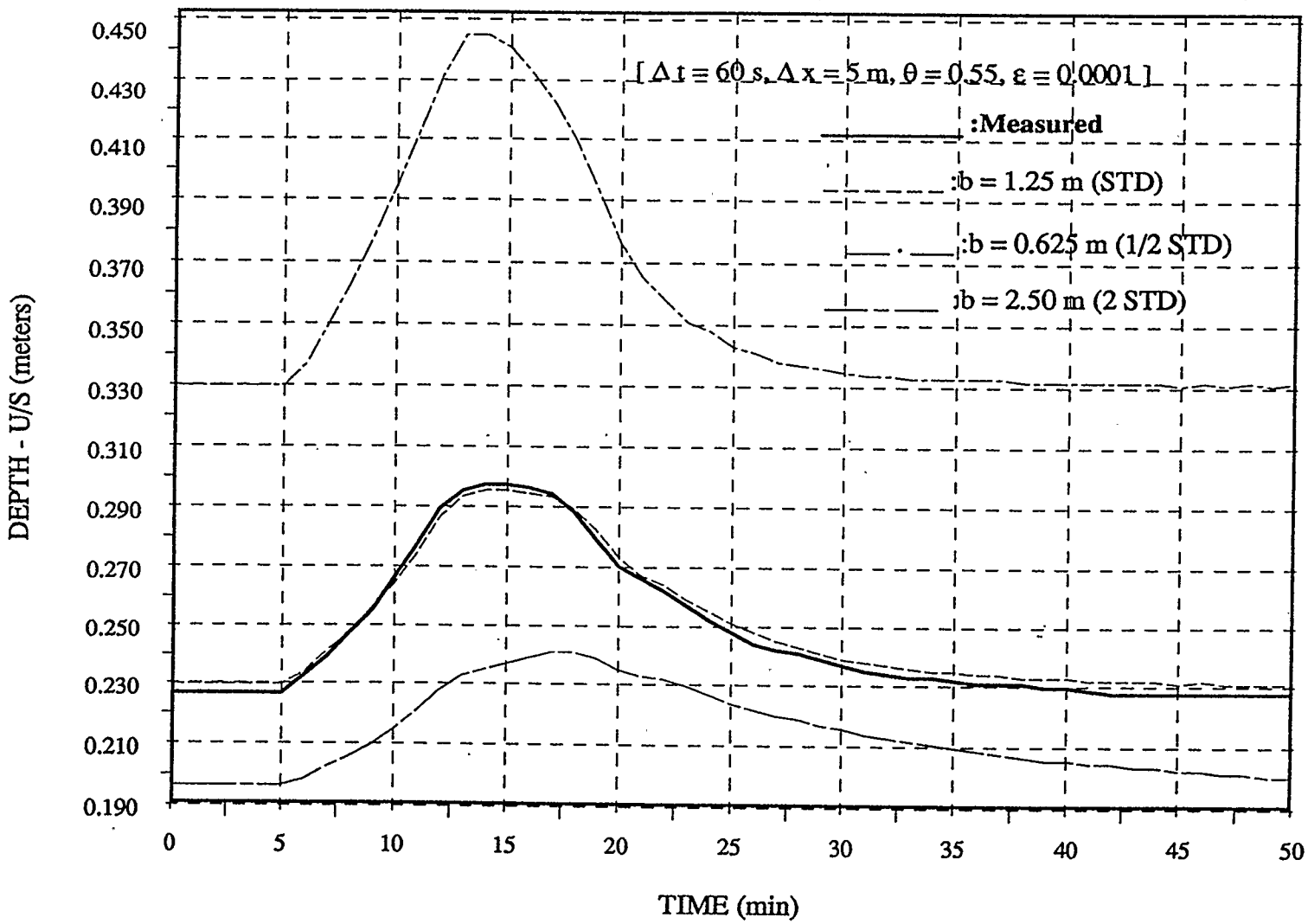

Figure 4.13

Measured and Computed Depth Hydrographs at Upstream Boundary of the Channel Reach for Varying Channel Width

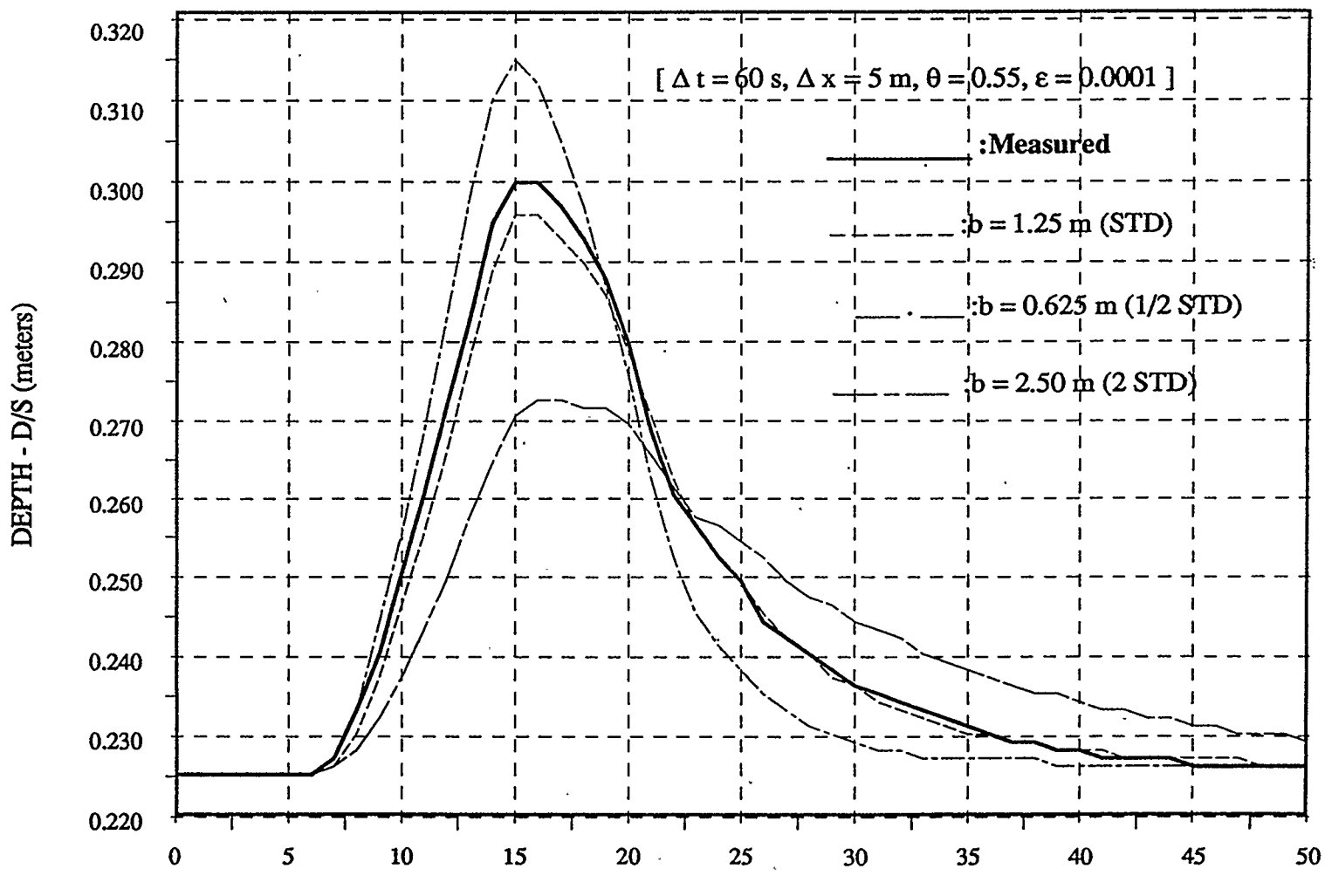

Figure 4.14

Measured and Computed Depth Hydrographs at Downstream Boundary of the Channel Reach for Varying Channel Width

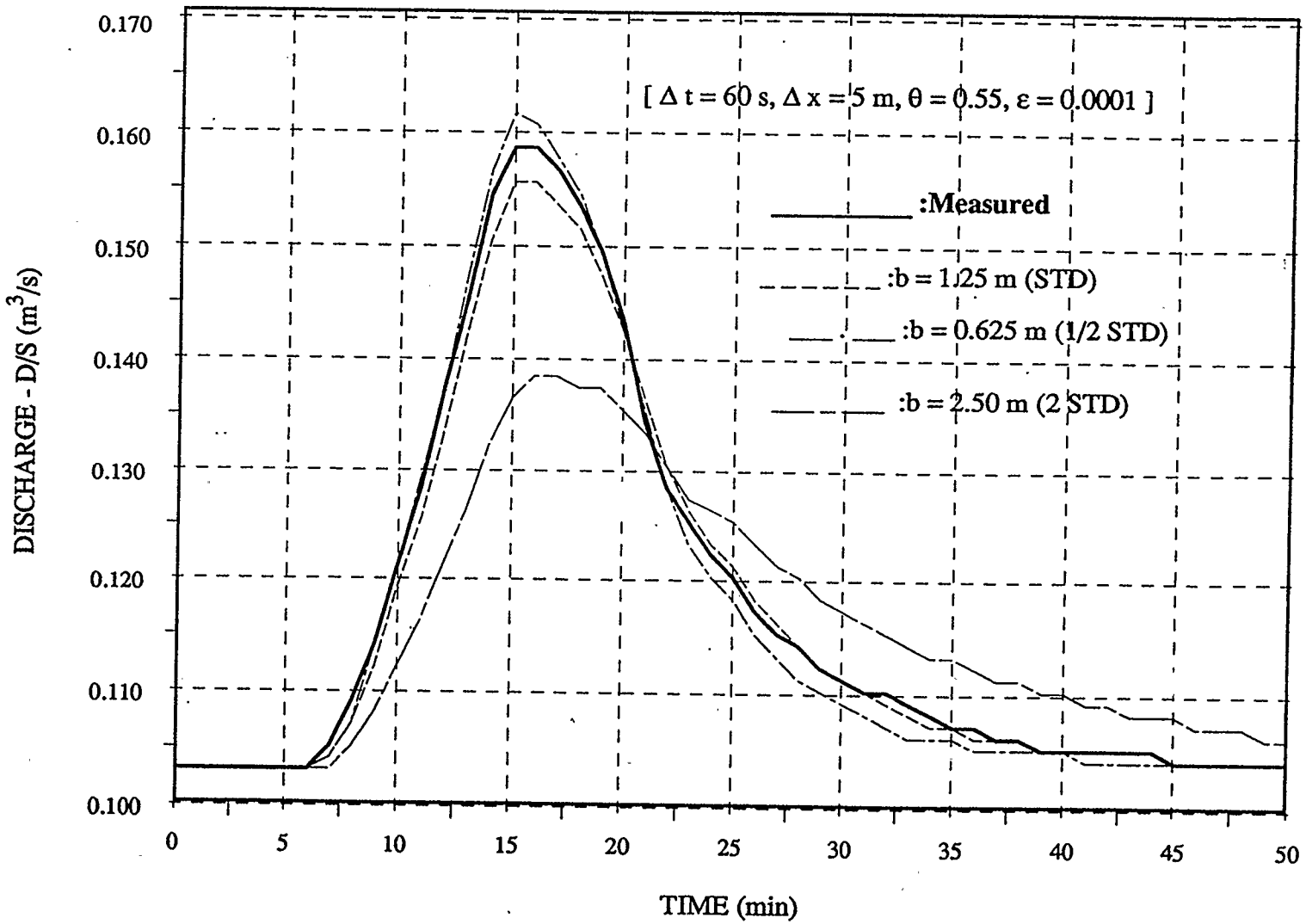

Figure 4.15

Measured and Computed Discharge Hydrographs at Downstream Boundary of the Channel Reach for Varying Channel Width

A summary of the results of the calibration experiments is shown in Table 4.4. Using this table strategies for performing calibration studies may be developed for situations where hydraulic control parameters unknown error. Also methods were developed and demonstrated by which optimum values of resistance coefficient could be estimated. The same technique could also be used to estimate optimum channel slope and cross-sectional geometry.

Table 4.4
Summary of Calibration Experiments

	Increase in n	Increase in S_0	Increase in b
upstream boundary	1. magnifies 2. no phase shift	1. dampens 2. no phase shift	1. dampens 2. no phase shift
downstream boundary	1. dampens 2. lagging phase shift	1. magnifies 2. no phase shift	1. dampens 2. very small lagging phase shift
POSSIBLE EFFECTS 1. dampening / magnifying of hydrograph 2. leading or lagging phase shift of hydrograph			

CHAPTER 5: CONCLUSION AND RECOMMENDATION

5.1 CONCLUSION

The numerical and simulation properties of the weighted four-point implicit finite difference scheme for hydraulic routing of unsteady open channel flows was investigated. This included an evaluation of the stability, convergency, verification and factors affecting the calibration properties of the method. Experimental data obtained by Treske (1980) was used extensively for all phases of the research, particularly the verification and calibration.

The stability and convergence properties of the weighted four-point implicit finite difference scheme are summarized as follows:

1. When values of time and distance interval are selected such that the term $\Delta t/\Delta x \cdot C \approx 1$, simulations can be expected to be stable and convergent and provide a more accurate representation of the flow profile. However, if values of distance increment are selected much greater than Δx_c, serious instabilities may result.

2. The time interval must be chosen sufficiently small to ensure adequate detail of the flow is provided to the numerical model.

3. The maximum value of time interval which would ensure solution stability decreases as the relative change in abrupt increase or decrease in flow increases, convergence considerations withstanding.

4. The magnitude of the time interval had a much greater impact on solution convergence than either distance interval or weighting factor.

5. The maximum value of time interval which would ensure solution stability appears to be less for flow increases as compared to decrease in flow of similar magnitude.

6. A value of weighting coefficient approaching 0.6 permits stable, convergent and accurate representation of the wave profile of abruptly varying flow. Weighting coefficients approaching 0.55 may be successfully used for changes in flow which are not abrupt.

7. If values of time and distance interval are selected such that the term $\Delta t/\Delta x \cdot C = 1$, the convergence criteria appears to have a negligible effect on solution results.

Using the high quality experimental data obtained by Treske 1980, the appropriately configured simulation model which employed the weighted four-point implicit method was verified. The model successfully predicted the measured flow conditions and may be considered verified.

Methods for calibration of the model of unsteady flow were developed. These methods were used to refine estimation of the resistance coefficient of the channel used by Treske to obtain his observation. This technique could also be used to estimate optimum channel slope and cross-sectional geometry. A number of numerical experiments were performed to obtain some knowledge of the significance of the various channel hydraulic control parameters affecting the calibration procedure. These are summarized in Table 4.4 It is clear that strategies for performing calibration studies may be developed using these results.

5.2 RECOMMENDATION FOR FUTURE RESEARCH.

1. Further research requirements on the present one-dimensional model are:

(a) Experimental studies on the rapidly varied unsteady flows with data recorded throughout the channel length with emphasis on accuracy.

(b) Further study is required to differentiate between rapidly fluctuating flows and gradually varied flows.

(c) An efficient technique for determination of the Manning's coefficient (or resistance coefficients) under various flow and channel conditions needs to be developed.

(d) Experimental studies should be conducted for the unsteady flow conditions in open channels with different degrees of wind effect and/or lateral inflows or outflows to investigate the effect of these parameters on the computational scheme.

(e) Additional research should be undertaken to determine the magnitude of the computational time step used in the weighted four-point implicit scheme.

2. The extension of the one-dimensional formulation of the numerical scheme can consider where those meandering channels, over-bank flow, lateral inflow or outflow and branched channels.

REFERENCES CITED

Amein, M., "An implicit Method for Numerical Flood Routing", Water Resource Research, V 4, no. 4, 1968, pp 719-26

Amein, M., and Fang, C.S., "Implicit Flood Routing in Natural Channel", Proceedings of the American Society of Civil Engineers, Journal of the Hydraulic Division, Vol. 96, No. HY12, December 1970, pp. 2481-2500

Amein, M., and Chu, H.L., "Implicit Numerical Modelling of Unsteady Flows", Proceedings of the American Society of Civil Engineers, Journal of the Hydraulic Division, Vol. 94, No. HY6, June 1975, pp. 717-731

Balzer, R.A., and Lac, C., "Computer Simulations of Unsteady Flows in Waterways", Proceedings of the American Society of Civil Engineers, Journal of the Hydraulics Division, Vol. 94, No. HY4, July 1968, pp. 1083-1117

Chaudry, Y.M., and Contractor, D.N., "Application of the Implicit Method to Surges in Open Channels", Water Resources Research, Vol. 9, No. 6, December 1973, pp. 1605-1612

Cungè, Jean A., "Rapidly Varying Flows in Power and Pumping Canals", Unsteady Flow in open channel, ed by K. Mahmood and V. Yevjevich, Vol II, Water Resource Publications, Ft. Collins, Colorado, 1975, pp 539-562.

Fread, D.L., "Numerical Properties of Implicit Four-Point Finite Difference Equations of Unsteady Flow", NOAA Technical Memorandum, NWS HYDRO, 18, NOAA, 1975a

Fread, D.L., and Smith, G.F., "Calibration Technique for I-D Unsteady Flow Models", Proceedings of the American Society of Civil Engineers, Journal of the Hydraulics Division, Vol. 104, No. HY7, July 1978, pp. 1027-1044

French, Richard H., Open-Channel Hydraulics, McGraw-Hill Book Company, New York, 1985

Guneratnam, D.J., and Perkins, F.E., "Numerical Solution of Unsteady Flows in Open Channels", Hydrodynamics Laboratory Report No. 127, MIT, July 1970, 260pp

Halliwell, A.R., and Ahmed, M., "Flood Routing in Non-Prismatic Channels Using an Implicit Method of Solution", International Symposium on River Mechanics, C3, 9-12 Jan. 1973, Bangkok, Thailand

Lai, C., "Numerical Modelling of Unsteady Open-channel Flow", Advance in Hydroscience, Vol. 14, 1986

Manz, D.H., 1985, "System Analysis of Irrigation Conveyance Systems", Ph.D thesis submitted to the Department of Civil Engineering, University of Alberta, Edmonton, Alberta

Price, R.K., "Comparison of Four Numerical Methods for Flood Routing", Journ. of the Hydraulics Division, V 100, No HY7, July 1974, pp 879-899.

Stoker, J.J., "Numerical Solution of Flood Prediction and River Regulation Problems", rep. IMM-200, Inst. for Math. and Mech., New York Univ., New York, 1953

Strelkoff, T., "Numerical Solution of St. Venant Equations", Journal of the Hydraulics Division, Vol. 96, No. HY1, Jan. 1970, pp. 223-252

Terzidis, G., and Strelkoff, T., "Computation of Open Channel Surges and Shocks", Journal of the Hydraulics Division, Vol. 96, No. HY12, December 1970, pp. 2581-2610

Treske, A., 1980, Experimentelle Uberpristung numerischer Berechningsuerfatinen Von Hachwasserwellen, in Blind, Report of Hydraulics Research Station, TU Munchen, 44: 1-133

APPENDIX A

NUMERICAL SOLUTION USING THE 4-POINT IMPLICIT FINITE DIFFERENCE SCHEME

The particular form of the St. Venant equations that was chosen for the numerical solution is given by equations 2.1(a) and 2.1(b) and are were written as:

$$\frac{A}{B} \cdot \frac{\partial V}{\partial x} + V \cdot \frac{\partial y}{\partial x} + \frac{\partial y}{\partial t} - \frac{q}{B} = 0 \qquad \text{...(A.1)}$$

and

$$\frac{\partial V}{\partial t} + V \cdot \frac{\partial V}{\partial x} + g \cdot \frac{\partial y}{\partial x} + g \cdot (\delta_f - \delta_o) + \frac{V}{A} \cdot g = 0 \qquad \text{...(A.2a)}$$

in which

$$S_f = n^2 \cdot V \cdot |V| \cdot \frac{P^{4/3}}{A^{4/3}} \qquad \text{...(A.2b)}$$

Note that these equations are only applicable to a prismatic channel.

Consider the representation of the space-time continuum by a number of discrete points, as indicated in Figure 2.1. At any time t^j the channel reach length is represented by N discrete points. The subscript (i) and the superscript (j) are used to designate the position along the x-axis and the t value respectively. For example, the velocity (v) at any particular point (i,j) is denoted by V_i^j.

Assume that the terms are known at all the grid points at time t^j. To determine the values of the terms at time t^{j+1}, consider a point M entirely within four grid points (i,j), (i+1,j), (i,j+1) and (i+1,j+1), as shown in Figure 2.1. The governing equations are required to be satisfied at the point M by substituting the respective finite difference operators (Eqns 2.2, 2.3, 2.4) for $\partial y/\partial t$, A/B , $\partial V/\partial x$, g/B , V , $\partial V/\partial t$ and S_f into

equations (A.1) and (A.2). After rearranging and gathering terms, the governing equations to be satisfied become:

$$F_i \cdot \left[y_i^{j+1}, V_i^{j+1}, y_{i+1}^{j+1}, V_{i+1}^{j+1}\right] = \left[y_{i+1}^{j+1} + y_i^{j+1}\right] + C_1$$

$$+ \frac{\Delta t}{\Delta x} \cdot \theta^2 \cdot \left[\left(\frac{A}{B}\right)_{i+1}^{j+1} + \left(\frac{A}{B}\right)_i^{j+1}\right] \cdot \left[V_{i+1}^{j+1} - V_i^{j+1}\right] \qquad \text{...(A.3)}$$

$$+ \frac{\Delta t}{\Delta x} \cdot \theta \cdot C_2 \cdot \left[V_{i+1}^{j+1} - V_i^{j+1}\right] + \frac{\Delta t}{\Delta x} \cdot C_3 \cdot \left[\left(\frac{A}{B}\right)_{i+1}^{j+1} + \left(\frac{A}{B}\right)_i^{j+1}\right] + C_4$$

$$+ \frac{\Delta t}{\Delta x} \cdot \theta^2 \cdot \left[V_{i+1}^{j+1} + V_i^{j+1}\right] \cdot \left[y_{i+1}^{j+1} - y_i^{j+1}\right] + \frac{\Delta t}{\Delta x} \cdot \theta \cdot C_5 \cdot \left[y_{i+1}^{j+1} - y_i^{j+1}\right]$$

$$+ \frac{\Delta t}{\Delta x} \cdot \theta \cdot C_6 \cdot \left[V_{i+1}^{j+1} + V_i^{j+1}\right] + C_7 - \Delta t \cdot q \cdot \theta \cdot \left[\left(\frac{I}{B}\right)_{i+1}^{j+1} + \left(\frac{I}{B}\right)_i^{j+1}\right] - C_8 = 0$$

and:

$$G_i \cdot \left[y_i^{j+1}, V_i^{j+1}, y_{i+1}^{j+1}, V_{i+1}^{j+1}\right] = \frac{1}{g} \cdot \frac{\Delta x}{\Delta t} \cdot \left[V_{i+1}^{j+1} + V_i^{j+1}\right]$$

$$+ C_g + \frac{\theta^2}{g} \cdot \left[\left(V_{i+1}^{j+1}\right)^2 - \left(V_i^{j+1}\right)^2 + C_{10} \cdot \frac{\theta}{g} \cdot \left[V_{i+1}^{j+1} = V_i^{j+1}\right]\right. \qquad \text{...(A.4)}$$

$$+ C_{11} \cdot \frac{\theta}{g} \cdot \left[V_{i+1}^{j+1} + V_i^{j+1}\right] + C_{12} + 2 \cdot \theta \cdot \left[y_{i+1}^{j+1} - y_i^{j+1}\right] + C_{13} + C_{14}$$

$$+ \Delta x \cdot \theta \cdot \left[\left(S_f\right)_{i+1}^{j+1} + \left(S_f\right)_i^{j+1}\right] + C_{15} + q \cdot \frac{\Delta x}{g} \cdot \theta \cdot \left[\left(\frac{V}{A}\right)_{i+1}^{j+1} + \left(\frac{V}{A}\right)_i^{j+1}\right] + C_{16} = 0$$

The energy-gradient S_f at point (i, j) can be written

$$S_{f_i}^{\,j} = \frac{\left[n_i^j\right]^2 \cdot V_i^j \mid V_i^j \mid \left[P_i^j\right]^{\frac{4}{3}}}{\left[A_i^j\right]^{\frac{4}{3}}} \qquad \text{...(A.5)}$$

where P is the wetted parameter, n is the Manning's resistance coefficient and C_1, C_2, C_3, ..., C_{16} are constants. The values of the constants depend upon the values of the terms, V, y, A, B, S_o, etc. at the known time step t^j, for example the channel bottom slope is expressed as:

$$S_o = \frac{\partial z}{\partial x} = \frac{\left[z_{i+1}^j - z_i^j\right]}{\Delta x} \qquad \text{...(A.6)}$$

in which z is the elevation from the reference datum point (stage).

There are (N-1) points like M in the space-time grid between the time t^j and t^{j+1}. Therefore, equations (A.3) and (A.4) provide 2(N-1) equations (with i taking values 1, 2, 3, ... (N-1)) which contain N unknown depths y_i and N unknown velocities V_i. The terms A_i, B_i, etc. are known in terms of y_i.

Two additional equations are obtained by considering the boundary conditions at each end of the channel. At the upstream boundary must be either the depth or the discharge as function of time. If the depth versus time relationship is known, then the upstream boundary condition can be written:

$$y_1 = f_1(t): \quad \text{i.e.} \quad G_0\,(y_i) = y_1 - f_1(t) = 0 \qquad \text{...(A.7a)}$$

If the discharge across the section is known as a function of time, then the upstream boundary condition can be written:

$$Q_1 = f_1(t) = A_1 \cdot V_1 : \quad \text{i.e.} \quad G_0(y_1, v_1) = V_1 \cdot A_1 - f_1(t) = 0 \qquad \text{...(A.7b)}$$

In similar fashion the downstream condition may be discharge as a function of time, or depth as a function of time and sometimes given in the form of a stage-discharge

relationship (rating curve) at the section. If the depth versus time relationship is known, then the downstream boundary condition can be written:

$$Y_N = f_N(t): \quad \text{i.e.} \quad F_N(y_N) = Y_N - f_N(t) = 0 \qquad \text{...(A.8a)}$$

If the discharge across the section is known as a function of time, then the downstream boundary condition can be written:

$$Q_N = V_N \cdot A_N = f_N(t): \quad \text{i.e.} \quad F_N(y_N, V_N) = V_N \cdot A_N - f_N(t) = 0 \qquad \text{...(A.8b)}$$

If the function relationship between the depth and discharge is known, then the downstream boundary condition can be written:

$$Y_N = f_N(Q_N): \quad \text{i.e.} \quad F_N(Y_N, V_N) = Y_N - f_N(Q_N) = 0 \qquad \text{...(A.8c)}$$

The non-linear partial-differential equations (A.1) and (A.2) have been replaced, using a four-point implicit finite-difference scheme, by a set of 2 N non-linear simultaneous equations (Equations (A.3) (A.4), (A.7) and (A.8).

The form of these equations is particularly suitable for the generalized iteration-method of Newton. In this method, the non-linear equations are reduced to a set of linear equations. Trial values are assigned to unknowns and substituted into the system of the equations. In general, the right hand side will not be zero but will have some residual values. The solution is obtained by adjusting the trial variable values until the residuals vanish or are reduced to a tolerable limit, known as convergence criterion ε. To demonstrate the application of the Newton Iteration Solution technique, assume that the computations are continued until the kth iteration cycle and let the values of the unknowns at the end of this cycle be denoted by the superscript k. Let the residuals of the kth iteration be designated by $r^k_{1,i}$ and $r^k_{2,i}$ for the F and G functions respectively. The set of simultaneous equations arising from equations (A.3), (A.4), (A.7) and (A.8) are therefore,

$$G_0(y^k_i, v^k_i) = r^k_{2,0}$$

$$F_1(y^k_1, v^k_1, y^k_2, v^k_2) = r^k_{1,1}$$

$$G_1(y_1^k\ ,\ V_1^k\ ,\ y_1^k\ ,\ V_2^k) = r_{2,1}^k$$

etc.

$$F_i(\ y_i^k\ ,\ V_i^k\ ,\ y_{i+1}^k\ ,\ V_{i+1}^k) = r_{1\ ,\ i}^k$$

$$G_i(\ y_i^k\ ,\ V_i^k\ ,\ y_{i+1}^k\ ,\ V_{i+1}^k) = r_{2\ ,\ i}^k$$

etc.

$$F_N(\ y_N^k\ ,\ V_N^k)\ \ldots = r_{1\ ,\ N}^k \qquad \ldots(A.9)$$

Note that the superscript at $j+1$ is dropped as the terms of j^{+1} are being determined.

The next approximations to the values of y and V are then given as,

$$y_i^{k+1} = y_i^k + dy_i$$

and

$$V_i^{k+1} = V_i^k + Dv_i \qquad \ldots(A.10)$$

where the values of dy_i and dv_i are given by set of 2N simultaneous linear equations:

$$\begin{aligned}
\frac{\partial G_0}{\partial y_i}\cdot dy_i + \frac{\partial G_0}{\partial V_1}\cdot dv_1 &= -r_{2,0}^k \\
\frac{\partial F_1}{\partial y_1}\cdot dy_1 + \frac{\partial F_1}{\partial V_1}\cdot dV_1 + \frac{\partial F_1}{\partial y_2}\cdot dy_2 + \frac{\partial F_1}{\partial V_2}\cdot dV_2 &= -r_{1,1}^k \\
\frac{\partial G_1}{\partial y_1}\cdot dy_1 + \frac{\partial G_1}{\partial V_1}\cdot dv_1 + \frac{\partial G_1}{\partial y_2}\cdot dy_2 + \frac{\partial G_1}{\partial V_2}\cdot dV_2 &= -r_{2,1}^k
\end{aligned}$$

etc.

$$\begin{aligned}
\frac{\partial F_i}{\partial y_i}\cdot dy_i + \frac{\partial F_i}{\partial V_i}\cdot dV_i + \frac{\partial F_i}{\partial y_{i+1}}\cdot dy_{i+1}\ \frac{\partial F_i}{\partial V_{i+1}}\cdot dV_{i+1} &= -r_{i,1}^k \qquad \ldots(A.11) \\
\frac{\partial G_i}{\partial y_i}\cdot dy_i + \frac{\partial G_i}{\partial V_i}\cdot dV_i + \frac{\partial G_i}{\partial y_{i+1}}\cdot dy_{i+1}\ \frac{\partial F_i}{\partial V_{i+1}}\cdot dV_{i+1} &= -r_{2,i}^k
\end{aligned}$$

etc

$$\frac{\partial F_N}{\partial Y_N}\cdot dY_N + \frac{\partial F_N}{\partial V_N}\cdot dV_N = r_{1,N}^k$$

All the partial derivatives are evaluated at the kth iteration cycle. The coefficients of the equations (i.e. the values of the function F and G) are obtained by differentiating the appropriate equation and substituting the values of y, V, B, A, etc., corresponding to the kth iteration cycle. Estimates of the unknown flow variables t^{j+1} are made and the residuals are calculated using Equation (A.9). These are then substituted into Equation (A.11) which is rearranged to solve for the estimates of the unknown flow variables. These are then substituted back into Equation (A.9) and a new set of residuals is calculated. If these residuals equal zero or are below a predetermined tolerance level (i.e. convergence criterion parameter), the flow variables are accepted as correct and the time step can change. If the residuals are still too large, the iteration is repeated

Note that Equation (A.11) is a set of 2 N simultaneous linear equations and the matrix of coefficients is a sparse diagonal matrix. The sparse diagonal matrix can be solved using several methods of solution such as gaussian elimination or matrix inversion.

APPENDIX B

HYDROGRAPHS

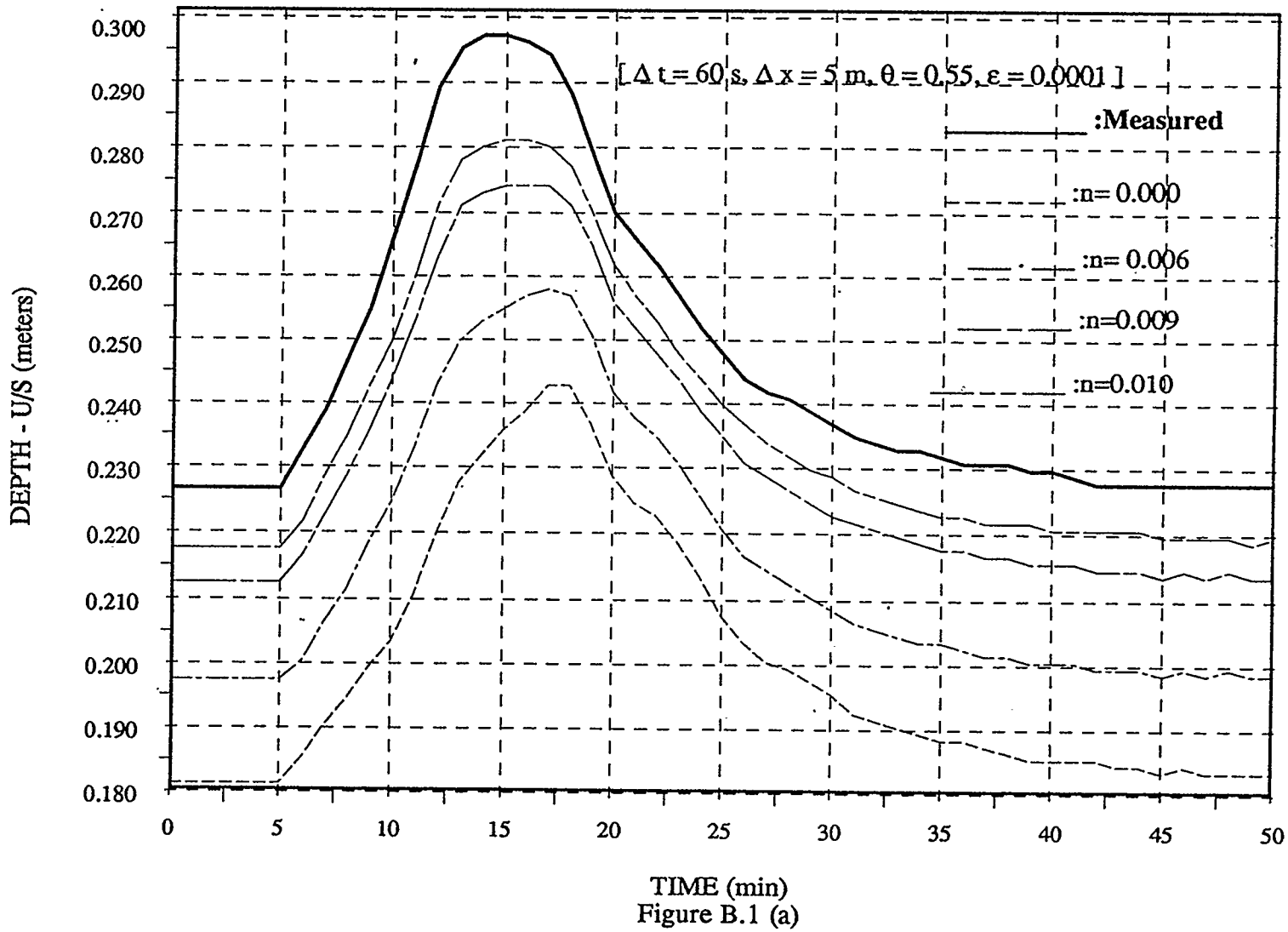

Figure B.1 (a)

Measured and Computed Depth Hydrographs at Upstream Boundary of the Channel Reach for Varying Resistance Coefficient

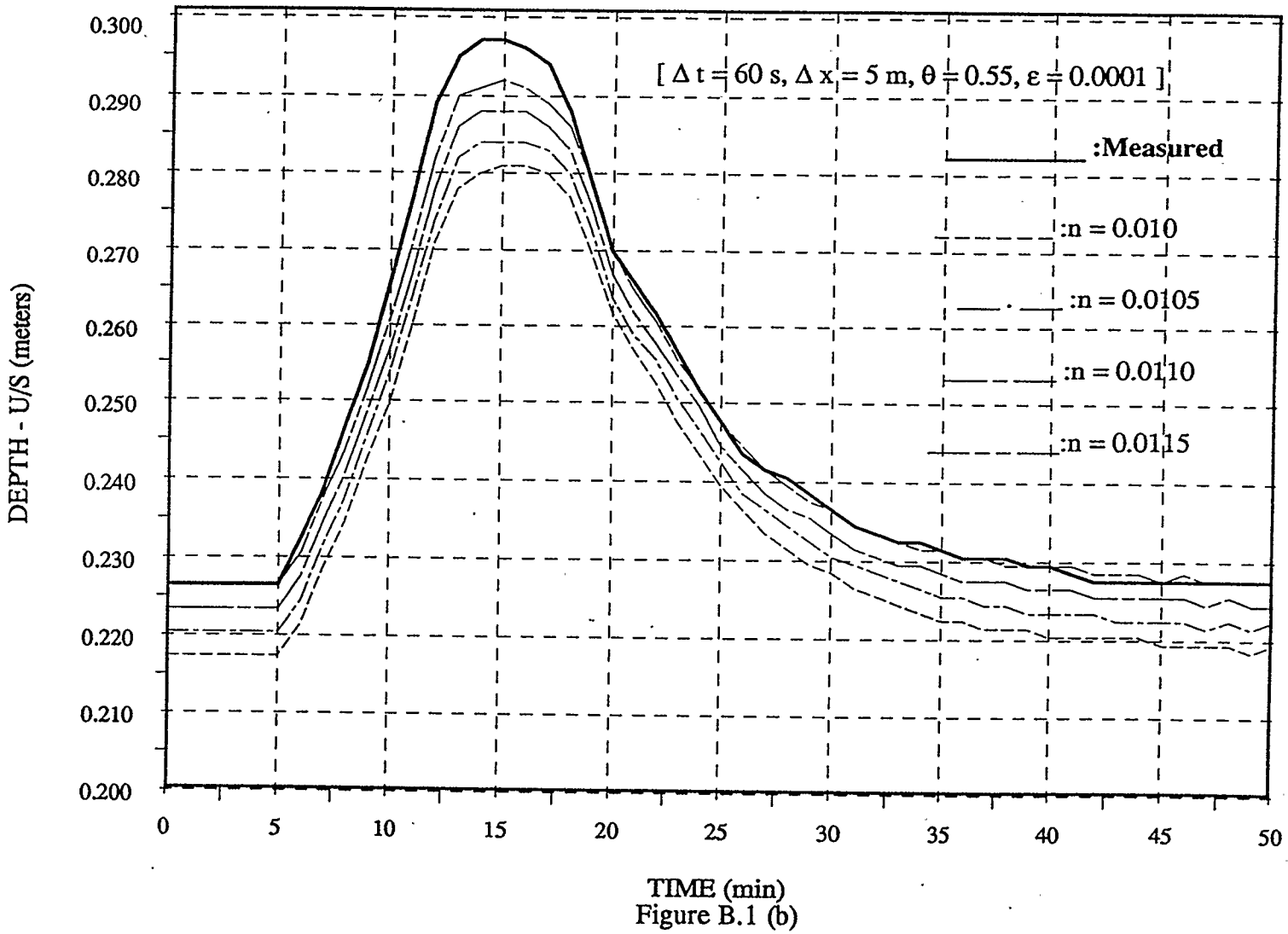

Figure B.1 (b)

Measured and Computed Depth Hydrographs at Upstream Boundary of the Channel Reach for Varying Resistance Coefficient

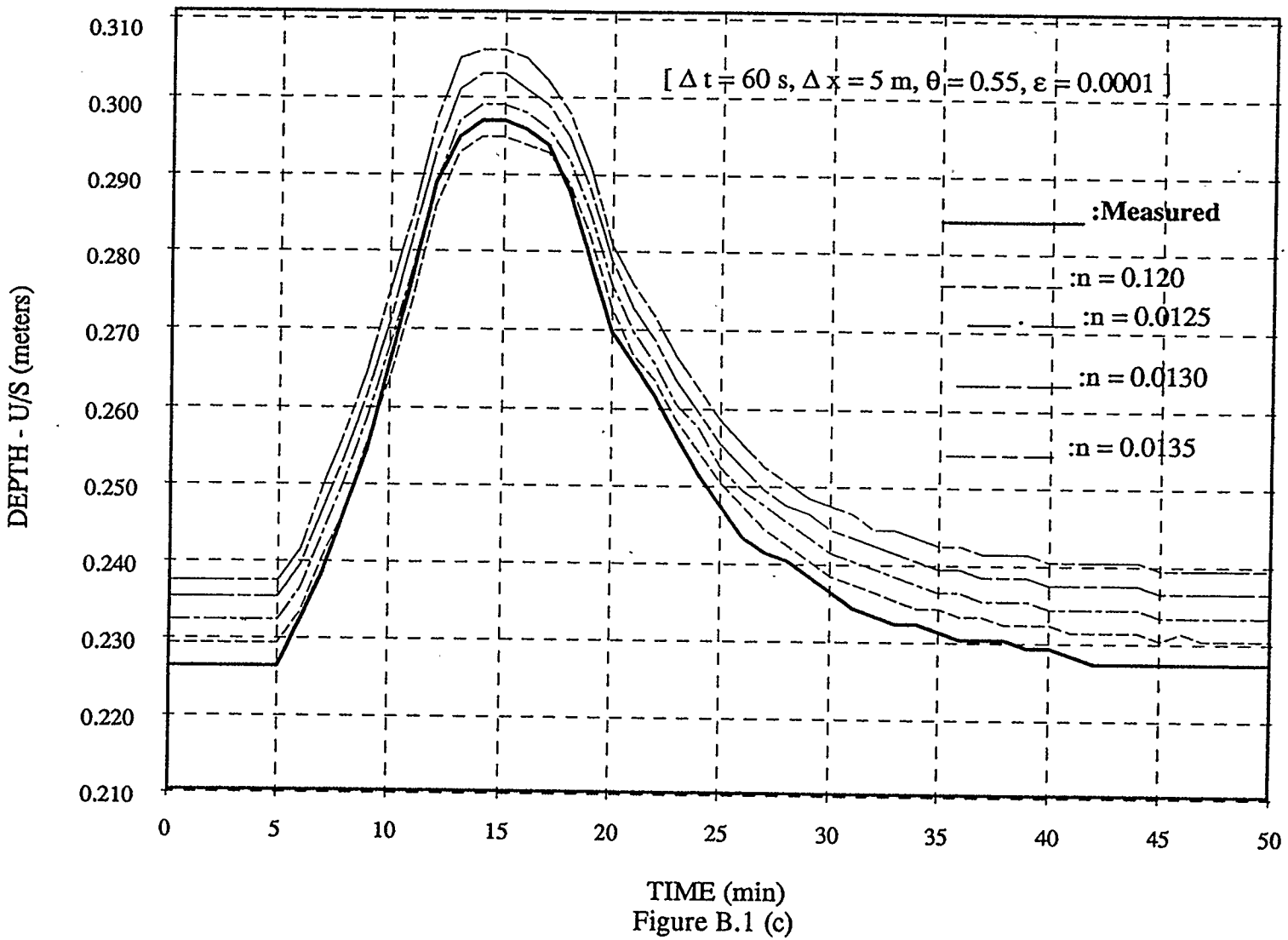

Figure B.1 (c)

Measured and Computed Depth Hydrographs at Upstream Boundary of the Channel Reach for Varying Resistance Coefficient

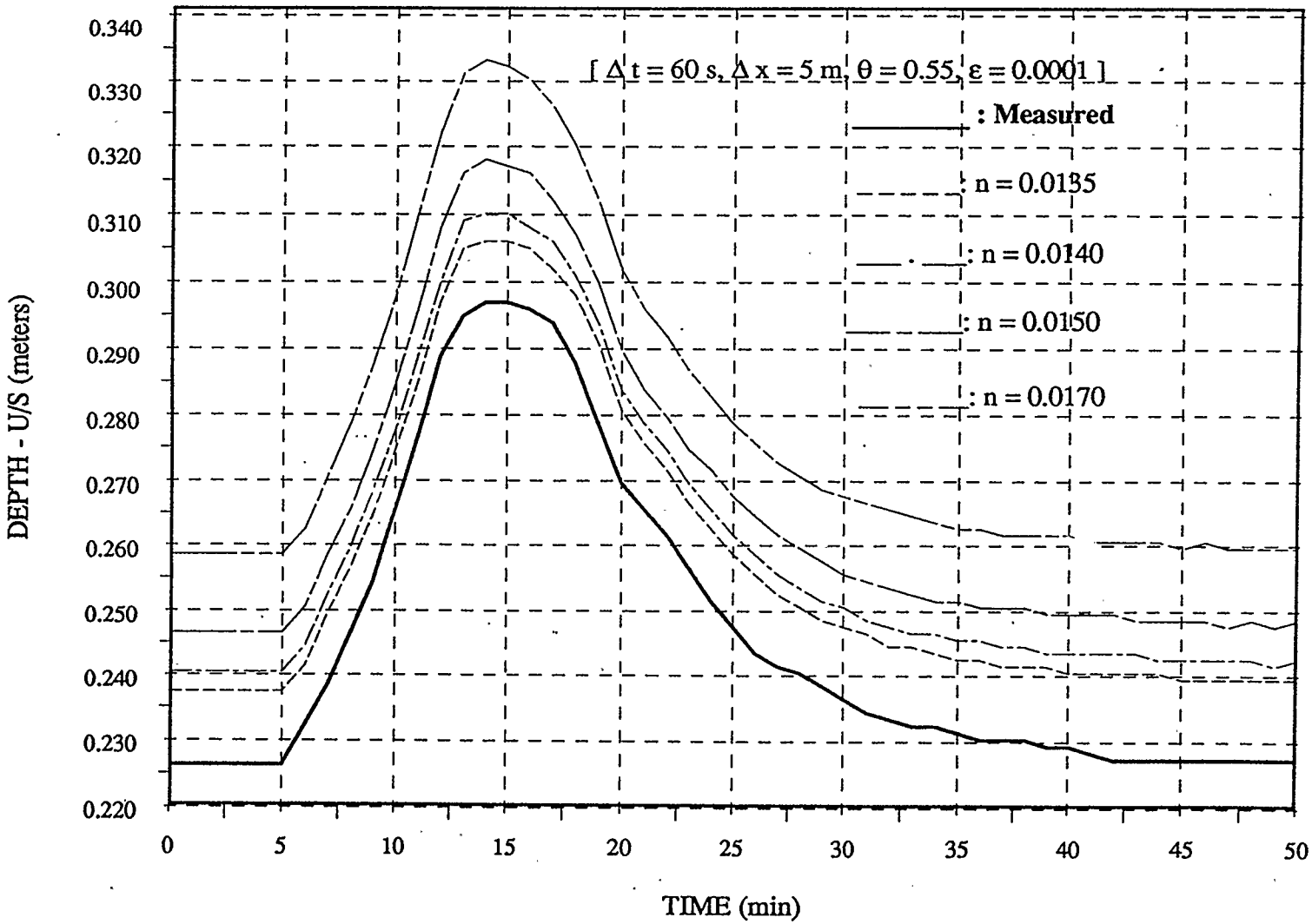

Figure B.1 (d)

Measured and Computed Depth Hydrographs at Upstream Boundary of the Channel Reach for Varying Resistance Coefficient

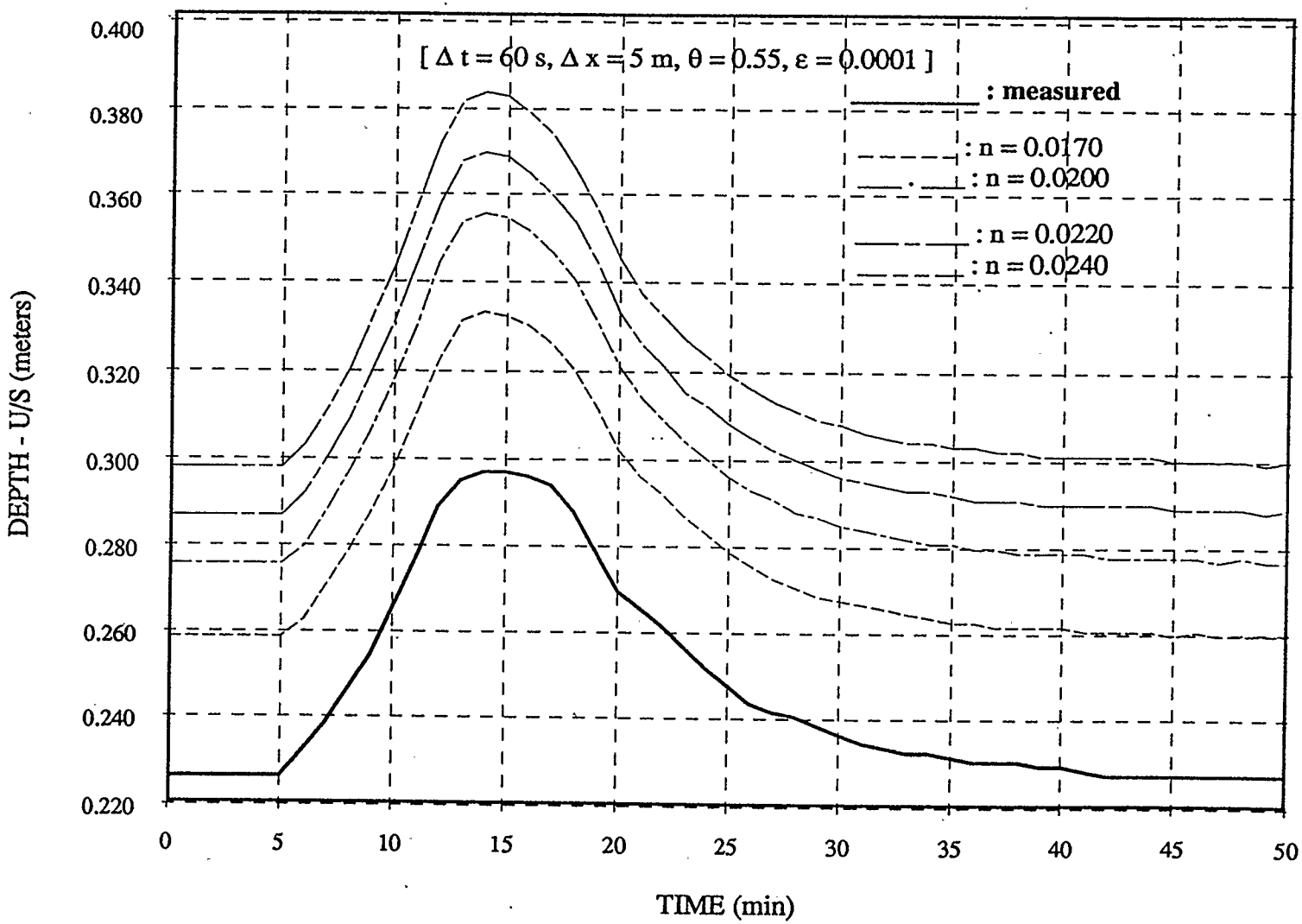

Figure B.1 (e)

Measured and Computed Depth Hydrographs at Upstream Boundary of the Channel Reach for Varying Resistance Coefficient

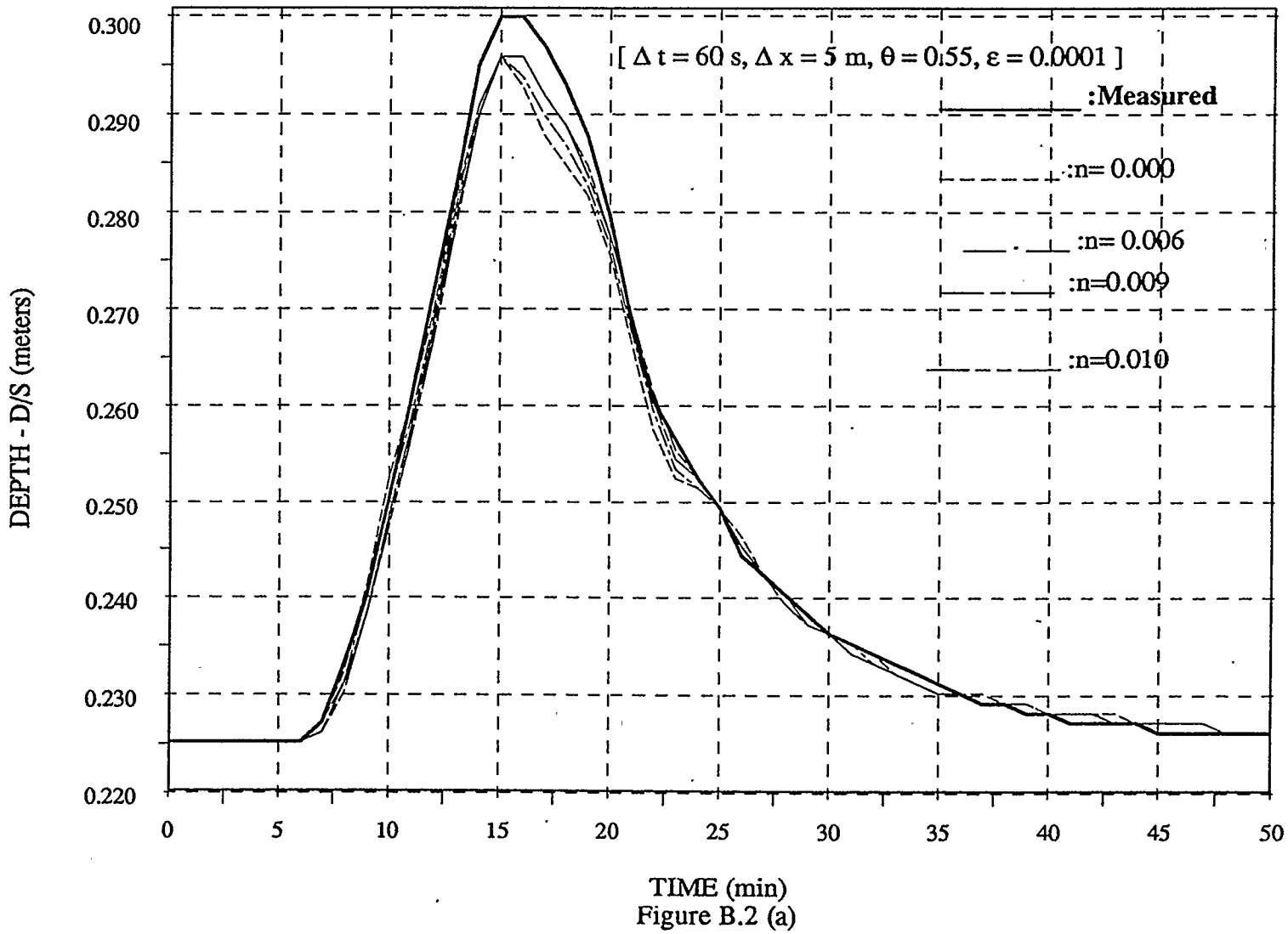

Figure B.2 (a)

Measured and Computed Depth Hydrographs at the Downstream Boundary of the Channel Reach for Varying Resistance Coefficient.

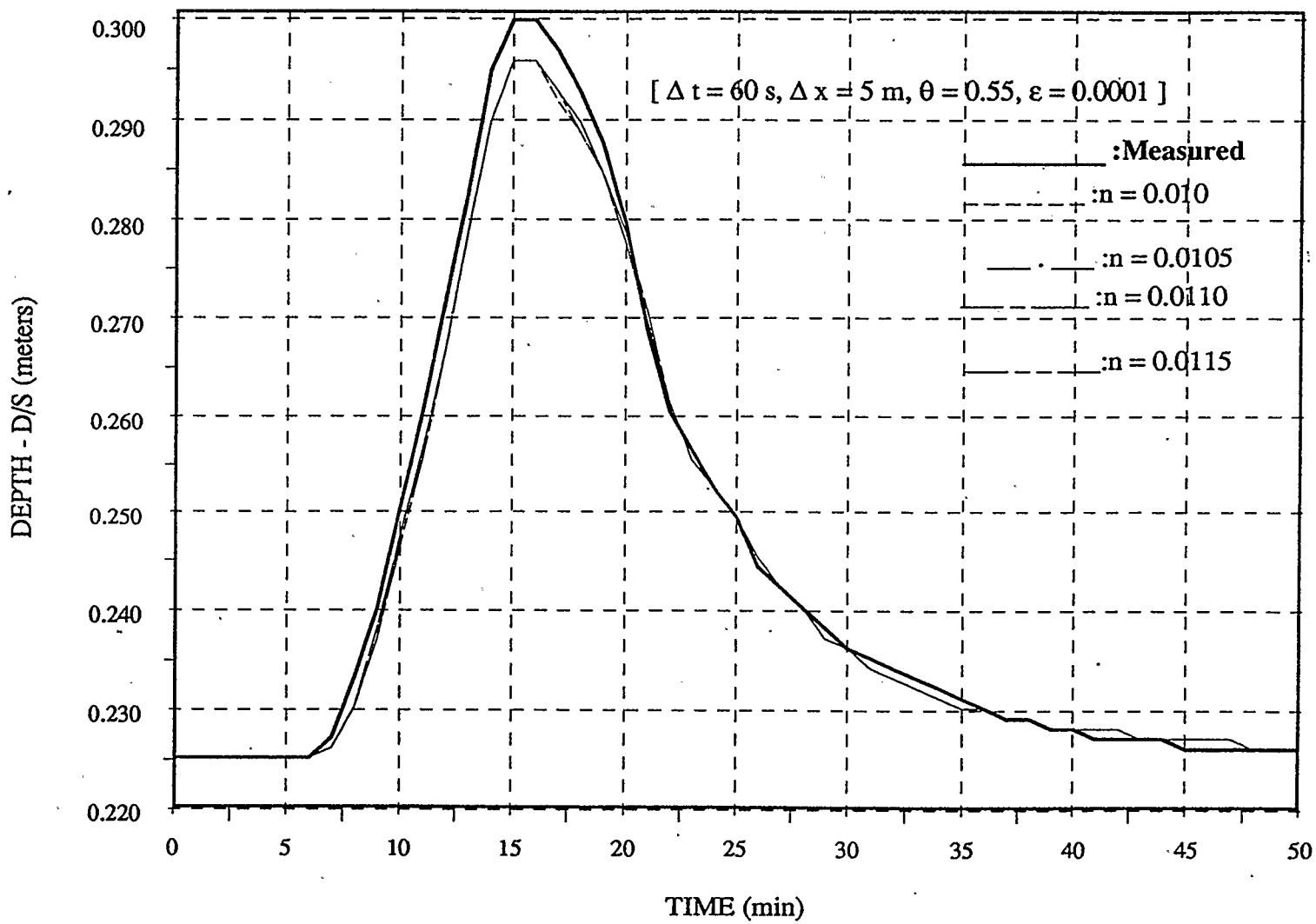

Figure B.2 (b)

Measured and Computed Depth Hydrographs at the Downstream Boundary of the Channel Reach for Varying Resistance Coefficient

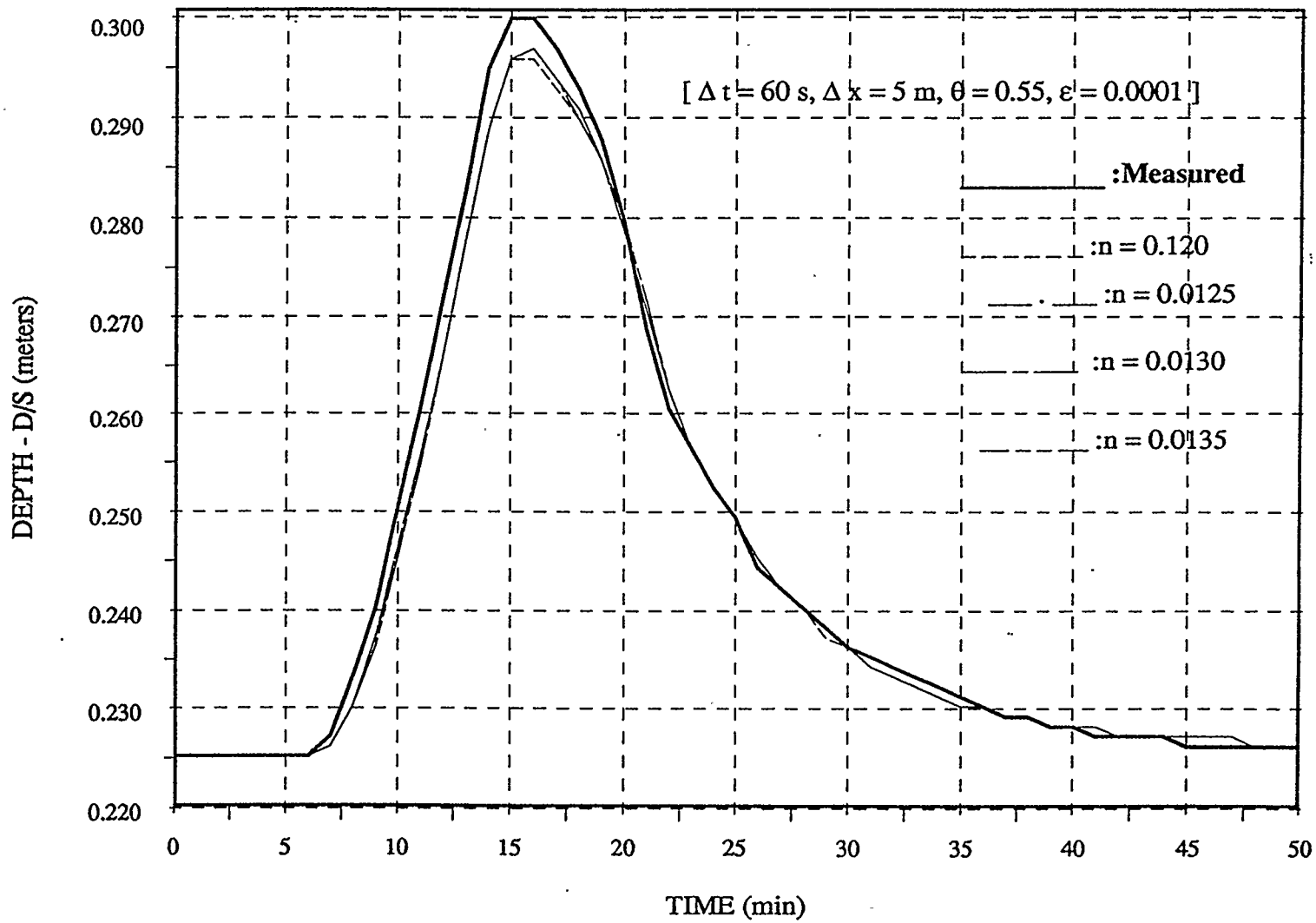

Figure B.2 (c)

Measured and Computed Depth Hydrographs at the Downstream Boundary of the Channel Reach for Varying Resistance Coefficient

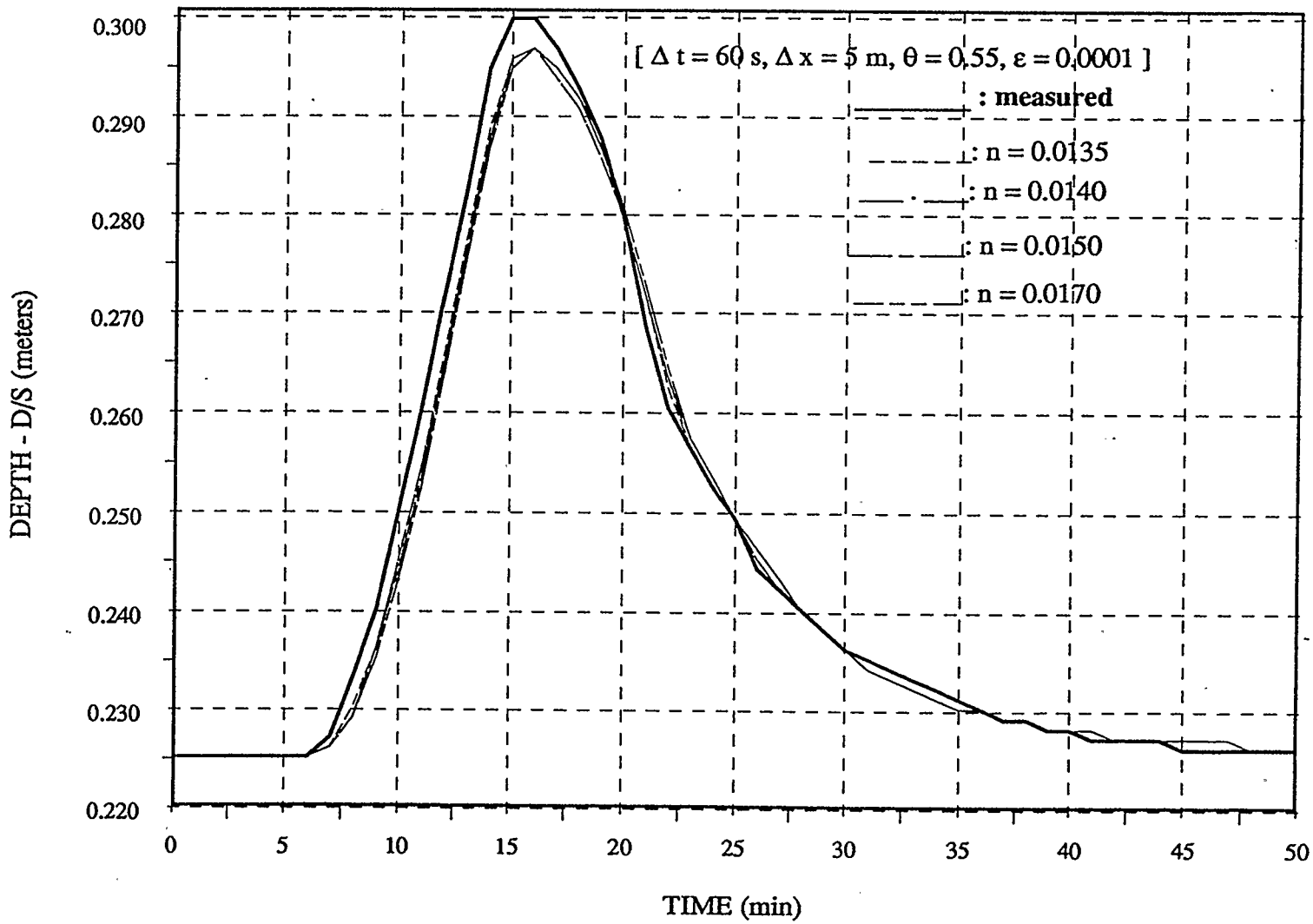

Figure B.2 (d)

Measured and Computed Depth Hydrographs at the Downstream Boundary of the Channel Reach for Varying Resistance Coefficient

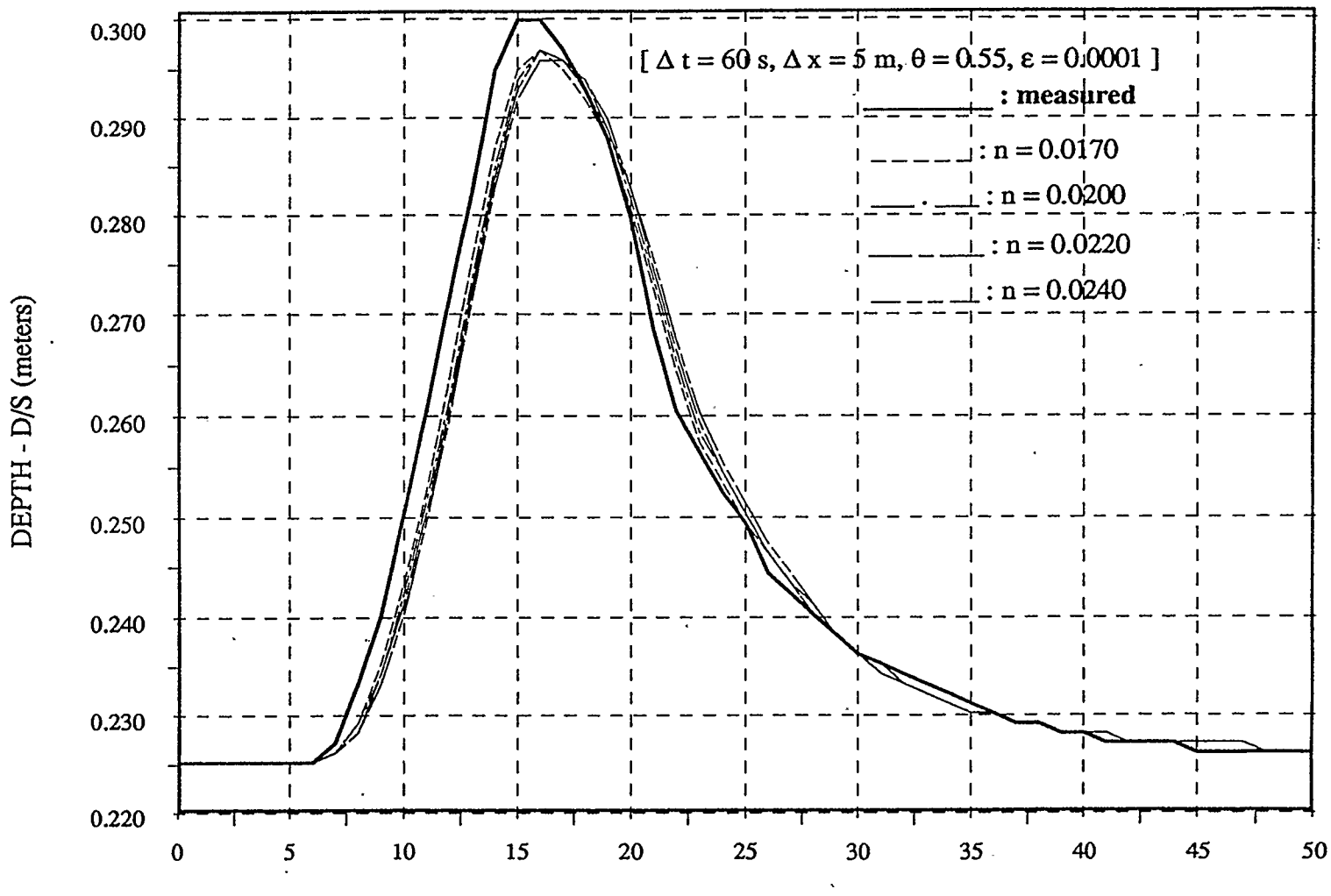

Figure B.2 (e)

Measured and Computed Depth Hydrographs at the Downstream Boundary of the Channel Reach for Varying Resistance Coefficient

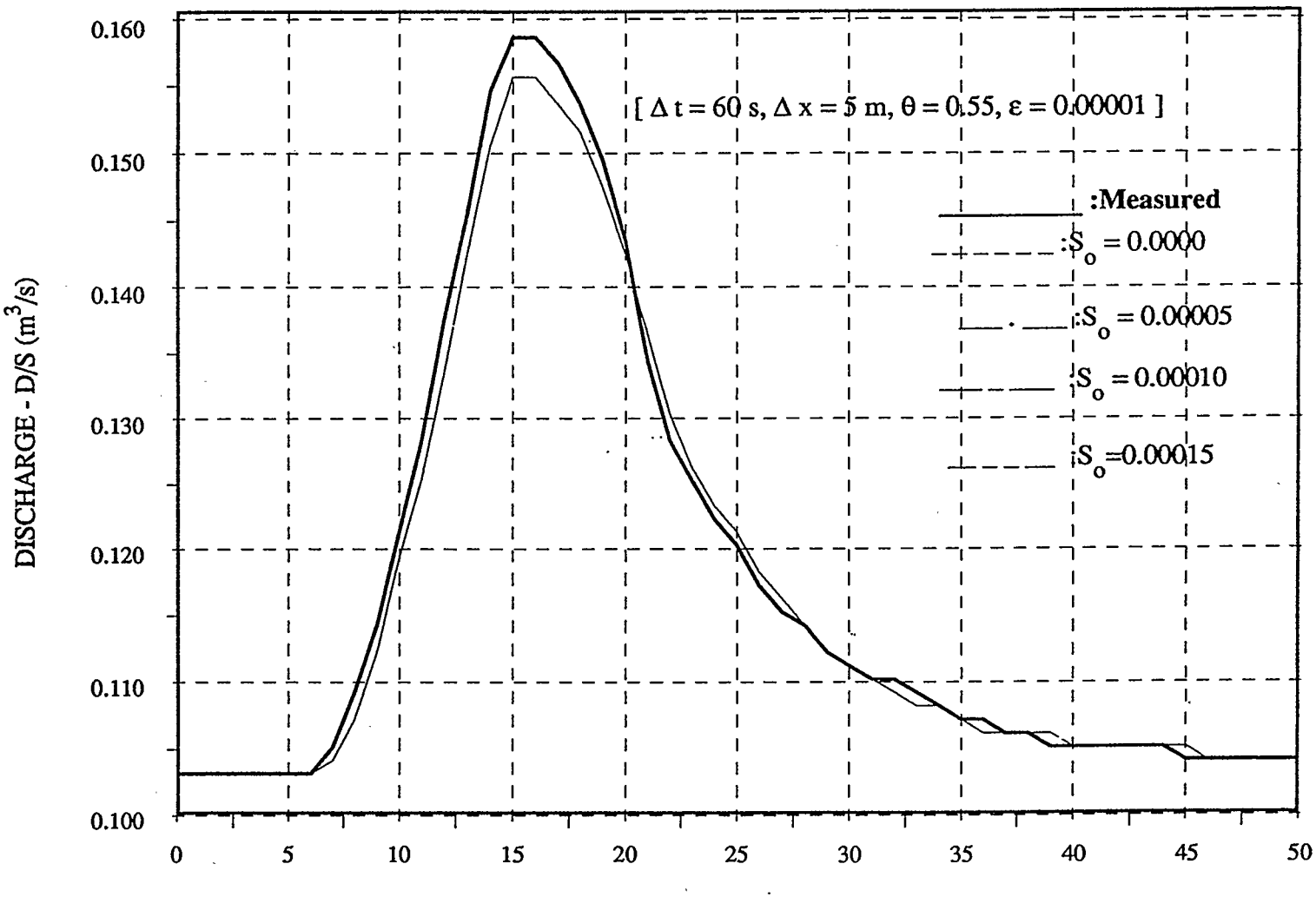

Figure B.3 (a)

Measured and Computed Discharge Hydrographs at Downstream Boundary of the Channel Reach for Varying Channel Bottom Slope

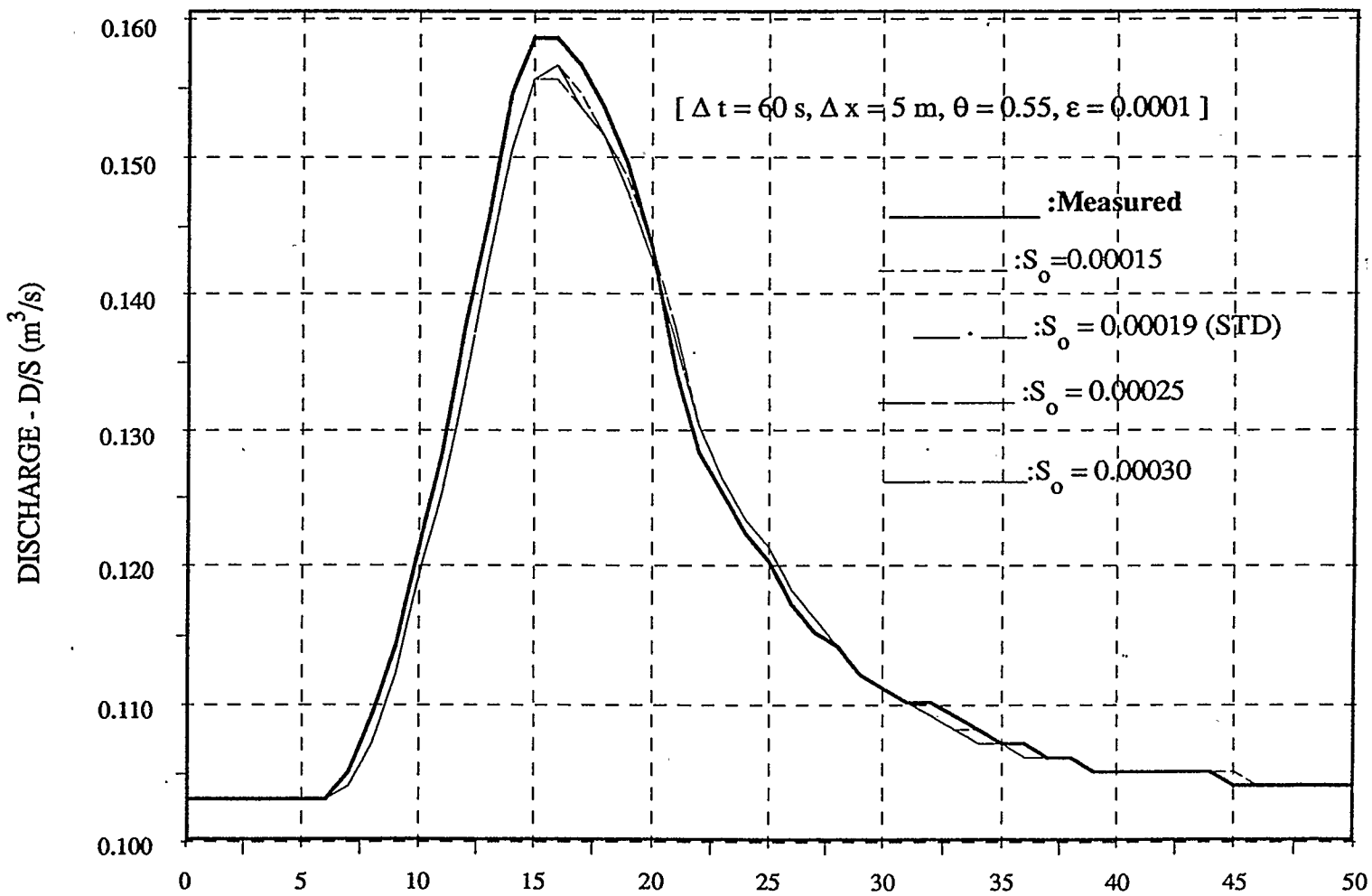

Figure B.3 (b)

Measured and Computed Discharge Hydrographs at Downstream Boundary of the Channel Reach for Varying Channel Bottom Slope

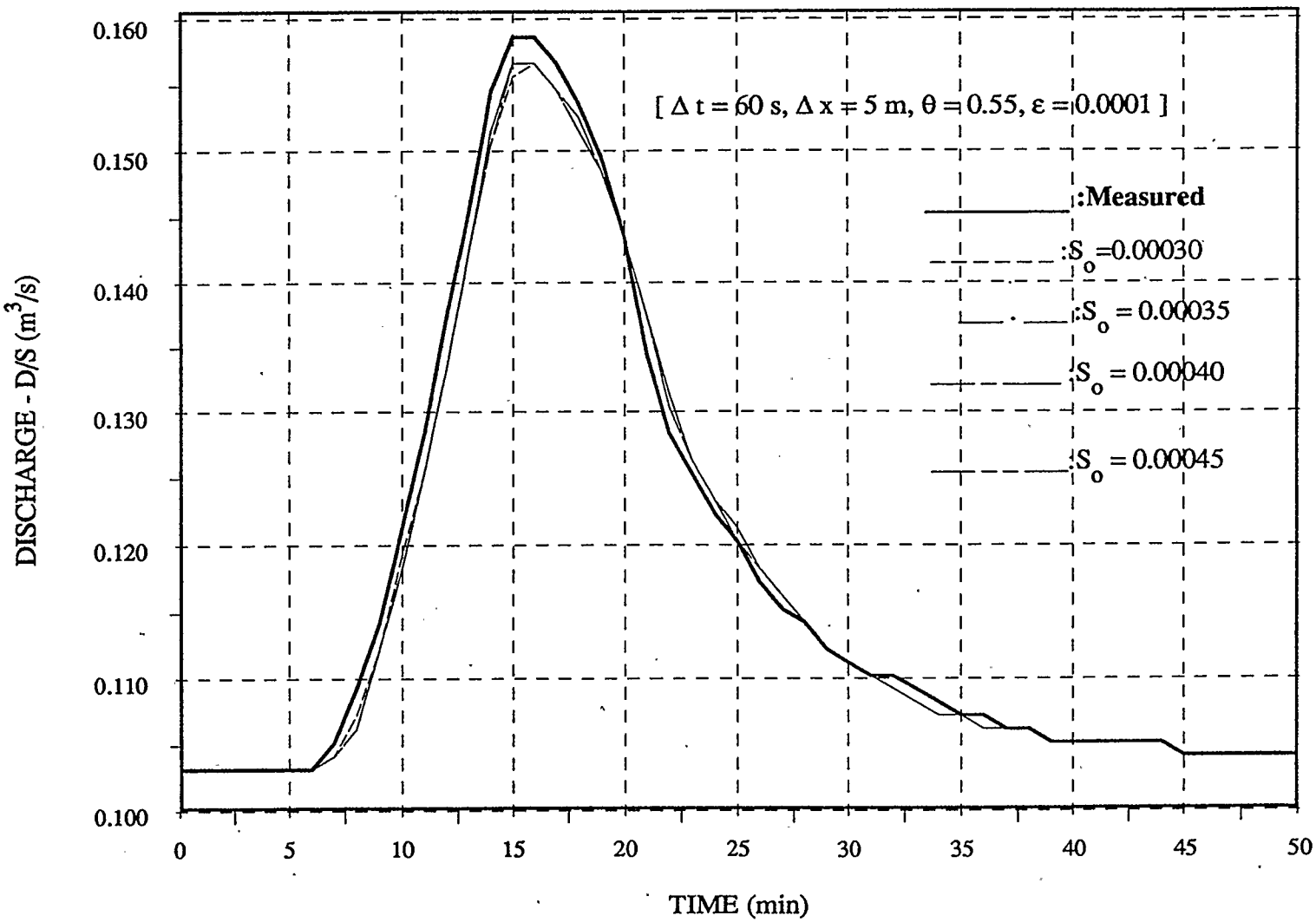

Figure B.3 (c)

Measured and Computed Discharge Hydrographs at Downstream Boundary of the Channel Reach for Varying Channel Bottom Slope

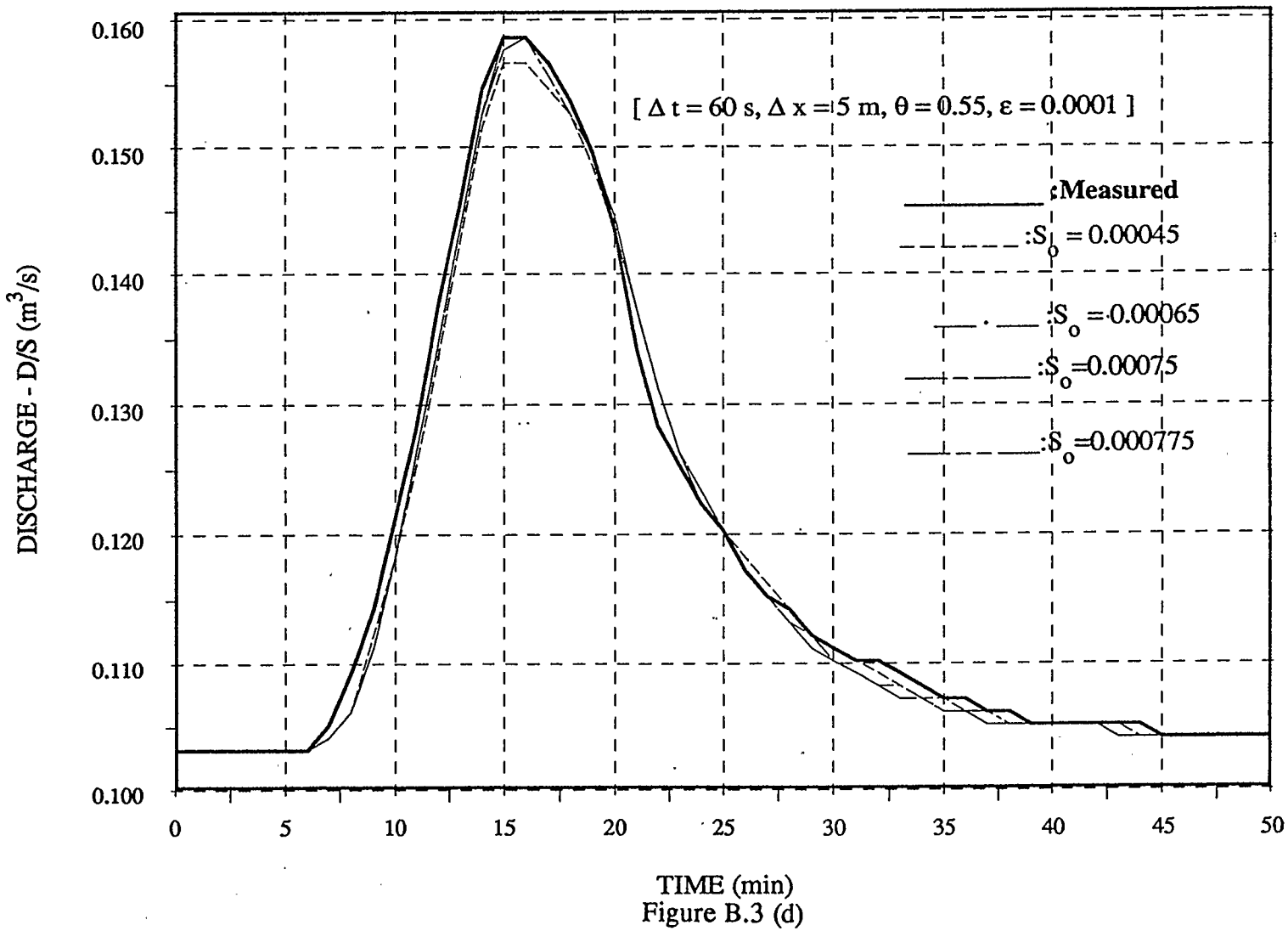

Figure B.3 (d)

Measured and Computed Discharge Hydrographs at Downstream Boundary of the Channel Reach for Varying Channel Bottom Slope

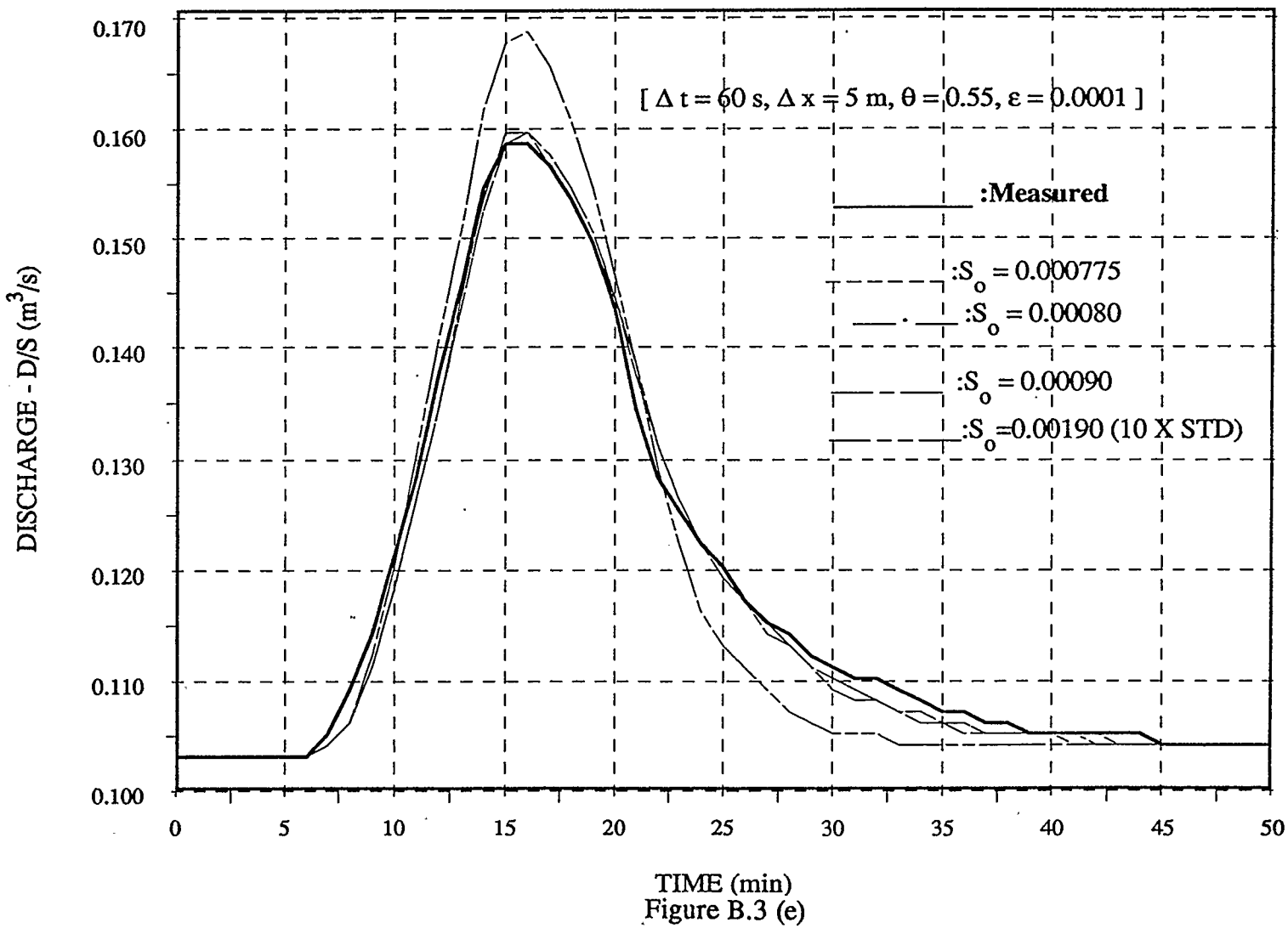

Figure B.3 (e)

Measured and Computed Discharge Hydrographs at Downstream Boundary of the Channel Reach for Varying Channel Bottom Slope

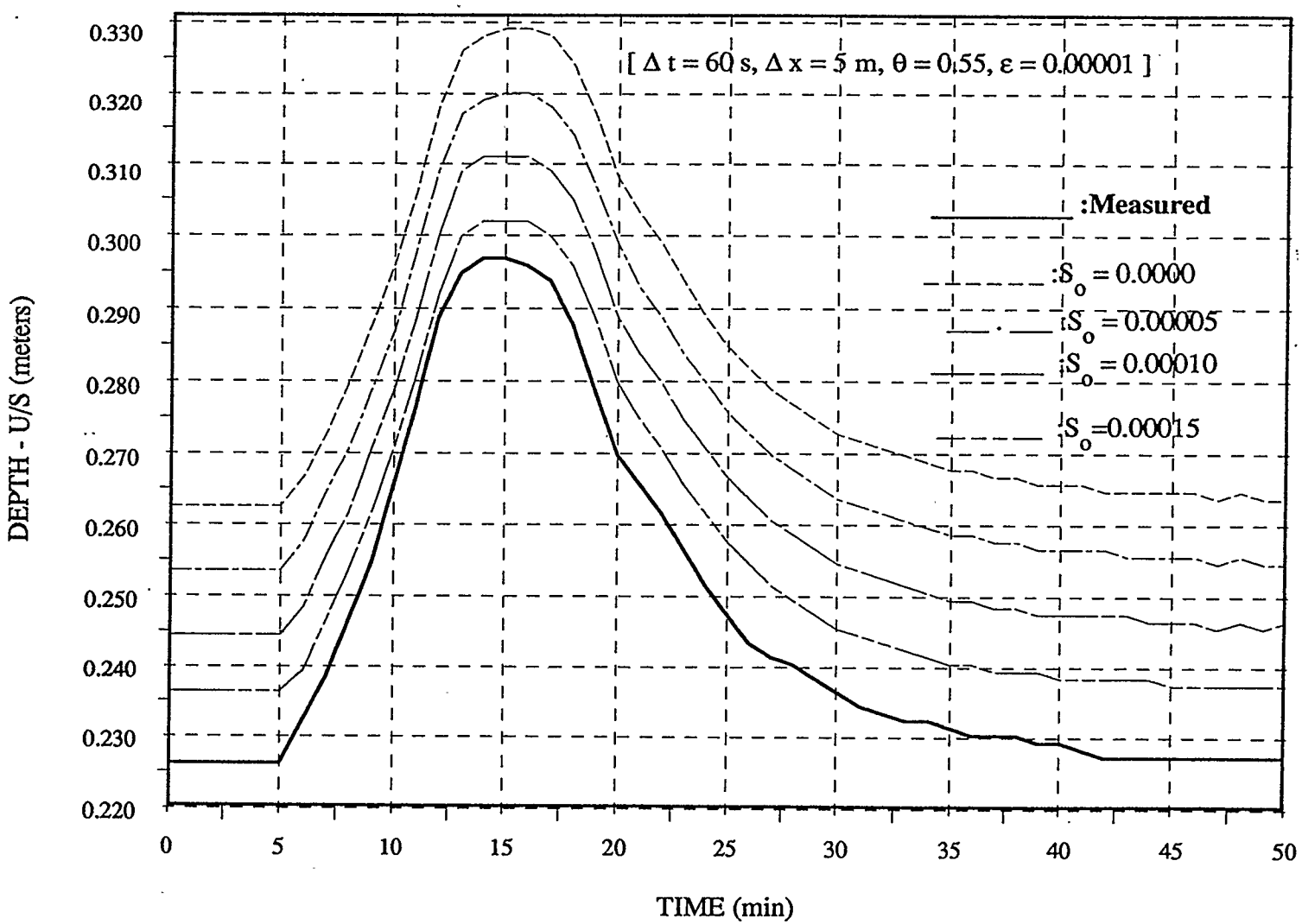

Figure B.4 (a)

Measured and Computed Depth Hydrographs at Upstream Boundary of the Channel Reach for Varying Channel Bottom Slope

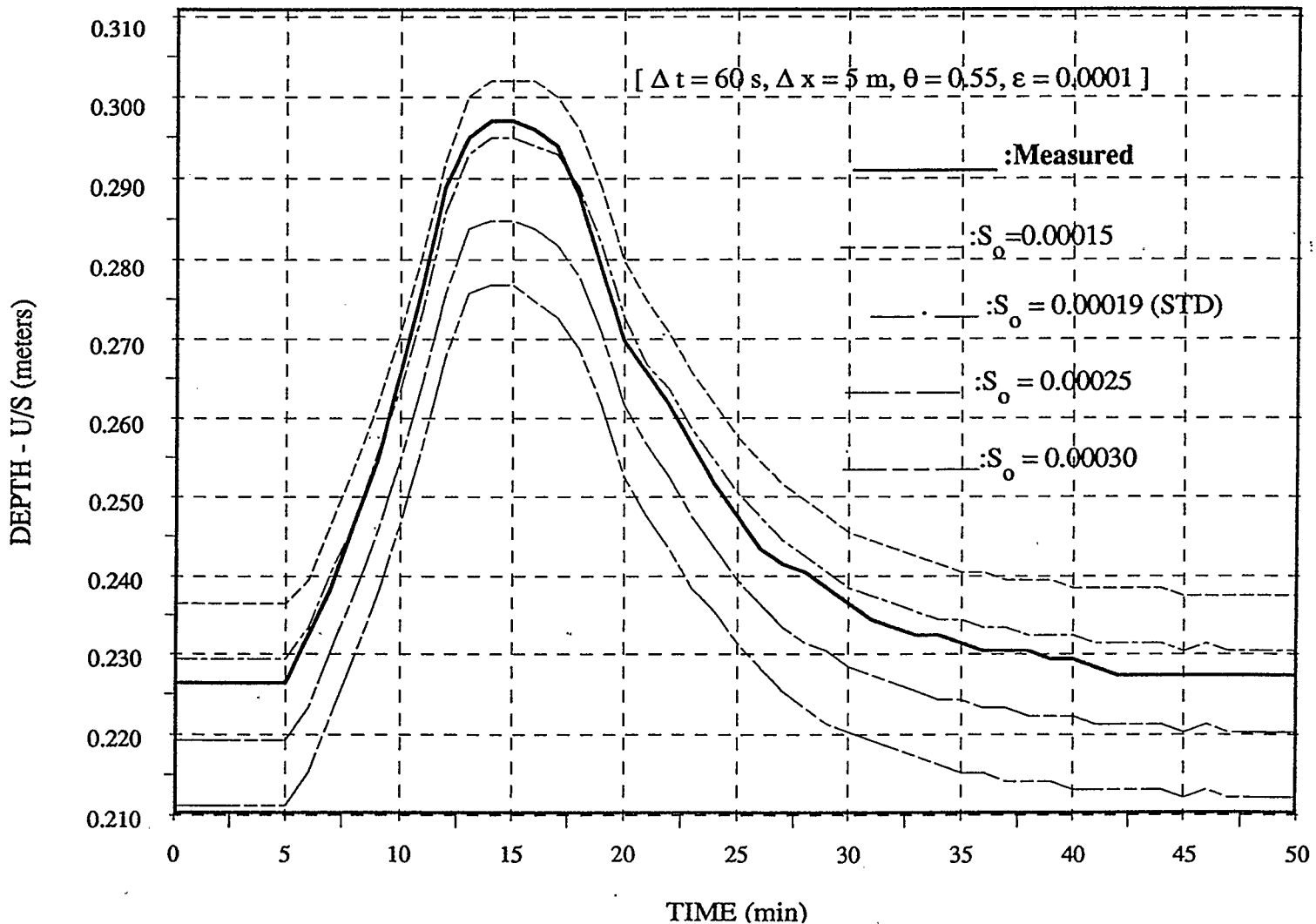

Figure B.4 (b)

Measured and Computed Depth Hydrographs at Upstream Boundary of the Channel Reach for Varying Channel Bottom Slope

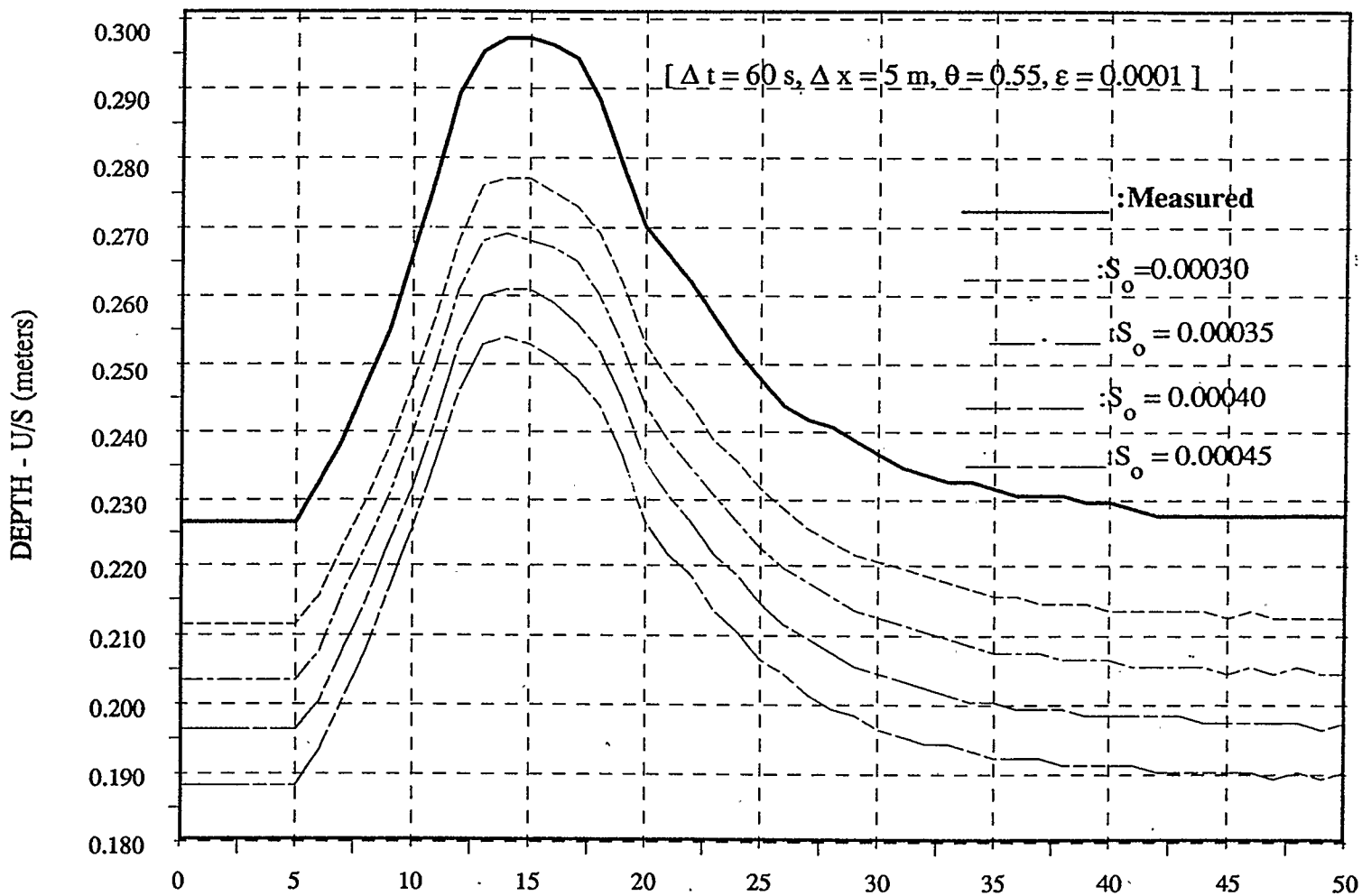

Figure B.4 (c)

Measured and Computed Depth Hydrographs at Upstream Boundary of the Channel Reach for Varying Channel Bottom Slope

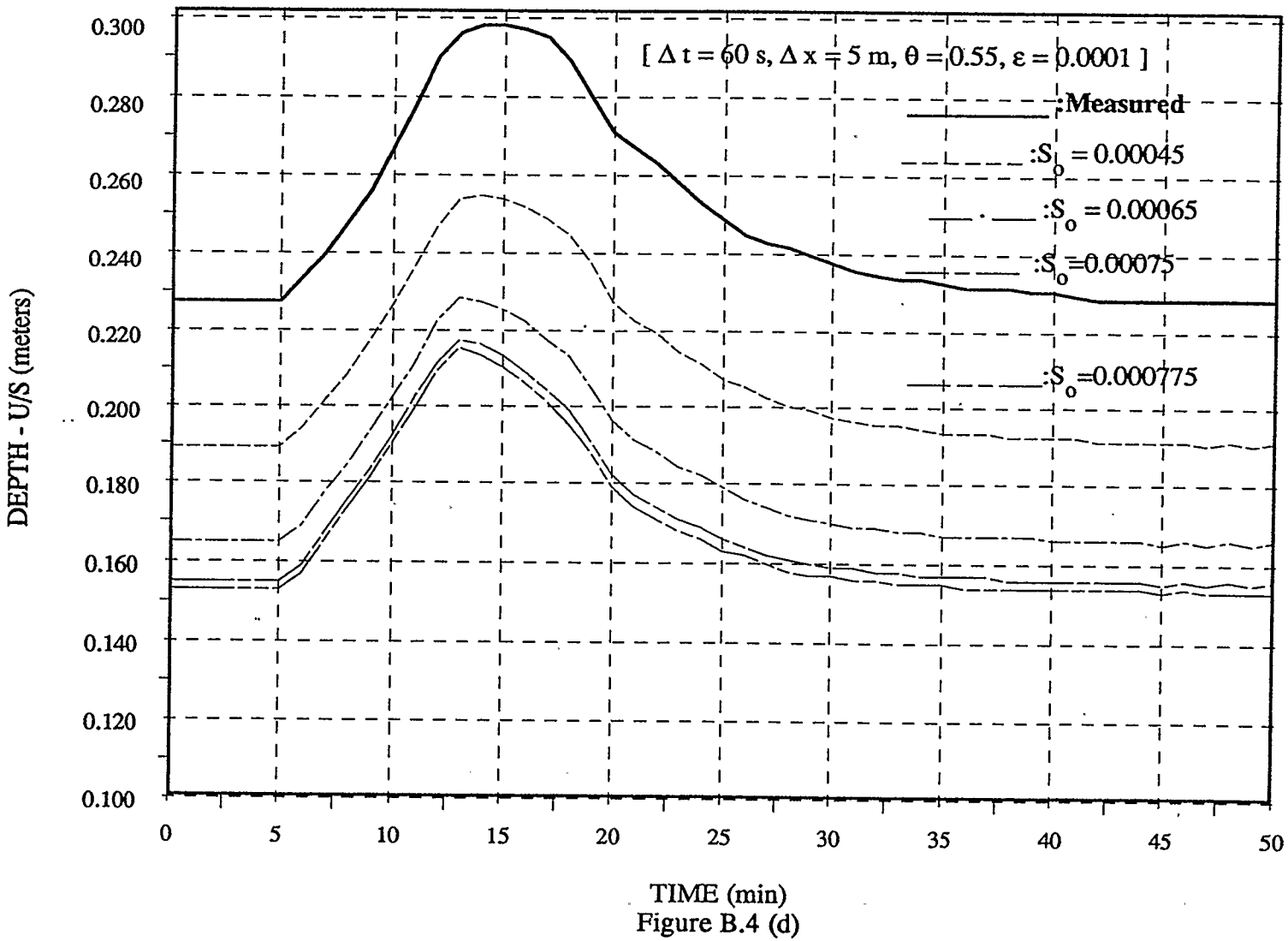

Figure B.4 (d)

Measured and Computed Depth Hydrographs at Upstream Boundary of the Channel Reach for Varying Channel Bottom Slope

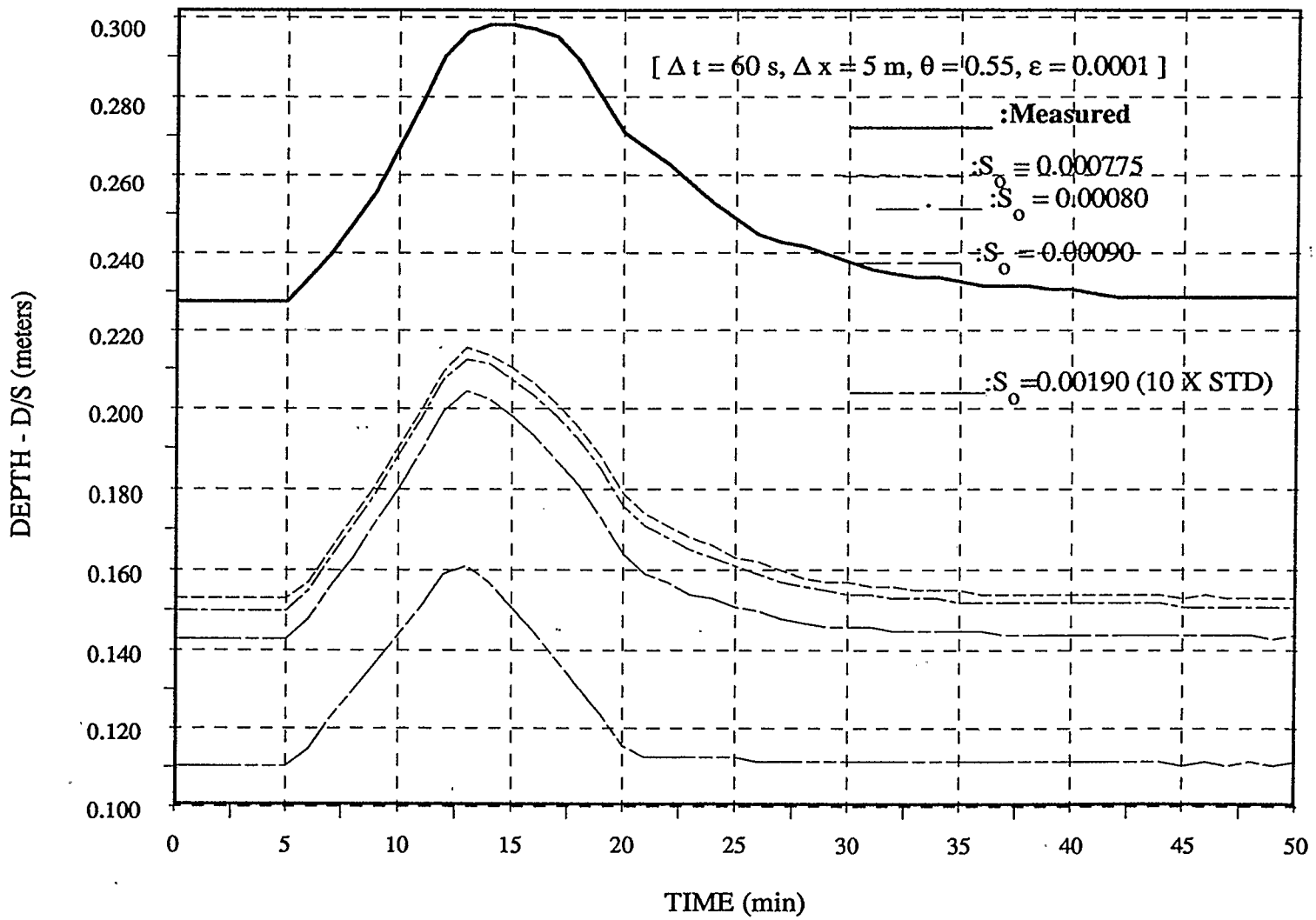

Figure B.4 (e)

Measured and Computed Depth Hydrographs at Upstream Boundary of the Channel Reach for Varying Channel Bottom Slope

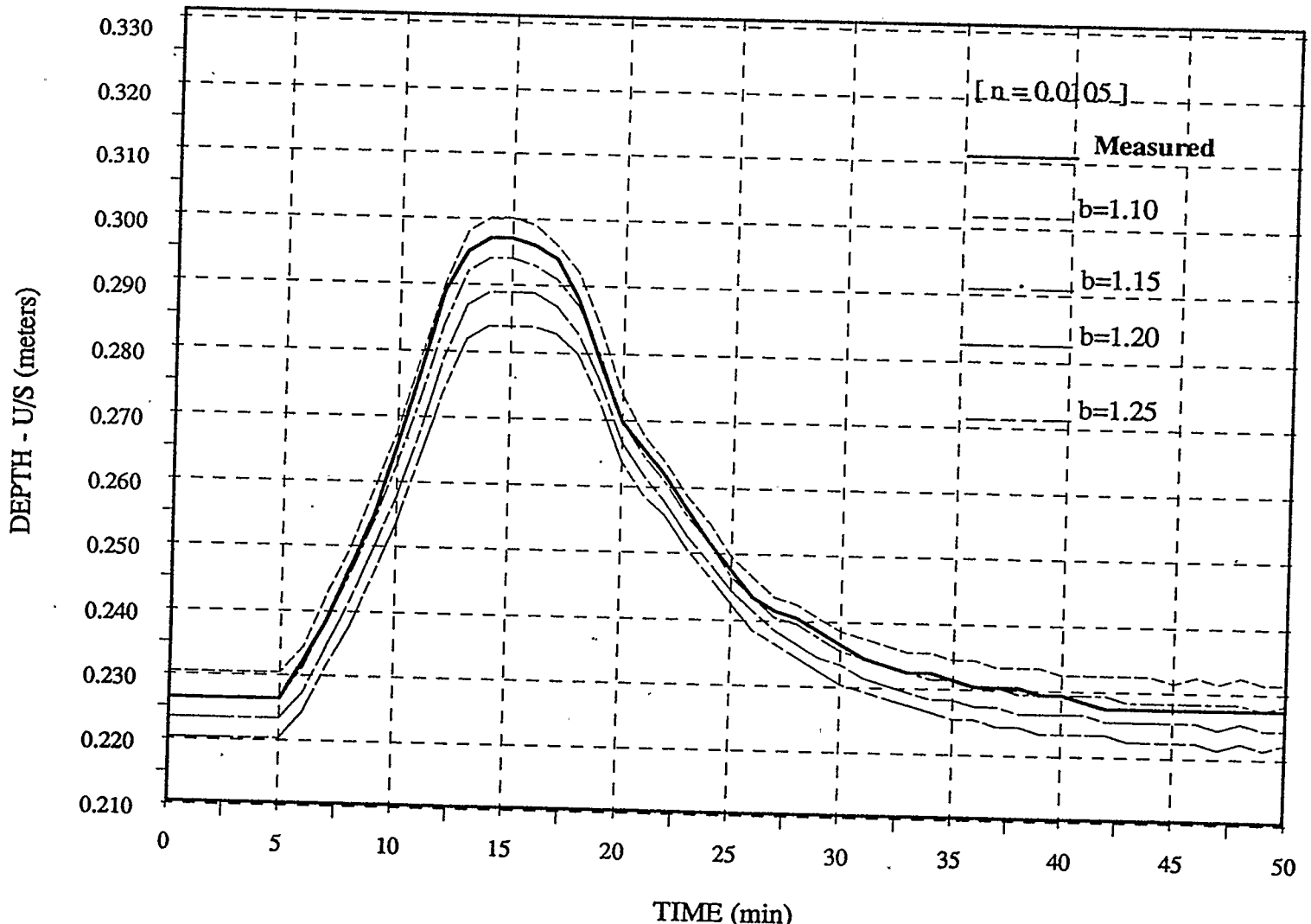

Figure B.5 (a)

Measured and Computed Depth Hydrographs at the Upstream Boundary of the Channel Reach for Varying Channel Widths and for Resistance Coefficient n=0.0105

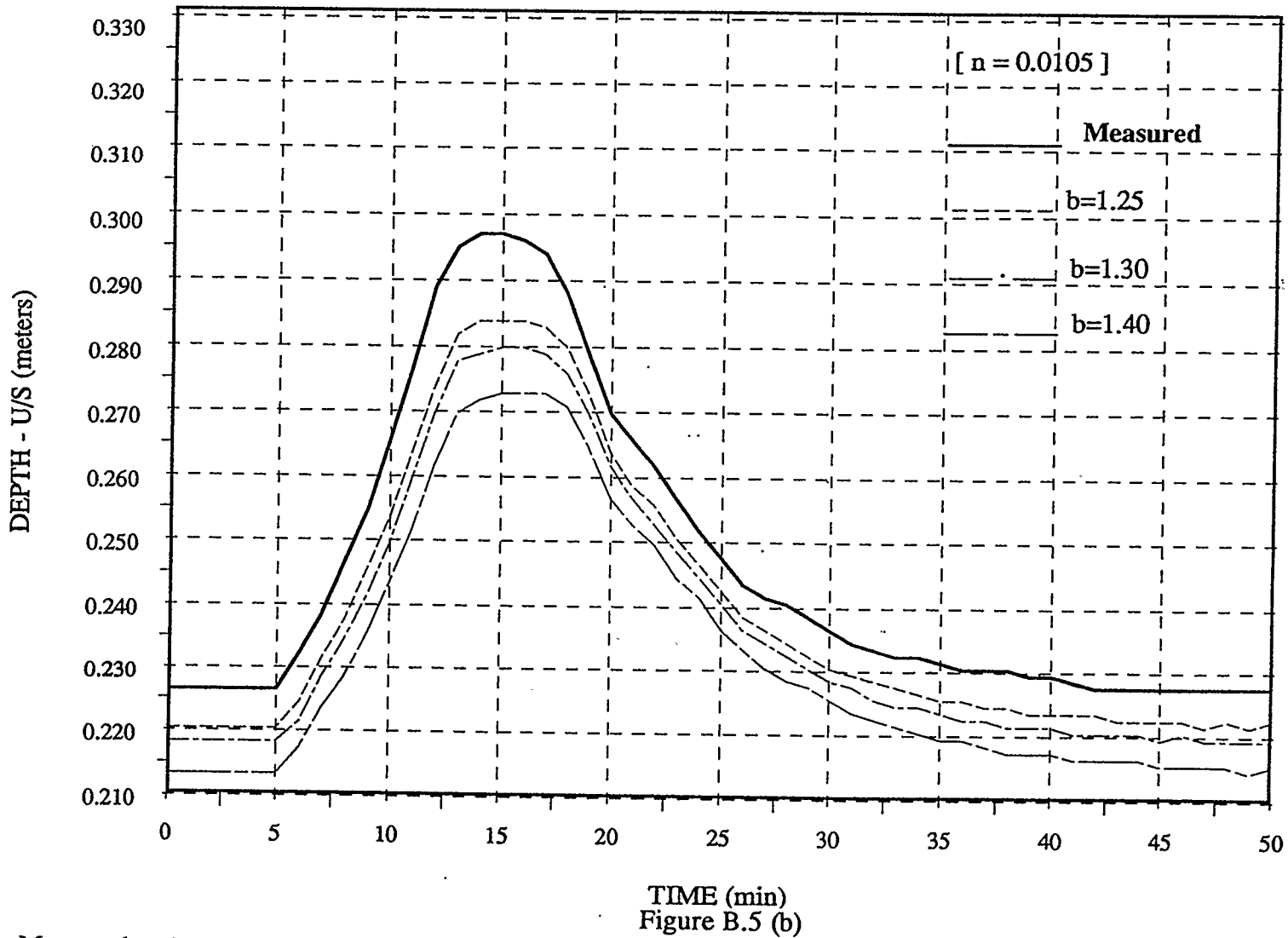

Figure B.5 (b)

Measured and Computed Depth Hydrographs at the Upstream Boundary of the Channel Reach for Varying Channel Widths and for Resistance Coefficient n=0.0105

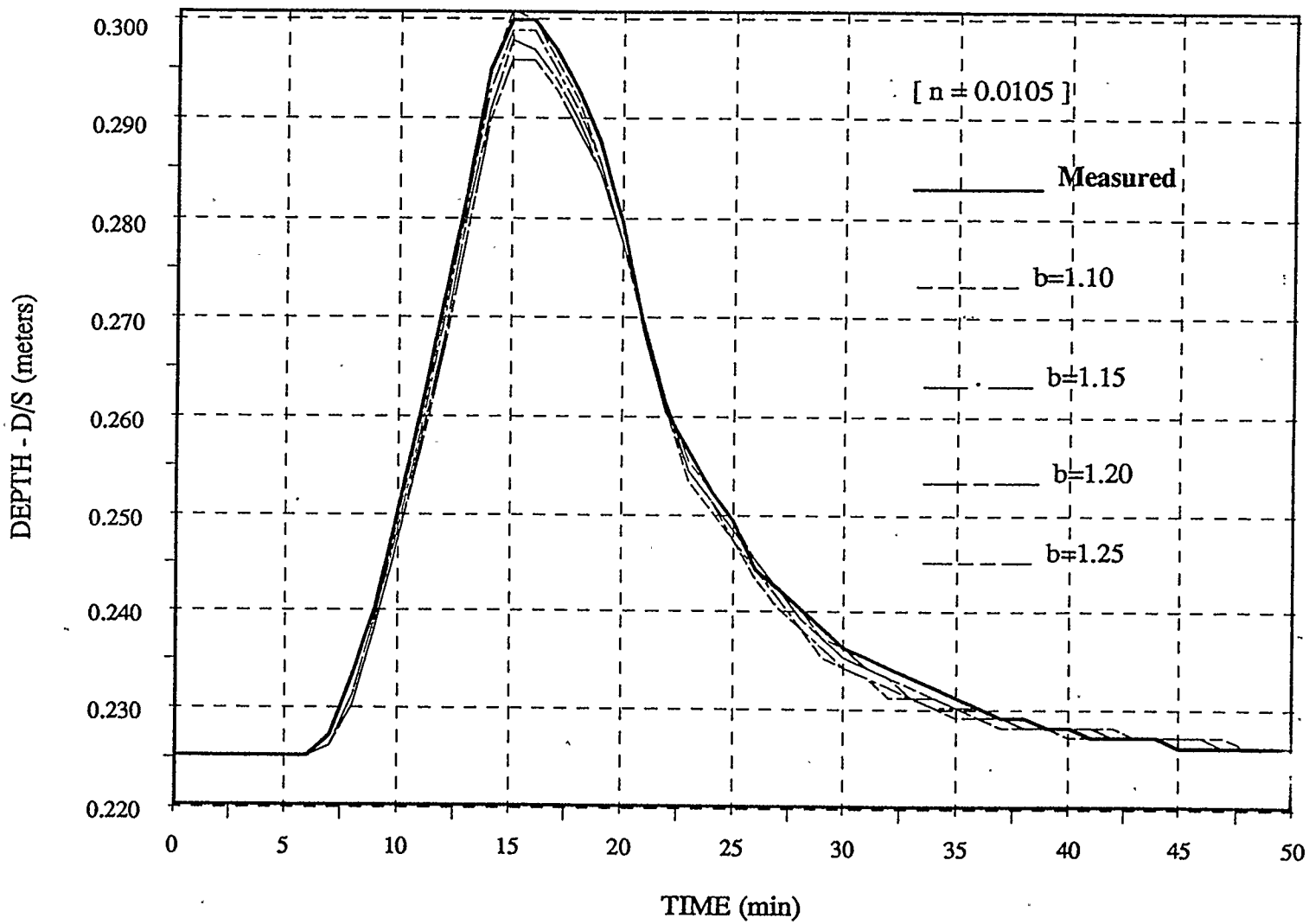

Figure B.5 (c)

Measured and Computed Depth Hydrographs at the Downstream Boundary of the Channel Reach for Varying Channel Widths and for Resistance Coefficient n=0.0105

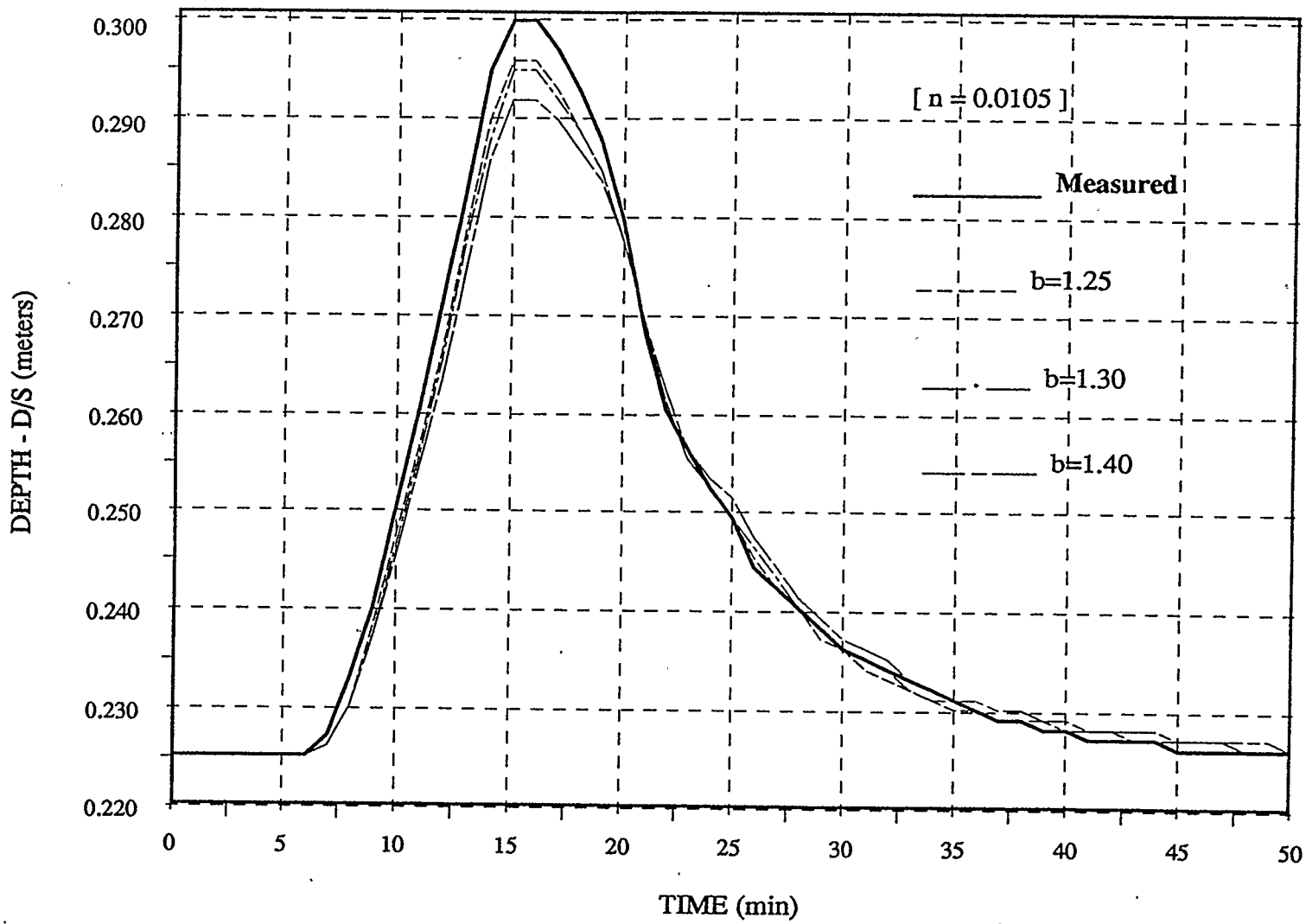

Figure B.5 (d)

Measured and Computed Depth Hydrographs at the Downstream Boundary of the Channel Reach for Varying Channel Widths and for Resistance Coefficient n=0.0105

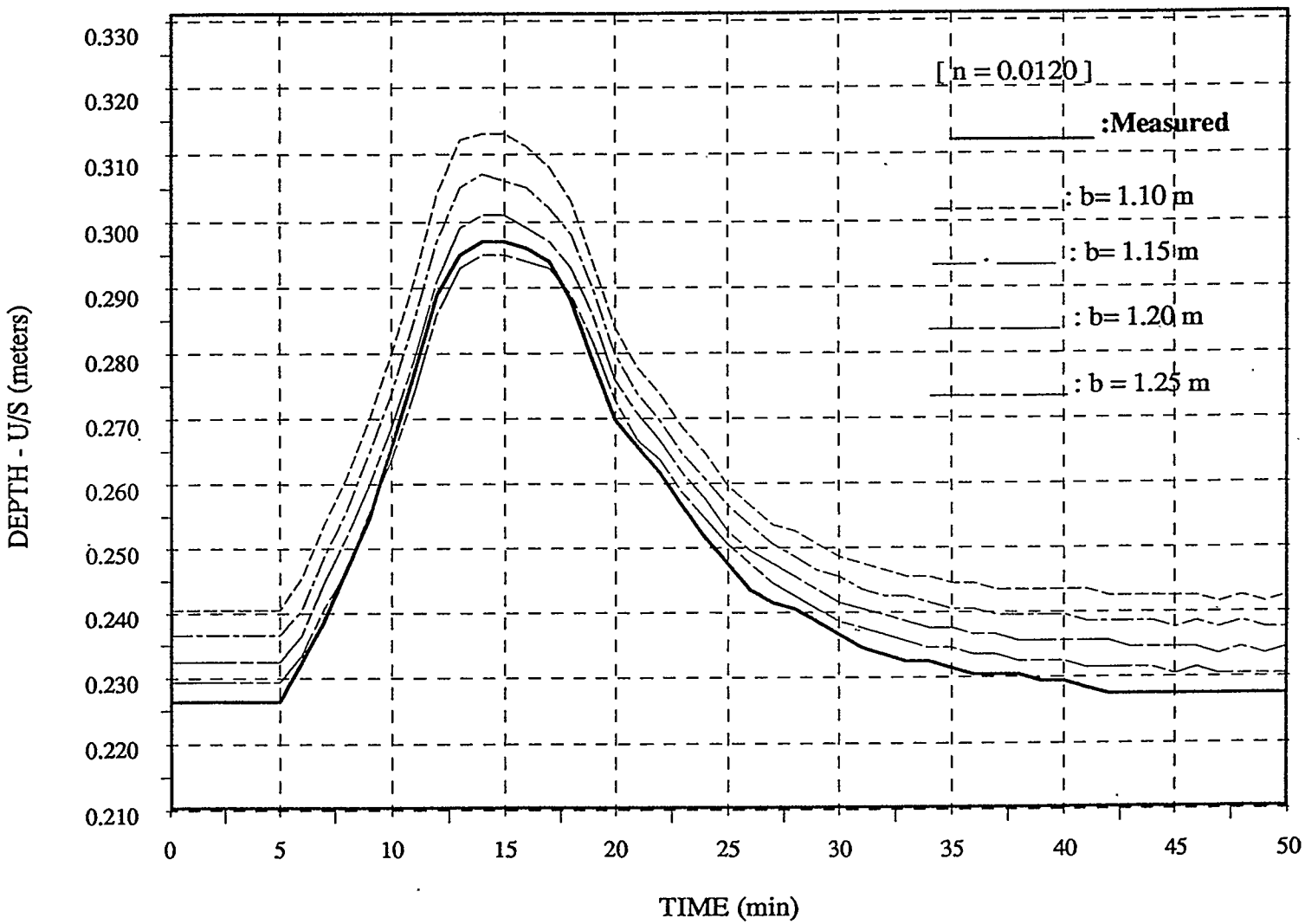

Figure B.6 (a)

Measured and Computed Depth Hydrographs at the Upstream Boundary of the Channel Reach for Varying Channel Width and for Resistance Coefficient n=0.0120

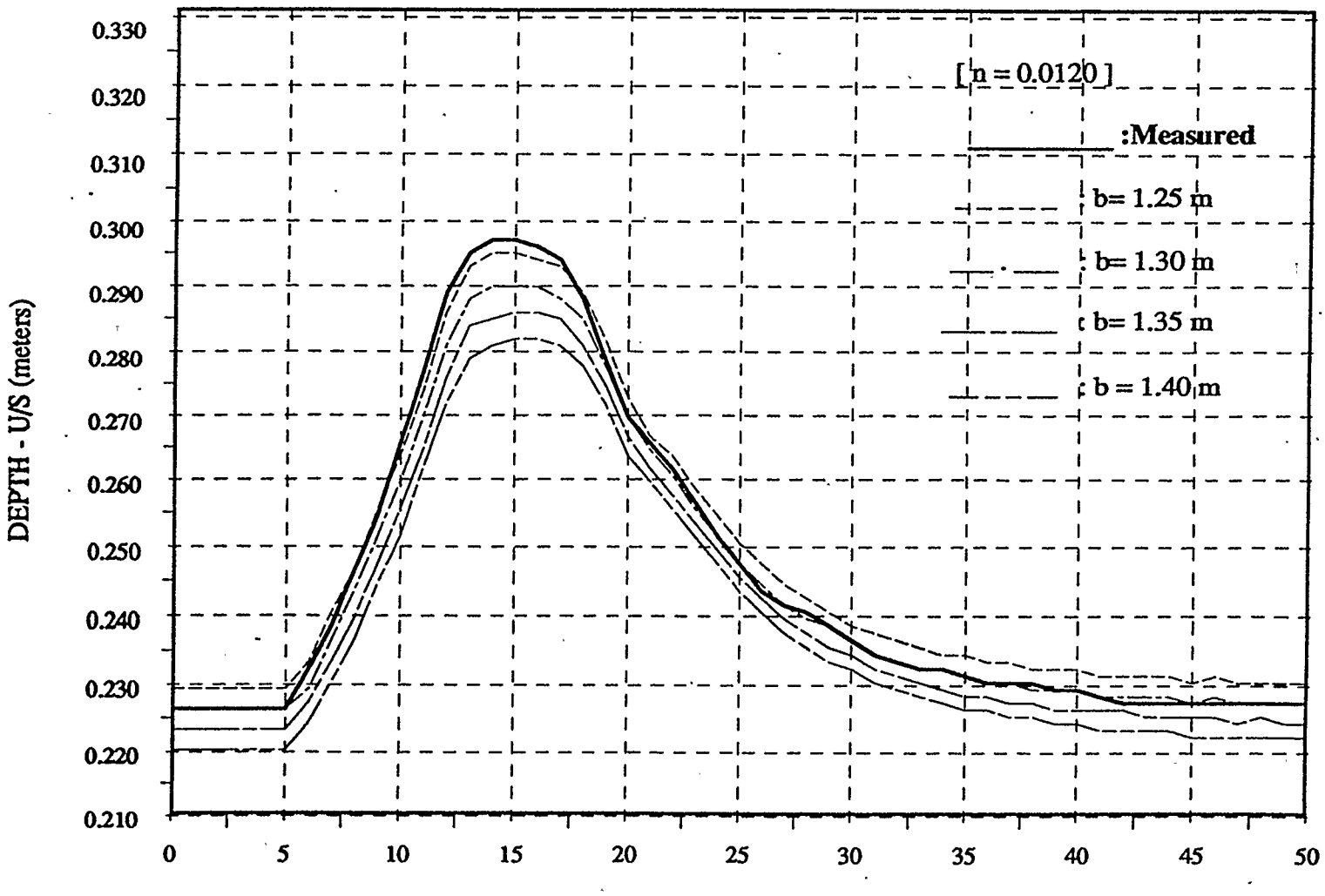

Figure B.6 (b)

Measured and Computed Depth Hydrographs at the Upstream Boundary of the Channel Reach for Varying Channel Width and for Resistance Coefficient n=0.0120

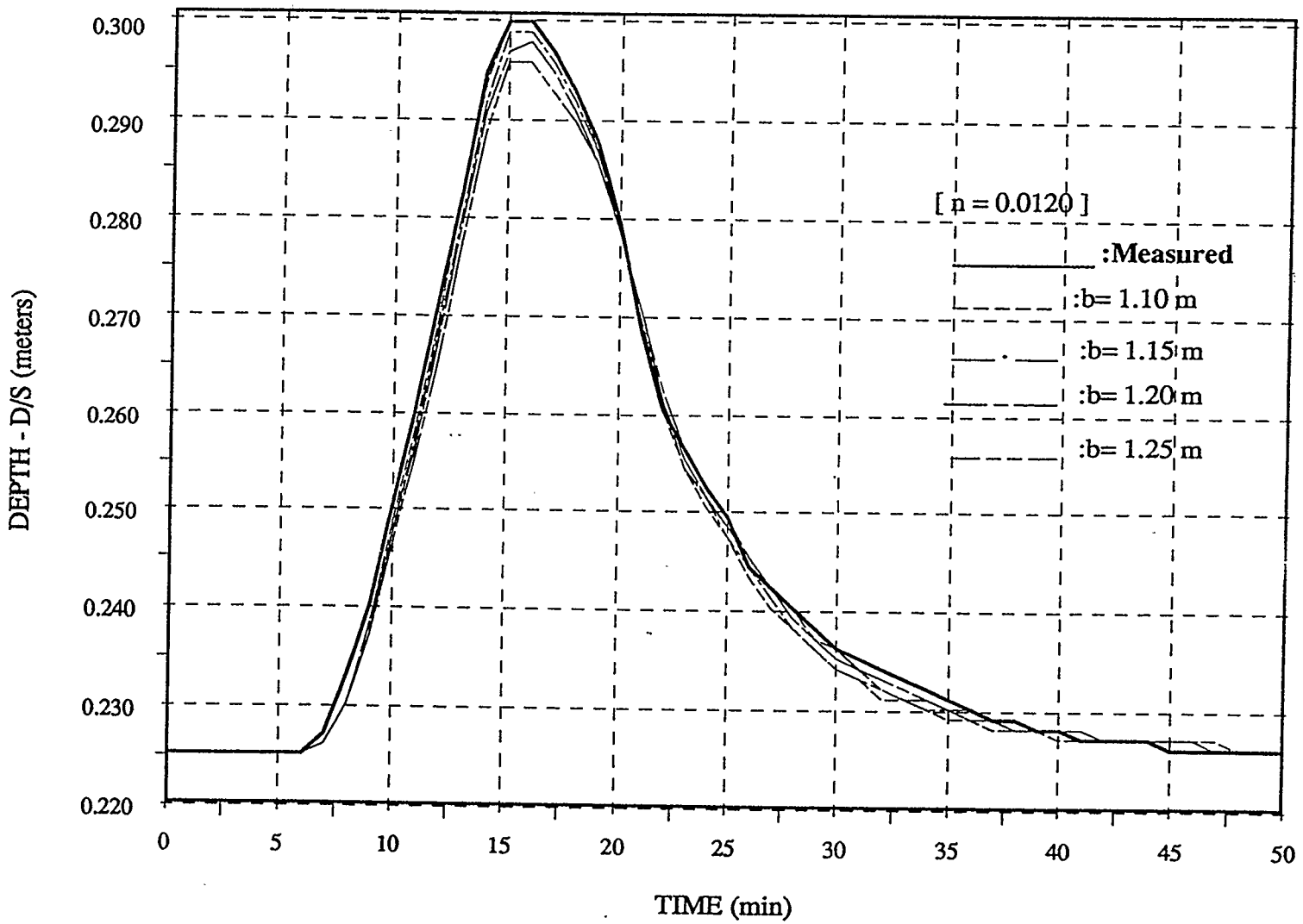

Figure B.6 (c)

Measured and Computed Depth Hydrographs at the Downstream Boundary of the Channel Reach for Varying Channel Width and for Resistance Coefficient n=0.0120

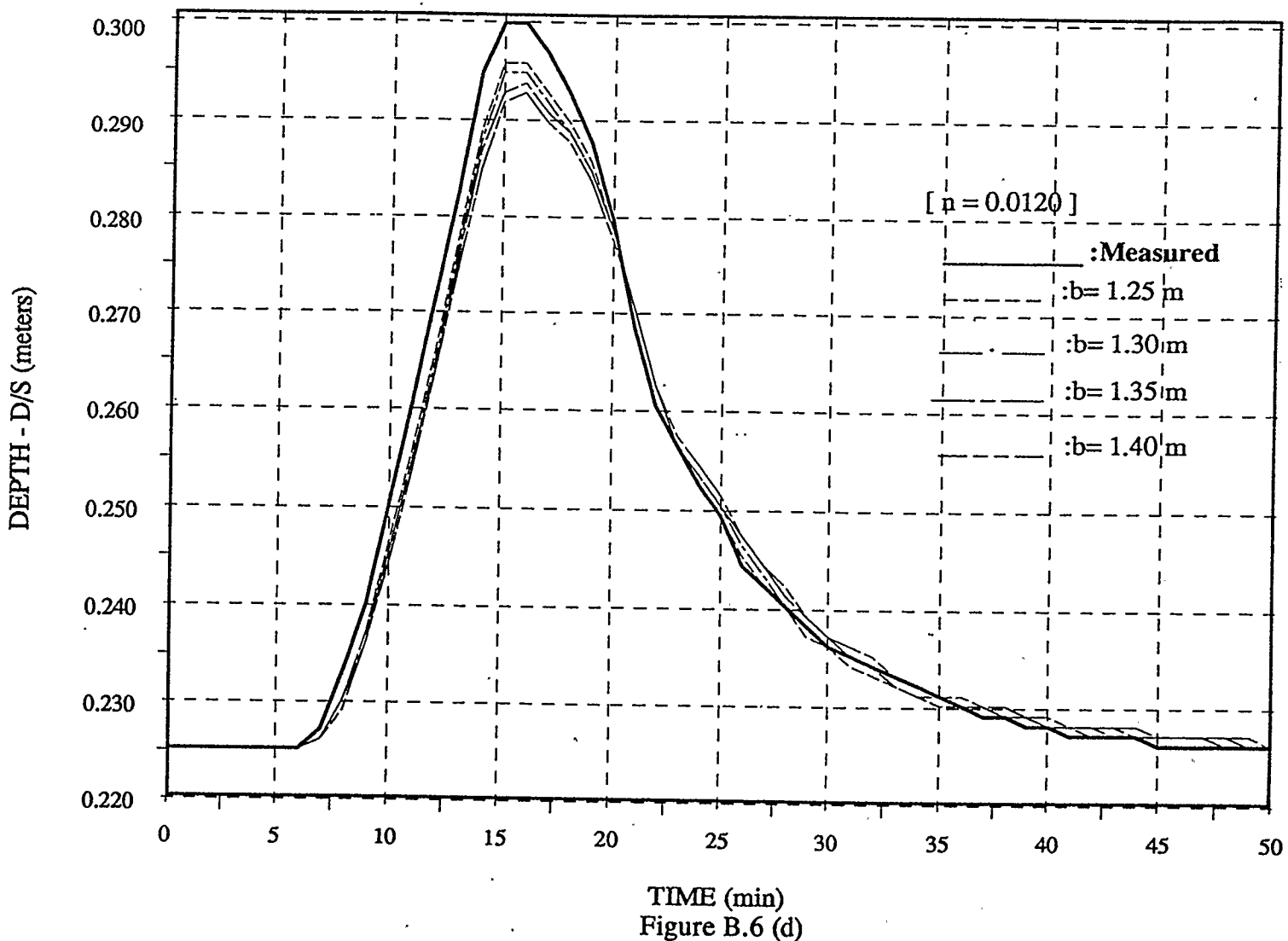

Figure B.6 (d)

Measured and Computed Depth Hydrographs at the Upstream Boundary of the Channel Reach for Varying Channel Width and for Resistance Coefficient n=0.0120

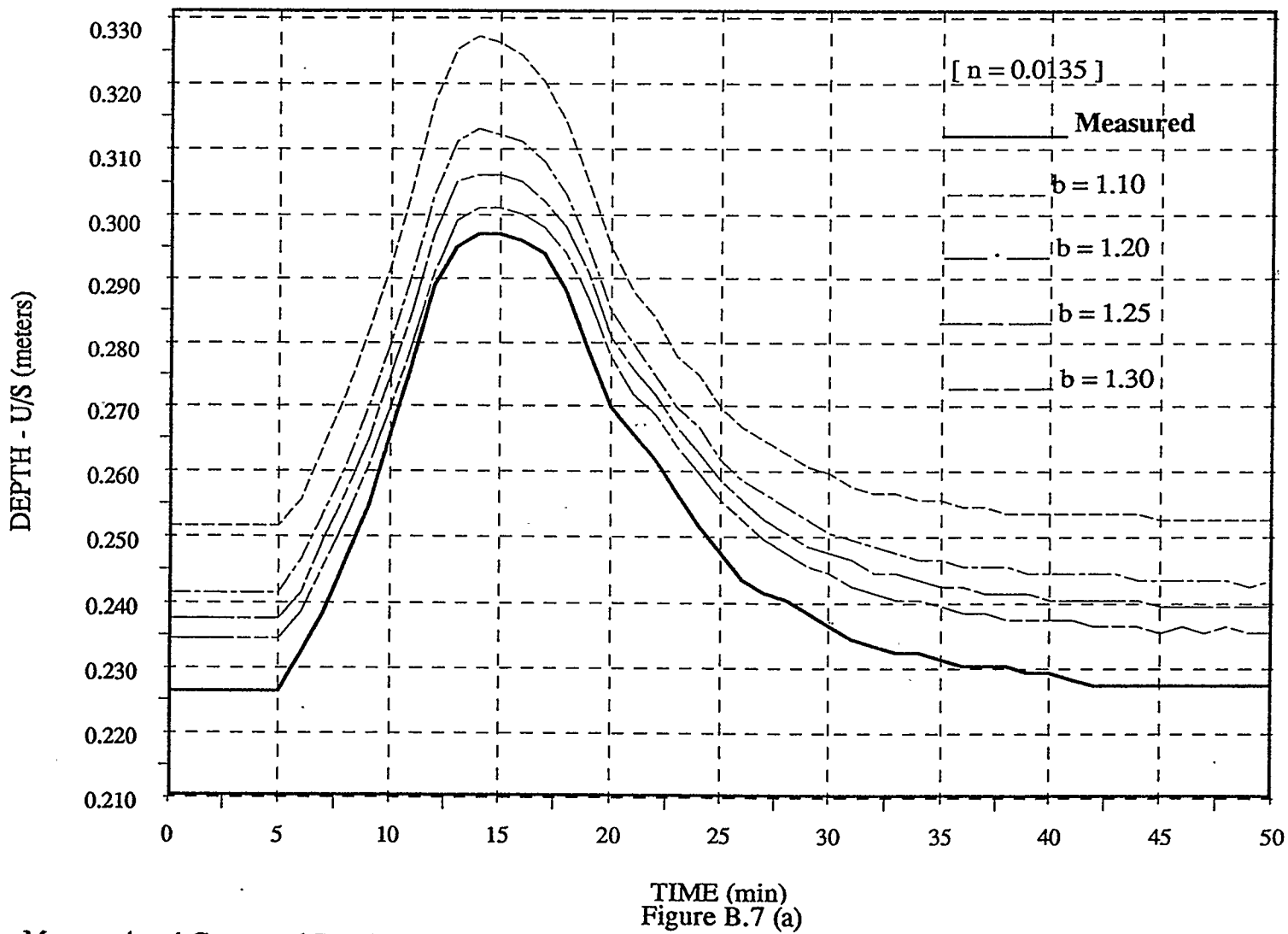

Figure B.7 (a)

Measured and Computed Depth Hydrographs at the Upstream Boundary of the Channel Reach for Varying Channel Width and for Resistance Coefficient n=0.0135

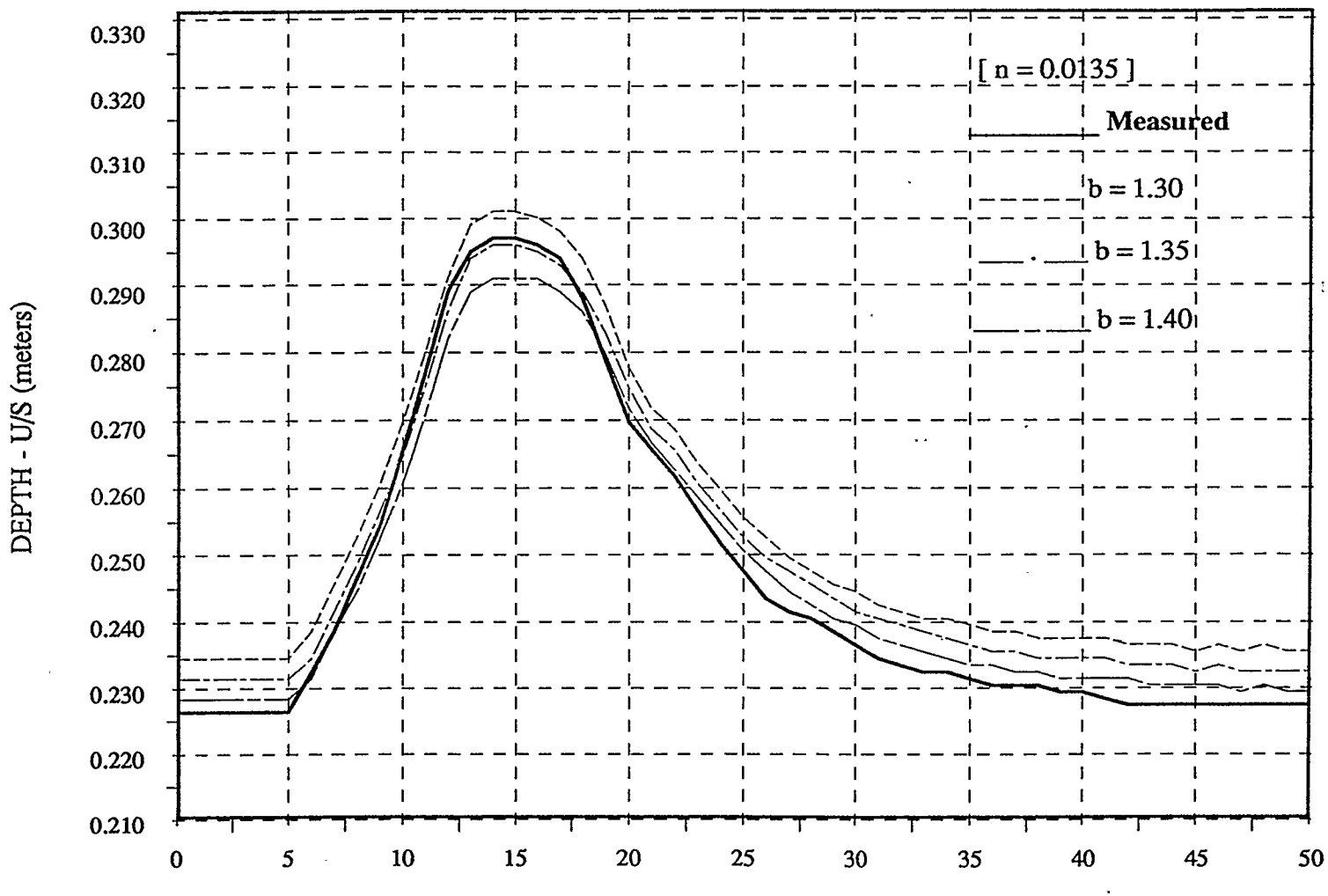

Figure B.7 (b)

Measured and Computed Depth Hydrographs at the Upstream Boundary of the Channel Reach for Varying Channel Width and for n=0.0135

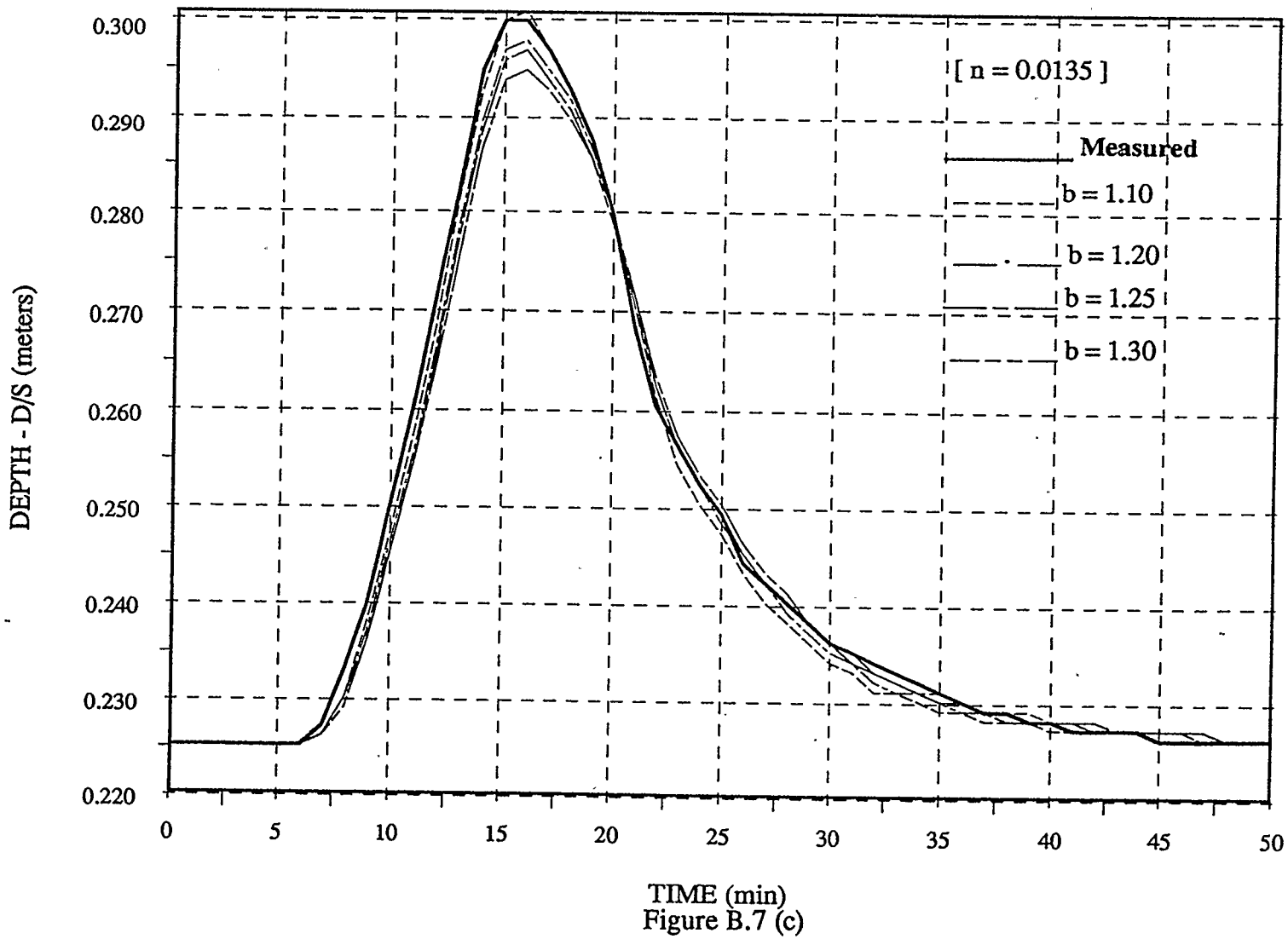

Figure B.7 (c)

Measured and Computed Depth Hydrographs at the Downstream Boundary of the Channel Reach for Varying Channel Width and for n=0.0135

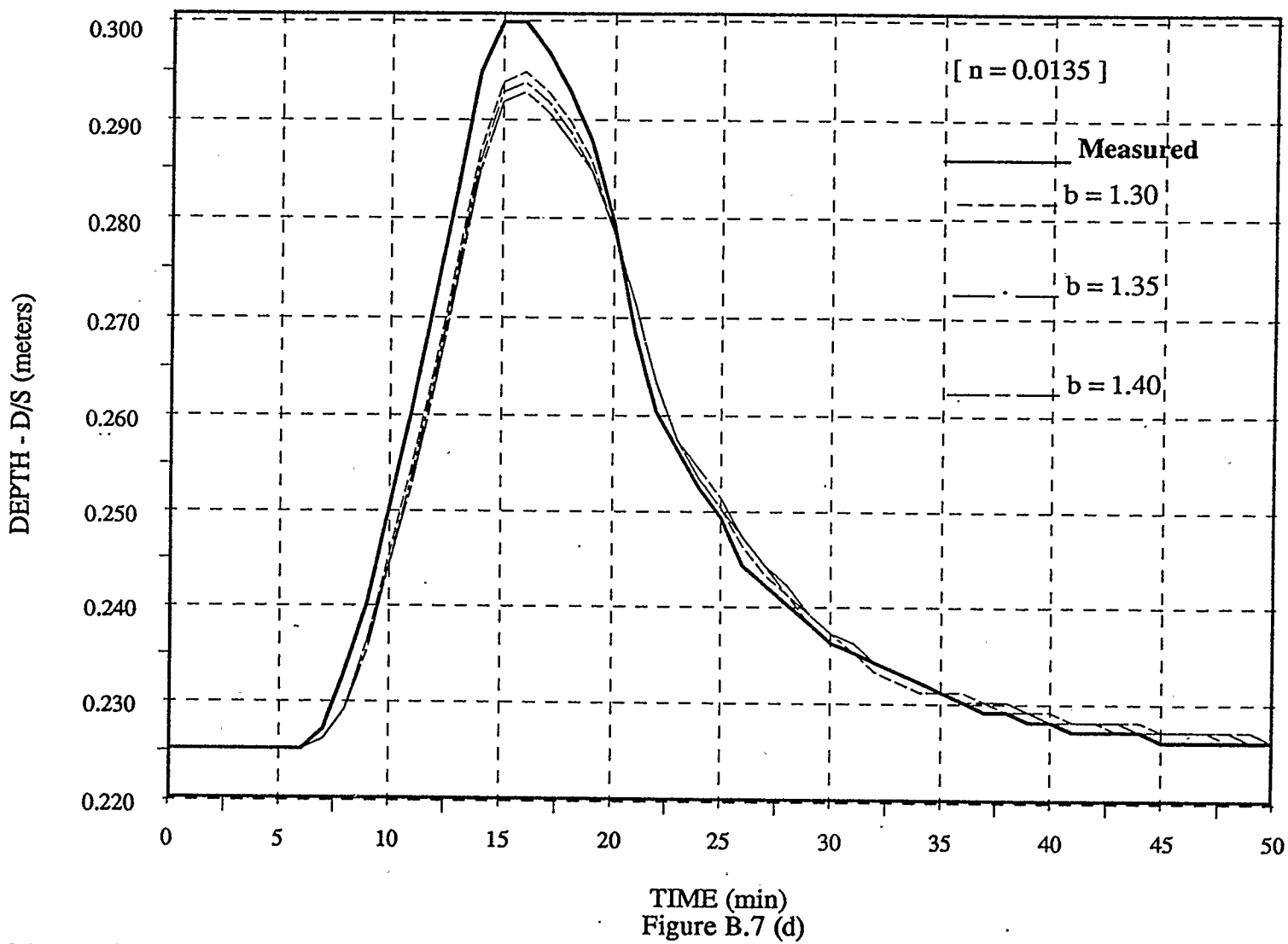

Figure B.7 (d)

Measured and Computed Depth Hydrographs at the Downstream Boundary of the Channel Reach for Varying Channel Width and for n=0.0135

APPENDIX C

BRIEF DESCRIPTION OF TRESKE'S CHANNEL AND DATA SET

Channel flow experiments were conducted at Treske's experimental facility for unsteady flow studies (Treske, 1980). Treske's experimental facility consists of three outdoor channels located side by side with a common head tank. Unsteady flow experiments were conducted for three different channel configurations, namely, straight channel, meandering channel, and straight channel with lateral inflow. Carefully planned unsteady flow experiments were carried out in the channels. Only the straight channel configuration will be described briefly here because model simulation was carried out only in this case.

A 210 m working length of the straight channel reach was used in the unsteady flow experiments. The working length (L=210 m) was chosen so that the flow readings at the downstream end of the working length was not affected by the flow control structure (weir) at the outlet of the channel. Neither was it affected at the upstream end of the working length by the inlet flow control structure at the inlet of the channel. A summary of the channel condition is given in Table C.1. Unsteady flow experiments were conducted for different characteristics of unsteady inlet flow at the inlet of the straight channel. The flow measurements taken were water surface elevations and the rating curve functional relationship between the depth and discharge was used to determine the discharges. The error of accuracy of depth measurements was in the range of 1.5 mm to 2.5 mm for all the unsteady flow conditions. The results of the flow readings both at the upstream and at the downstream ends of the working lengths which were used in the verification and calibration of the model in Chapter 3 are shown in Table C.2.

The discharge-depth relationship (rating curve) was determined from the measured depth and discharge at the downstream end of the working length in Table C.2 and is given as:

$$Y(L)=1.344 \cdot Q(L)+0.08565 \qquad \text{...(C.1)}$$

where Y(L) is the depth in meters at the downstream end and Q(L) is the discharge in m^3/S at the downstream end.

A similar characteristic of unsteady flow conditions in the working length channel as shown in Table C.2 was conducted by Treske but with higher magnitudes of unsteady flow rates. The maximum unsteady inflow rate recorded at the upstream boundary of the working length is Q = 0.387 m^3/s. This maximum value of upstream inflow rate (Q = 0.387 m^3/s) and the maximum value recorded in Q = 0.186 m^3/s shown in Table C.2 were used in the sensitivity analysis in Chapter 3.

Table C.1
Data Summary of Treske's Experimental Channel Conditions

Configuration & alignment	straight prismatic rectangular channel
Working reach length, L	210 m
Channel bottom width, B	1.25 m
Channel bottom slope, S_o	0.00019
Channel resistance, n	0.0120
Channel uniform flow condition:	
Initial uniform flow rate, Q_0	0.103 m^3/s
Initial uniform flow depth, Y_0	0.225 m

Table C.2
Data Summary of Treske's Experimentally Measured Depth and Discharge of the Flow at Upstream and Downstream Boundary of the Channel Reach Length, L=210m

Time (min)	y u/s -m	Q u/s -m³/s	y d/s -m	Q d/s -m³/s
0	0.226	0.103	0.225	0.103
1	0.226	0.103	0.225	0.103
2	0.226	0.103	0.225	0.103
3	0.226	0.103	0.225	0.103
4	0.226	0.103	0.225	0.103
5	0.226	0.103	0.225	0.103
6	0.232	0.111	0.225	0.103
7	0.238	0.124	0.227	0.105
8	0.246	0.134	0.233	0.109
9	0.254	0.146	0.24	0.114
10	0.265	0.157	0.25	0.121
11	0.276	0.17	0.26	0.128
12	0.288	0.183	0.271	0.137
13	0.294	0.186	0.282	0.145
14	0.296	0.175	0.294	0.154
15	0.296	0.164	0.299	0.158
16	0.295	0.153	0.299	0.156
17	0.293	0.142	0.296	0.156
18	0.287	0.131	0.292	0.153
19	0.278	0.119	0.287	0.149
20	0.269	0.107	0.279	0.143
21	0.265	0.105	0.268	0.134
22	0.261	0.106	0.26	0.128
23	0.256	0.105	0.256	0.125
24	0.251	0.106	0.252	0.122
25	0.247	0.105	0.249	0.12
26	0.243	0.105	0.244	0.117
27	0.241	0.104	0.242	0.115
28	0.24	0.104	0.24	0.114
29	0.238	0.104	0.238	0.112
30	0.236	0.104	0.236	0.111
31	0.234	0.104	0.235	0.11
32	0.233	0.104	0.234	0.11
33	0.232	0.104	0.233	0.109
34	0.232	0.104	0.232	0.108
35	0.231	0.104	0.231	0.107
36	0.23	0.104	0.23	0.107
37	0.23	0.104	0.229	0.106
38	0.23	0.104	0.229	0.106
39	0.229	0.104	0.228	0.105
40	0.229	0.104	0.228	0.105
41	0.228	0.104	0.227	0.105
42	0.227	0.104	0.227	0.105
43	0.227	0.104	0.227	0.105
44	0.227	0.104	0.227	0.105
45	0.227	0.103	0.226	0.104
46	0.227	0.104	0.226	0.104
47	0.227	0.103	0.226	0.104
48	0.227	0.104	0.226	0.104
49	0.227	0.103	0.226	0.104
50	0.227	0.104	0.226	0.104

APPENDIX D

IRRIGATION CONVEYANCE SYSTEM SIMULATION (ICSS) MODEL

The numerical computations carried out in this study were made by the Irrigation Conveyance System Simulation (ICSS) computer model. The ICSS program is described by Manz (1985). The ICSS Model was written in FORTRAN and executed interactively on a Control Data Corporation Cyber 186 computer system at the University of Calgary.

The first step in the use of the ICSS program is the creation of two auxiliary programs called SIMDAT and RCHDAT. The program SIMDAT creates the data file called SIM1 containing the general information on simulation including the hydraulic time step, weighting factor, convergence criterion parameter, and gravitational constant. The program RCHDAT creates the data file called RCH1 containing the physical parameters necessary to describe the simulated channel and the downstream and upstream boundary parameters. The most important physical data for the channel are channel length, channel bottom slope, distance interval, Manning's resistance coefficient, lateral inflow and/or outflows, and cross-section geometry coefficients for the channel reach. The downstream parameters include the boundary condition and initial flow condition.

In the ICSS program, the unsteady flow routing sub-program was interactively programmed to accept the upstream and downstream boundary condition, the initial conditions in the channel, the functional relationships between depth and area or channel surface width or wetted perimeter for each reach of the channel, appropriate values of Manning's n, and all other data necessary for unsteady flow routing.These information are contained in different subroutines in the ICSS program. These subroutines include the SMD and DATAM subroutine programs to read the data files SIM1 and RCH1 respectively. The functional relationship between the depth and area or channel surface width or the wetted perimeter, and their respective derivative with respect to depth were the

third-degree polynomial. Channel area, surface width, wetted perimeter, and their derivatives with respect to depth were made available throughout the program using function subroutines AREA, TOPW, WETP, DAREA, DTOPW, and DWETP. The initial flow conditions in the iterative procedure of unsteady flow routing, was provided by the backwater calculations in the subroutine BACKW. The gradually varying flow equations of steady spatially varied channel flow were used in the backwater calculations. The equations (see Manz, 1985) were solved using the finite difference technique. The upstream and downstream boundary conditions were described in subroutines UBC band DBC respectively.

The numerical algorithms used in the unsteady flow routing sub-program are describe in Appendix A. The Gaussian elimination procedure was used to solve the sparse diagonal matrix of Equation A.11. The results from program execution were written in output files named REPORTS 1 to 2. The REPORT 1 contained the initial storage at time t=0; cumulative volume of inflow and outflow, and storage in the reach at time t=t. These results are used in Mass Conservation Error (E) calculations. The REPORT 2 file contain the depth and discharge at both upstream and downstream boundaries of the channel length from time t=0 to t=t in increments of hydraulic time step.

The various values of each time interval or weighting factor or convergence criterion parameter in the numerical computations conducted in this study using the ICSS Model were made in the auxiliary data file SIM1. Values for each of distance interval or physical channel parameter were made in the auxiliary file RCH1.